



Numerical Methods for the Simulation of Acoustic Resonances

Diplomarbeit zur Erlangung des akademischen Grades

Diplom Ingenieur

im Diplomstudium Technische Mathematik

Angefertigt am Institut für Numerische Mathematik

Betreuung:

Dipl.-Ing. Dr. Joachim Schöberl

Eingereicht von:

Maria Rechberger

Linz, November 2005

For my father

Abstract

The Helmholtz eigenvalue problem on infinite domains appear in many fields such as acoustics, geophysics, electromagnetics, aerodynamics, meteorology and so on. Therefore it is very important to provide methods or boundary conditions that terminate the infinite domain and absorb the waves totally without any reflection.

One method is the PML method by Bérenger, the other is called wavefactorization. The first absorbs all waves independent from their direction or frequency by analytic continuation of the governing equations into the complex domain. The latter splits up the wave into an exponential term and a smooth amplitude. The exponential term is responsible for the oscillation raising with distance to the origin.

This thesis introduces and discusses both methods and their combination in the one- and two-dimensional case.

Starting from the Helmholtz eigenvalue problem the mathematical model is derived, which is the variational formulation of the eigenvalue problem with absorbing boundary condition.

For picking out artificial eigenvalues of the set of computed eigenvalues a special strategy has been developed and successfully tested.

The matrices obtained from the Finite Element discretisation are large and sparse and so the Arnoldi method solves the eigenvalue problem.

Zusammenfassung

Das Eigenwert Problem abgeleitet von der Helmholtzgleichung in unbeschränkten Gebieten betrifft viele Fachbereiche: Akkustik, Geophysik, Elektromagnetic, Aerodynamik, Meteorologie usw. Deshalb ist es sehr wichtig, Methoden die das unendliche Gebiet beschränken und Randbedingungen, welche die ausstrahlenden Wellen ohne jedwellige Reflektion absorbieren, zur Verfügung zu stellen.

Ein solches Verfahren ist die "Perfectly Matched Layer Methode", das andere heißt "Wavefactorization". Erstere absorbiert alle Wellen egal welcher Richtung oder Frequenz indem die Helmholtzgleichung in den komplexen Raum analytisch fortgesetzt wird. Letztere faktorisiert die Welle in einen exponentiellen Term und einer stetigen Amplitude, wobei der exponentielle Faktor verantwortlich ist für die Oszillation, welche mit Abstand zum Ursprung zunimmt.

Diese Diplomarbeit stellt beide Methoden und deren Kombination vor und behandelt jeweils den ein- und zwei-dimensionalen Fall.

Ausgehend von der Helmholtzgleichung wird das mathematische Model, also die Variationsformulierung des Eigenwert Problems mit absorbierender Randbedingung, abgeleitet.

Eine spezielle, vielversprechende Strategie zur Auslese künstlicher Eigenwerte aus der Menge der berechneten Eigenwerte wurde entwickelt und erfolgreich getestet.

Die aus der Finite Element Diskretisierung erhaltenen Matrizen sind groß und dünnbesetzt, deshalb wird als Eigenwertlöser die Arnoldi Methode herangezogen.

Acknowledgements

First of all I would like to thank my supervisor Dr. Joachim Schöberl for giving me the chance to write this thesis, for various discussions and for his time. He supported me in getting started in programming and in debugging.

Special Thanks to Larissa Vorhauer and Sabine Zaglmayr, who had always an open ear to my questions.

Thanks to Dr. Werner Koch from *Deutsche Luft- und Raumfahrt Institut (DLR)* for pointing out this problem and for financial support.

Also, I want to thank Thorsten Hohage of the University of Göttingen for his interest in my work and his physical explanation of various themes.

Last but not least I acknowledge the Institute of Computational Mathematics at the Johannes Kepler university of Linz for the environment and the technical support.

Maria Rechberger
Linz, Nov. 2005

Contents

| | | |
|----------|------------------------------------------------------------------------|-----------|
| 1 | Introduction | 1 |
| 2 | Problem Formulation | 5 |
| 2.1 | Physical Model and Governing Equations | 5 |
| 2.1.1 | Conservation of Mass | 5 |
| 2.1.2 | Equation of Motion | 6 |
| 2.2 | The Sommerfeld Condition | 7 |
| 2.3 | Wave Equation and Absorbing Boundary Conditions in 1D | 7 |
| 2.4 | Plane Waves | 8 |
| 3 | Source and Eigenvalue Problems on Bounded and Unbounded Domains | 10 |
| 3.1 | Source Problem on Bounded Domain | 10 |
| 3.2 | Bounded Eigenvalue Problem | 11 |
| 3.3 | Unbounded Eigenvalue Problem | 12 |
| 3.3.1 | The Oscillating String | 13 |
| 4 | Analytical Solutions of the Helmholtz Problem | 15 |
| 4.1 | Separation of Variables | 15 |
| 4.1.1 | Cartesian Coordinates | 15 |
| 4.1.2 | Spherical Coordinates | 16 |
| 4.1.3 | Cylindrical Coordinates | 19 |
| 4.2 | Problems in Variational Formulation | 20 |
| 5 | The Perfectly Matched Layer | 21 |
| 5.1 | Sketch of the PML Method in 1D | 21 |
| 5.2 | Variational Derivation | 24 |
| 5.3 | Examples | 26 |
| 5.3.1 | The Oscillating String Problem with PML | 26 |
| 5.3.2 | Unbounded Eigenvalue Problem | 28 |
| 5.3.3 | Unbounded two dimensional Eigenvalue Problem | 30 |
| 5.4 | Properties of Complex Symmetric Matrices | 32 |
| 6 | Methods of Discretization/Modelling | 33 |
| 6.1 | PML: Problems and Fixes | 33 |
| 6.1.1 | Reduced Integration | 34 |
| 6.1.2 | Dispersion Analysis for the FE-Solution | 38 |

| | | |
|----------|-----------------------------------------------------------|-----------|
| 6.1.3 | Derivatives and Sensitives | 42 |
| 6.2 | Wavefactorization | 47 |
| 6.2.1 | Wavefactorization: one-dimensional case | 48 |
| 6.2.2 | Wavefactorization in higher dimensions | 51 |
| 6.3 | Combination of Wavefactorization and PML method | 53 |
| 6.3.1 | The One Dimensional Case | 54 |
| 6.3.2 | Higher Dimensions | 55 |
| 7 | Example: Slat Cove of an Aeroplane | 58 |
| 7.1 | Geometry | 58 |
| 7.2 | PML Method | 58 |
| 7.3 | Wavefactorization | 61 |
| 7.4 | Wavefactorization and PML Method combined | 63 |
| 8 | The Eigenvalue Solver | 67 |
| 8.1 | The Arnoldi Method | 68 |
| 8.1.1 | The algorithm | 68 |
| 8.2 | Future Work on the Eigenvalue Solver | 70 |
| 8.2.1 | Deflation | 70 |
| 8.3 | Other Eigenvalue Solver | 72 |
| 9 | Conclusion and Future Work | 73 |
| A | List of Notations | 74 |
| B | The Finite Element Method | 76 |
| B.1 | The Galerkin Ritz Method | 76 |
| B.2 | Finite Elements - FE | 77 |
| B.3 | Courant Elements | 78 |
| B.3.1 | Courant Elements on Intervals | 78 |
| B.3.2 | Linear Courant Elements on Triangles | 81 |
| B.3.3 | High order ansatz functions in \mathbb{R}^2 | 82 |

Chapter 1

Introduction

In industry acoustic waves are interesting phenomena with important application. Engineers are interested in the reliable simulation of scattering problems. Such problems appear everywhere but its mathematical description or solution is highly untrivial.

Just consider the pipe of an organ. The air stream comes into the pipe through a narrow gap. In the interior this air stream forms a longitudinal wave. The length of the wave and thus the frequency depends on the length of the organ pipe. Large pipes produce low frequency and small pipes high frequency tones.

This problem is an wave eigenvalue problem. The organ pipe whistles if the air stream oscillates with its resonance. So the governing equations (wave) and the type (eigenvalue) of the problem are known. Nevertheless one huge problem remains: the extent of the computational domain.

The pipe is not closed so the computational domain is not only the interior of the pipe but its surroundings. Thus the domain is infinite/unbounded or at least too large for computation.

Reducing an infinite domain to a finite extent might cause troubles if the bounded domain is too small. Then events that should happen inside the domain are outside and neither considered nor computed.

If the bounded domain is too large unnecessary computational work arises.

Assuming an optimal bounded domain, that means it is not too large or too small, the next question arising handles with the boundary conditions. Waves coming through the boundary should not be reflected but absorbed.

With Dirichlet boundary conditions the air pressure at the boundary is fixed. Neumann conditions state that the pressure changes in normal direction as a certain function and Robin conditions fix the exchange of pressure. So no boundary condition is able to absorb waves.

In this thesis two methods that absorb waves are presented. The first is the Perfectly Matched Layer method introduced by Bérenger [5],[6]. The second is the newly developed Wavefactorization.

After terminating the unbounded domain and inclining methods that absorb waves the problem can be numerically solved.

Another example as simple as the organ pipe is a bottle where you blow over its open-

ing. If you blow in a certain direction you create some sound, an eigenfrequency. This is also an unbounded resonance problem.

Here a problem of aeronautics is considered: the box of the landing gear of an aeroplane, see Figure 1.1. The air streaming over this part creates oscillations that express in sound (as a blow over a bottle) or maybe even in destruction of the box, which has fatal consequences for the passenger.



Figure 1.1: The landing gear of an aeroplane

Task of this thesis:

The task of this thesis is to model the acoustic scattering of the landing gear of an aeroplane, to compute dangerous eigenvalues near reality, to find a mathematical strategy to pick out the artificial from the interesting, dangerous eigenvalues and finally to improve the eigenvalue solver so that the artificial eigenvalues are already picked out during computation. This thesis examines two types of approaches of modelling infinite domains. One is the **Perfectly Matched Layer (PML) method**, the other is called **Wavefactorization**. In the end both are combined and tested.

In fact there are four major components involved:

1. The **Finite Element method (FEM)** is used to discretize the eigenvalue problem. For an introduction [4] and [7] is recommended. Appendix B will outline the methods needed here.
2. The **Perfectly Matched Layer (PML)** terminates the infinite domain to a finite one. It can be seen as a sponge layer that totally absorb all waves, independent of their

frequency and direction. The PML method was first introduced by Bérenger [5],[6] in 1994 and is usually used for Maxwell equations. Here it is adapted to acoustic scattering. Promising results have been obtained with **Reduced Integration**.

3. **Wavefactorization** is a method to factorize the wave into two components: the smooth amplitude and a spherical wave. The arising variational formulation depends only on the amplitude and the exponential term vanishes. Wavefactorization also terminates the computational domain. With this method the wave will not decay as in the PML method.
4. The **Arnoldi method** is an eigenvalue solver method, that is recommended for large and sparse matrices. It is an orthogonal projection method onto a Krylov subspace, see [32].

Organization of this thesis:

Chapter 2: Problem Formulation

Deriving the physical model for acoustics results in the Helmholtz eigenvalue problem on an unbounded domain. Although the domain is infinite some "boundary condition" at infinity has to be provided (Sommerfeld condition). Finally the wave equations are presented for the one dimensional case and plane waves are explained.

Chapter 3: Source and Eigenvalue Problems on Bounded and Unbounded Domains

The essential difference between source and eigenvalue problems and eigenvalue problems on bounded and unbounded domains are outlined in this chapter.

Chapter 4: Analytical Solutions of the Helmholtz Problem

With the method of separation of variables exact solutions of several cases of geometry are computed. A major problem in variational form is described as well.

Chapter 5: The Perfectly Matched Layer (PML)

This chapter is an introduction into the use and handling of Perfectly Matched Layers. It is described how to terminate the infinite domain with the help of PML. Three examples where and how to use PML are described. In addition the qualities of complex symmetric matrices are listed.

Chapter 6: Methods of Discretization/Modelling

This is the main part of the thesis. Here the PML method, Wavefactorization and a combination of both is formulated, tested and discussed. In addition a method to distinguish between artificial and interesting eigenvalues is developed.

Chapter 7: Example: Slat Cove of an Aeroplane

A special geometry, that is the wing of an aeroplane, is considered and the eigenvalue problem is computed with the various methods.

Chapter 8: The Eigenvalue Solver

The Arnoldi method is used to get the eigenvalues and -vectors. The algorithm and its advantages are described in this Chapter. For future work some deflation strategies and some special algorithms, like the Jacobi Davidson for complex symmetric matrices and the Block Arnoldi algorithm are recommended.

The conclusion can be found at the end.

Chapter 2

Problem Formulation

In this Chapter the basic relations of linear wave physics are outlined. Acoustic waves and the time-harmonic case are of special interest. We follow the construction of [17].

2.1 Physical Model and Governing Equations

Acoustic waves (sound) are small oscillations of pressure in a compressible ideal fluid (acoustic medium). These oscillations interact in a way that energy is propagated through the medium. The governing equations are obtained from fundamental laws of compressible fluids.

2.1.1 Conservation of Mass

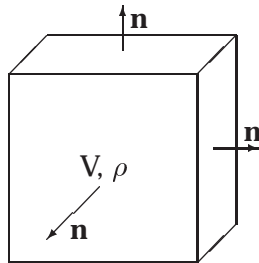


Figure 2.1: A volume element V with definition of normal direction n

The flow of fluid material with the air pressure p , the density ρ and the particle velocity v (vector field) is considered. Let V be a volume element with boundary ∂V and let n ($= n(x)$ with $x \in \partial V$) be the normal unit vector directed into the exterior of V , see Figure 2.1. The conservation of mass in a unit time interval through some volume element V is expressed by the relation

$$-\frac{\partial}{\partial t} \int_V \rho dV = \oint_{\partial V} \rho(vn) dS, \quad (2.1)$$

with (vn) the normal flux through ∂V . Using the Gauss theorem $\oint_{\partial V} (\rho v) n dS = \int_V \text{div}(\rho v) dV$ onto the surface integral, we obtain the equation

$$\int_V \left(\frac{\partial \rho}{\partial t} + \text{div}(\rho v) \right) dV = 0. \quad (2.2)$$

This leads to the *continuity equation* in differential form

$$\frac{\partial \rho}{\partial t} + \text{div}(\rho v) = 0. \quad (2.3)$$

2.1.2 Equation of Motion

Now assume the volume element V is subject to some pressure p . The total force along the boundary of V equals $F = - \oint p n dS$, with n as above. Applying the second Newtonian law leads to

$$\int_V \rho \frac{\partial v}{\partial t} dV = - \oint_{\partial V} p n dS. \quad (2.4)$$

Generally the differential on the left in equation (2.4) should be the total differential $\frac{dv}{dt} := \frac{\partial v}{\partial t} + (v \cdot \nabla)v$. Here small oscillations are assumed and therefore this relation can be linearized as above.

From the Gauss theorem it follows that $- \oint_{\partial V} p n dS = - \int_V \nabla p dV$ and so the *equation of motion* which is also called Euler equation is

$$\rho \frac{\partial v}{\partial t} = -\nabla p. \quad (2.5)$$

Recall that sound is a small perpetuation (p, ρ) of a constant state (p_0, ρ_0) of an compressible, ideal fluid. At any point x the functions p and ρ represent vibrations with a small amplitude. Therefore the velocities are also small (Euler equation). That's why a linear material law $p = c^2 \rho$ with c the speed of sound can be assumed. Derivation of the continuity equation (2.3) by t and then inserting the Euler equation (2.5) gives

$$\frac{\partial^2 p}{\partial t^2} = c^2 \frac{\partial^2 \rho}{\partial t^2} = -c^2 \text{div}(\rho \partial_t v) = c^2 \text{div}(\nabla p) = c^2 \Delta p \quad \Leftrightarrow \quad \frac{\partial^2 p}{\partial t^2} - c^2 \Delta p = 0. \quad (2.6)$$

For the time harmonic case $p(\mathbf{x}, t) = p(\mathbf{x}) \exp(-i\omega t)$ the above equation (2.6) changes to the Helmholtz equation

$$-\Delta p - k^2 p = 0, \quad (2.7)$$

with

$$k = \frac{\omega}{c}, \quad (2.8)$$

the wavenumber. This physical parameter k is of dimension m^{-1} and it counts the number of waves per unit (2π) length. In the one dimensional case the wavelength $\lambda = \frac{2\pi}{k}$ of a wave p is the length where $p(x + \lambda) = p(x)$ for all x .

2.2 The Sommerfeld Condition

Consider wave propagation in free space (unbounded acoustic domain). Sommerfeld postulated that at infinity all waves are outgoing. For the mathematical and physical derivation see [17]. The Sommerfeld condition in spaces with dimension d is

$$u = O(r^{-(d-1)/2}) \text{ for } r \rightarrow \infty, \quad (2.9)$$

$$(\partial_n u - i\omega u) = o(r^{-(d-1)/2}) \text{ for } r \rightarrow \infty, \quad (2.10)$$

$$\text{with } r = |x| = \sqrt{x_1^2 + x_2^2 + \dots + x_d^2},$$

for real ω . Without the o - and O -notation the condition looks like

$$\exists c \in \mathbf{R} : u \leq c(r^{-(d-1)/2}) \text{ for } r \rightarrow \infty, \quad (2.11)$$

$$\lim_{r \rightarrow \infty} \left(\frac{(\partial_n u - i\omega u)}{r^{-(d-1)/2}} \right) = 0. \quad (2.12)$$

Strictly speaking the Sommerfeld condition consists of the two conditions (2.9) and (2.10). But it can be shown (see [31] and also [10], p. 18) that any function u that fulfills (2.10) and the Helmholtz equation (2.7) automatically satisfies (2.9). So condition (2.9) can be neglected. From now on, if it is referred to the Sommerfeld condition, only (2.10) respectively (2.12) is meant.

In 1D the Sommerfeld condition equals

$$\lim_{|x| \rightarrow \infty} (u' - i\omega u) = 0. \quad (2.13)$$

Unlike the higher-dimensional case this condition can be imposed for finite x as a usual mixed boundary condition $\frac{\partial u}{\partial n} = i\omega u$ (Robin condition) that selects the outgoing wave e^{ikx} from the set of solutions $\{e^{ikx}, e^{-ikx}\}$ as will be shown in the following chapter.

Remark:

Sommerfeld holds only for real ω . If ω is complex the Pole condition [28],[29] is recommended.

2.3 Wave Equation and Absorbing Boundary Conditions in 1D

All functions of the form $p(x, t) = f(kx - \omega t)$ are solutions of the one-dimensional wave equation $-p'' - k^2 p = 0$. The value of the function f does not change if $\frac{dx}{dt} = \frac{\omega}{k}$. This expression $v_{phase} = \frac{dx}{dt}$ is called phase velocity of f . The phase velocity v_{phase} of the one-dimensional solution f is equal to the speed of sound c in the acoustic medium and hence depend on material properties only.

Now consider steady-state solutions $p(x, t) = p(x)e^{-i\omega t}$. The stationary part satisfies the Helmholtz equation (2.7) with the general solution $p(x) = ae^{ikx} + be^{-ikx}$ (a and b scalars). The solution is periodic, which means that there exists a wavelength λ of the stationary wave p so that $p(x + \lambda) = p(x)$ for all x with $\lambda = \frac{2\pi}{k}$. The corresponding time-dependent solution is $p(x, t) = ae^{i(kx - \omega t)} + be^{-i(kx + \omega t)}$. Computing the phase velocities v_{phase} it is clearly to

see, that $e^{i(kx-\omega t)}$ is an outgoing wave, traveling from the right boundary to the right with $v_{phase} = \frac{\omega}{k} = c$, whereas $e^{-i(kx+\omega t)}$ is an incoming wave traveling from the right boundary to the left with $v_{phase} = -c$.

If at any point $x = x_0$ the boundary condition $\frac{\partial p}{\partial t} - ikp = 0$ is applied, all incoming waves are eliminated.

The following table gives a short summary.

| | | |
|-----------------------------------|---------------------------------------------|-----------------------------------------------|
| | $p(x, t) = p(x)e^{-i\omega t}$ | |
| solution (time-dep.) | $p_1(x, t) = e^{i(kx-\omega t)}$ | $p_2(x, t) = e^{-i(kx+\omega t)}$ |
| wavedirection | $\frac{dx}{dt} = \frac{\omega}{k} = c$ → | $\frac{dx}{dt} = -\frac{\omega}{k} = -c$ ← |
| | outgoing | incoming |
| non reflecting boundary condition | $\frac{\partial p}{\partial x} - ikp = 0$ | $\frac{\partial p}{\partial x} + ikp = 0$ |

2.4 Plane Waves

Important particular solutions of the Helmholtz equation are the plane waves

$$u(\vec{x}) = e^{i\vec{k}\vec{x}}, \quad (2.14)$$

with $|\vec{k}|$ equal to the wave number k .

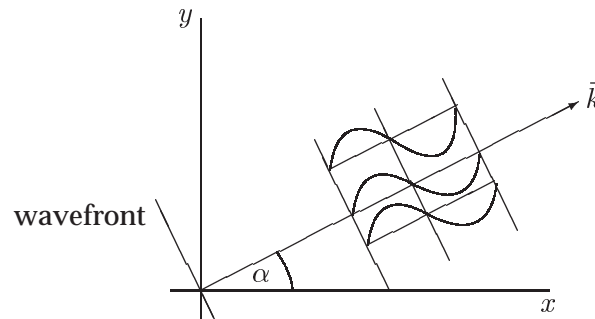


Figure 2.2: Plane wave in 2D

In 2D where $\vec{k} = (k \cos \alpha, k \sin \alpha)$ the plane wave $u(x, y) = \exp(i k(x \cos \alpha + y \sin \alpha))$ describes a wave with wave number k moving in direction α , which is shown in Figure 2.2. The wave front is a plane (a line in 2D) through the point (x, y) with normal $\vec{n} = \vec{k}/k = (\cos \alpha, \sin \alpha)$. Along an axis a in direction \vec{k} , plane waves are one dimensional waves e^{ika} .

A non reflecting boundary condition for a plane wave can be prescribed if its direction \vec{n} is known. Just take the Robin boundary condition

$$\frac{\partial u}{\partial \vec{n}} = i\omega u, \quad (2.15)$$

with a known \vec{n} . This condition absorbs the waves coming from direction \vec{n} . All other waves are reflected. Thus with non reflecting boundary conditions as in (2.15) it is not possible to absorb all waves (except in the one dimensional case).

Therefore absorbing boundary conditions as an alternative to non reflecting conditions have to be prescribed.

Here and in future, ω alone instead of $k = \frac{\omega}{c}$ is taken. It can easily be rescaled to the original problem.

Chapter 3

Source and Eigenvalue Problems on Bounded and Unbounded Domains

This Chapter shows the essential differences between source and eigenvalue problems and between eigenvalue problems on bounded and on unbounded domains.

3.1 Source Problem on Bounded Domain

Assume a bounded domain Ω with boundary $\partial\Omega = \Gamma_D \cup \Gamma_N \cup \Gamma_R$ where the solution u satisfies the Helmholtz equation on Ω with the various boundary conditions, a source f and a given frequency ω . The problem is as follows

$$\text{Find } u \in X : \quad -\Delta u - \omega^2 u = f \quad \text{for } x \in \dot{\Omega}, \quad (3.1)$$

$$u = g_1 \quad \text{for } x \in \Gamma_D, \quad (3.2)$$

$$\partial_n u = g_2 \quad \text{for } x \in \Gamma_N, \quad (3.3)$$

$$\partial_n u + \alpha u = g_3 \quad \text{for } x \in \Gamma_R, \quad (3.4)$$

$$\text{with } X := C^2(\dot{\Omega}) \cap C^1(\dot{\Omega} \cup \Gamma_N \cup \Gamma_R) \cap C^0(\bar{\Omega}). \quad (3.5)$$

The variational form is

$$\begin{aligned} \text{Find } u \in V_g : \quad & \overbrace{\int_{\Omega} \nabla u \nabla v dx - \omega^2 \int_{\Omega} u v dx + \int_{\Gamma_R} \alpha u v dx}^{a_{\omega}(u,v)} = \\ & \underbrace{\int_{\Omega} f v dx + \int_{\Gamma_N} g_2 v dx + \int_{\Gamma_R} g_3 v dx}_{f(v)} \quad \text{for all } v \in V_0 \end{aligned} \quad (3.6)$$

$$V_g = \{v \in H^1(\Omega) : v|_{\Gamma_D} = g_1\}, \quad (3.7)$$

$$V_0 = \{v \in H^1(\Omega) : v|_{\Gamma_D} = 0\}. \quad (3.8)$$

This is a boundary value problem

$$\text{Find } u \in V_g : \quad a_{\omega}(u, v) = f(v) \quad \text{for all } v \in V_0, \quad (3.9)$$

with a bilinearform $a_\omega(u, v)$ and a linearform $f(v)$. Fredholm Theory provides existence, uniqueness and stability of the solution u for given frequencies ω that are no singular values of $a(u, v)$, i.e. for all ω that fulfill $\forall u \neq 0 \exists v : a_\omega(u, v) \neq 0$.

3.2 Bounded Eigenvalue Problem

The domain Ω is bounded and the solution u satisfies the Helmholtz eigenvalue problem on Ω . Let Γ_D denote the Dirichlet boundary, Γ_N the Neumann boundary and Γ_R the Robin boundary with $\partial\Omega = \Gamma = \Gamma_D \cup \Gamma_N \cup \Gamma_R$. Assume homogeneous boundary conditions $u = 0$ on Γ_D , $\partial_n u = 0$ on Γ_N and $\partial_n u + \alpha u = 0$ on Γ_R . The frequency ω is not known. The problem is

$$\text{Find } u \in X, \omega \in \mathbf{C} : \quad -\Delta u - \omega^2 u = 0 \quad \text{for } x \in \overset{\circ}{\Omega}, \quad (3.10)$$

$$u = 0 \quad \text{for } x \in \Gamma_D, \quad (3.11)$$

$$\partial_n u = 0 \quad \text{for } x \in \Gamma_N, \quad (3.12)$$

$$\partial_n u + \alpha u = 0 \quad \text{for } x \in \Gamma_R, \quad (3.13)$$

$$\text{with } X := C^2(\overset{\circ}{\Omega}) \cap C^1(\overset{\circ}{\Omega} \cup \Gamma_N \cup \Gamma_R) \cap C^0(\overline{\Omega}). \quad (3.14)$$

The variational form is

$$\text{Find } u \in V_0, \omega \in \mathbf{C} : \quad \int_{\Omega} \nabla u \nabla v dx + \int_{\Gamma_R} \alpha u v dx = \omega^2 \int_{\Omega} u v dx \quad \text{for all } v \in V_0, \quad (3.15)$$

$$V_0 = \{v \in H^1(\Omega) : v|_{\Gamma_D} = 0\}. \quad (3.16)$$

The eigenvalue is $\lambda = \omega^2$ and the frequency ω is searched for. Unlike as in source problems the boundary conditions should be homogeneous otherwise no eigenvalue problem is obtained. Just take any eigenfunction u fulfilling $Lu = \omega^2 \rho u$ (L the Laplacian operator, $Lu := \Delta u$). This eigenfunction satisfies $L(cu) = cLu = c\omega^2 \rho u = \omega^2 \rho(cu)$ for any constant c only if homogeneous boundary conditions are assumed.

Before investigating the unbounded eigenvalue problem some relations between bounded and unbounded eigenvalue problems are listed.

Consider a bounded square domain as in Figure 3.1 on the left. If the bounded domain

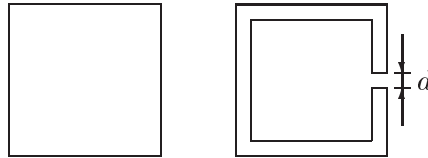


Figure 3.1: Bounded (left) and unbounded (right) domain

is slightly changed, e.g. cut in at one edge then it is not bounded any more, see right picture in Figure 3.1. The computational domain is not a square any more but the whole domain except the border area.

Assume a hole of small diameter d as in Figure 3.1. The eigenfunctions and -values of the unbounded problem should intuitively converge to those of the bounded problem if the diameter d goes to zero.

Bounded eigenvalue problem have a discrete spectrum, whereas the unbounded problem has continuous eigenvalues (a continuous spectrum).

Computing the eigenvalues and -functions of the unbounded problem involves a lot of problems. First the computational domain has to be terminated to finite extent. Then absorbing boundary conditions have to be prescribed. Finally the solution should be a good approximation of the infinite case.

3.3 Unbounded Eigenvalue Problem

An eigenvalue problem with the Sommerfeld condition as a "boundary" condition has to be solved. An eigenpair $(\omega \in \mathbf{C}, u \in C^2(\Omega))$ is searched so that the following equations hold in an unbounded (or at least semi-unbounded) domain $\Omega \in \mathbf{R}^d$.

$$\begin{aligned} -\Delta u - \omega^2 u &= 0 \text{ for } x \in \Omega, \\ \lim_{|x| \rightarrow \infty} \left(|x|^{(d-1)/2} (\partial_n u - i\omega u) \right) &= 0, \end{aligned} \quad (3.17)$$

with u the air pressure and ω acoustic resonances.

In the variational setting of problem (3.17), a solution pair (ω, u) with $\omega \in \mathbf{C}$ and u in the Sobolev space $H_{loc}^1(\Omega)$ with Ω as above is searched for, which fulfills

$$\begin{aligned} \int_{\Omega} \nabla u \nabla v dx - \int_{\partial\Omega} \frac{\partial u}{\partial n} v ds_x &= \omega^2 \int_{\Omega} u v dx \text{ for all } v \in V_c, \\ \lim_{|x| \rightarrow \infty} \left(|x|^{(d-1)/2} (\partial_n u - i\omega u) \right) &= 0, \end{aligned} \quad (3.18)$$

with the test spave $V_c = \{v \in H^1(\Omega) : \text{supp}(v) \text{ compact}\}$. The term *loc* on the above Sobolev space means that if u is in $H_{loc}^1(\Omega)$ with Ω an unbounded domain, then u restricted to Ω_F is a local member of $H^1(\Omega_F)$ with Ω_F any compact subdomain of Ω .

Since Ω is infinite the boundary $\partial\Omega$ in the variational form (3.18) does not exist but is needed for the exact mathematical formulation. Soon Ω will be terminated with the PML or the wavefactorization. So problem (3.18) is not the final model, but an intermediate result (for comparison) where the Sommerfeld condition is not yet inclined into the variational equation.

Instead of the Sommerfeld condition at infinity it is sometimes useful to incline a non continuous material parameter ρ into the Helmholtz equation. For better understanding a one dimensional example:

3.3.1 The Oscillating String

The bounded string eigenvalue problem on $\Omega = [x_0, x_1]$ with $x_0 = 1/3$ and $x_1 = 2/3$ reads as:

$$\text{Find } u \in C^2[x_0, x_1], \omega \in \mathbf{R} : \quad u''(x) + \omega^2 u(x) = 0 \text{ in } [x_0, x_1], \quad (3.19)$$

$$u(x_0) = 0 = u(x_1). \quad (3.20)$$

It is easy to verify that the solution pair (u, ω) is $u(x) = c \sin(\omega x)$ and $\omega = 3n\pi, n = 1, 2, \dots$ with c any constant value. Four solutions u with $c = 1$ are shown in Figure 3.2.

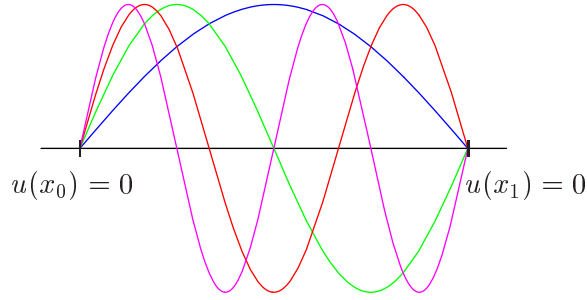


Figure 3.2: Solutions u with $n = 1, 2, 3, 4$ of the bounded eigenvalue problem

Now take the unbounded string eigenvalue problem with $\rho = \rho_0$ in the interior $[x_0, x_1]$ and $\rho = \rho_1$ elsewhere. The interface points x_0, x_1 are the same as above. The unbounded string eigenvalue problem is:

$$\text{Find } u \in X, \omega \in \mathbf{R} : \quad u''(x) + \omega^2 \rho_0 u(x) = 0 \text{ in } (x_0, x_1), \quad (3.21)$$

$$\frac{\partial u}{\partial n} = i\omega \sqrt{\rho_1} u \quad \text{at } x = 0, 1, \quad (3.22)$$

$$u(x_{0-}) = u(x_{0+}) \quad \text{and} \quad u(x_{1-}) = u(x_{1+}), \quad (3.23)$$

$$\partial_n u(x_{0-}) = \partial_n u(x_{0+}) \quad \text{and} \quad \partial_n u(x_{1-}) = \partial_n u(x_{1+}), \quad (3.24)$$

$$\text{with } X = C^2(x_0, x_1) \cap C^1[0, 1] \cap C[0, 1]. \quad (3.25)$$

Condition (3.22) is the Sommerfeld condition. If it is fulfilled at the boundary $x = 0$ and at $x = 1$ then it is fulfilled at the exterior $[0, x_0)$ and $(x_1, 1]$. The final analytical solution pair (u, ω) is

$$u(x) = c \begin{cases} -i(c_0 \sin(\omega \sqrt{\rho_0}/3) + \cos(\omega \sqrt{\rho_0}/3)) \exp(i\omega \sqrt{\rho_1}(1/3 - x)) & x \in [0, x_0) \\ (-i)c_0 \sin(\omega \sqrt{\rho_0}x) - i \cos(\omega \sqrt{\rho_0}x) & x \in [x_0, x_1] \\ -i(c_0 \sin(2\omega \sqrt{\rho_0}/3) + \cos(2\omega \sqrt{\rho_0}/3)) \exp(i\omega \sqrt{\rho_1}(x - 2/3)) & x \in (x_1, 1] \end{cases} \quad (3.26)$$

$$\text{with } c_0 = \frac{\sin(\omega \sqrt{\rho_0}/3) - i \sqrt{\frac{\rho_1}{\rho_0}} \cos(\omega \sqrt{\rho_0}/3)}{i \sqrt{\frac{\rho_1}{\rho_0}} \sin(\omega \sqrt{\rho_0}/3) + \cos(\omega \sqrt{\rho_0}/3)}$$

$$\text{and } \omega = \frac{3n\pi}{\sqrt{\rho_0}} - 2\pi i, \quad (3.27)$$

with c any real constant value and $n = 1, 2, \dots$

The solution obtained with $\rho_0 = 0.1$ and $\rho_1 = 1$ is shown in Figure 3.3. This solution oscil-

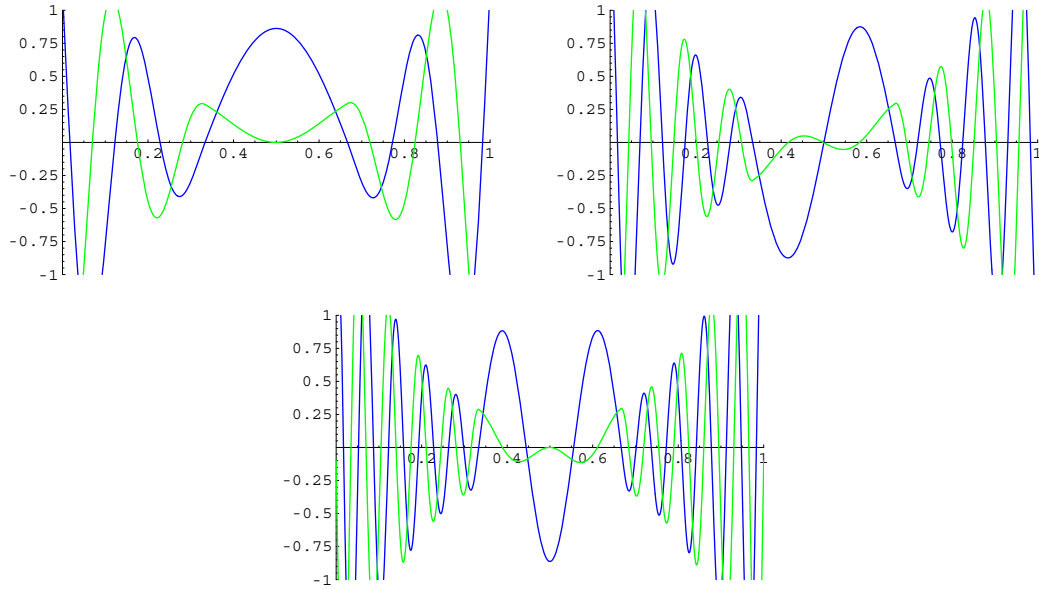


Figure 3.3: Solution $Re(u)$ and $Im(u)$ with $n = 1$ (left top), $n = 2$ (right top) and $n = 3$ (bottom) of the unbounded eigenvalue problem with $\rho_0 = 0.1$ and $\rho_1 = 1$

lates regularly until plus or minus infinity, which is the essential difference to the bounded problem. The eigenfunctions oscillate the more the farther from the origin. In the interior $[x_0, x_1]$ this solution is approximately the analytical solutions $\sin(3n\pi x)$, $n = 1, 2, 3$.

Thus inserting a non continuous material parameter ρ avoids the use of absorbing boundary conditions for analytical computation. All solutions converge to the solution of the bounded string problem in the interior $[x_0, x_1]$. The solutions in the exterior $(0, x_0)$ and $(x_1, 1)$ oscillate until infinity, which makes a lot of troubles. Just think of computing the solution numerically. No boundary condition fits in a way to terminate the domain.

Chapter 4

Analytical Solutions of the Helmholtz Problem

The aim of this Chapter is to analyse the behaviour of the solutions of the unbounded Helmholtz problem. We are especially interested in the solution behaviour in the exterior region where the Finite Element solution must be modeled.

At the end of this Chapter the problems of the variational formulation of the exterior Helmholtz model are described.

On simple domains, solutions of partial differential problem can be found by separation of variables.

4.1 Separation of Variables

This technique is illustrated on Helmholtz problems in cartesian, spherical and cylindrical coordinates.

4.1.1 Cartesian Coordinates

The usual Helmholtz equation $\Delta u + \omega^2 u = 0$ in \mathbf{R}^3 is considered. Inserting the Ansatz $u(x, y, z) = X(x)Y(y)Z(z)$ into the Helmholtz equation gives

$$X''YZ + XY''Z + XYZ'' + \omega^2 XYZ = 0, \quad (4.1)$$

which is the same as

$$-\frac{X''}{X} = \frac{Y''}{Y} + \frac{Z''}{Z} + \omega^2. \quad (4.2)$$

The term on the left is independent of y and z and the term on the right is independent of x . Therefore the equality can only hold if both sides are equal to a constant ν .

$$-\frac{X''}{X} = \nu = \frac{Y''}{Y} + \frac{Z''}{Z} + \omega^2. \quad (4.3)$$

Repeating the above argument for the second part, the functions X, Y and Z have to satisfy

$$X'' + \nu X = 0, \quad (4.4)$$

$$Y'' + \mu Y = 0, \quad (4.5)$$

$$Z'' + (\omega^2 - \nu - \mu)Z = 0, \quad (4.6)$$

for independent constants ν and $\mu \in \mathbf{C}$. Since only propagating waves are interesting, only positive values $\nu = \alpha^2$ and $\mu = \beta^2$ have to be considered. The equations can be rewritten as

$$X'' + \alpha^2 X = 0, \quad (4.7)$$

$$Y'' + \beta^2 Y = 0, \quad (4.8)$$

$$Z'' + \gamma^2 Z = 0 \quad \text{with } \gamma^2 = \omega^2 - \alpha^2 - \beta^2, \quad (4.9)$$

with solutions $X(x) = \exp(\pm i\alpha x)$, $Y(y) = \exp(\pm i\beta y)$ and $Z(z) = \exp(\pm i\gamma z)$ Now the solution u has to be of the form

$$u(x, y, z) = ce^{i(\pm\alpha x \pm \beta y \pm \gamma z)}, \quad (4.10)$$

with the only restriction that $\omega^2 = \alpha^2 + \beta^2 + \gamma^2$, but this does not matter since for the eigenvalue problem ω^2 is also searched for. Here only *plane* waves (see Section 2.4) are considered

$$u(x, y, z) = e^{i(\alpha x + \beta y + \gamma z)}. \quad (4.11)$$

If either α, β or γ is complex and the other constants real, the solution decays in either x, y or z -direction. Such solutions are called *evanescent* waves.

Finally u has the following form depending of the eigenvalue ω

$$u(x, y, z) = e^{i(\alpha x + \beta y + \sqrt{\omega^2 - \alpha^2 - \beta^2} z)}, \quad (4.12)$$

with α and $\beta \in \mathbf{C}$.

4.1.2 Spherical Coordinates

The Neumann problem in the exterior of a sphere with radius a is considered.

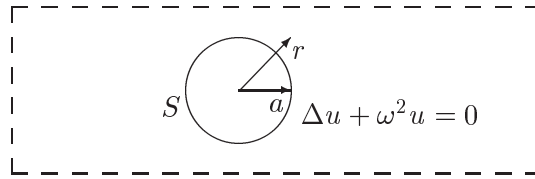


Figure 4.1: Exterior Neumann problem with sphere S of radius a in 2D

It is searched for a function $u(r, \phi, \theta)$ and for an eigenvalue $\omega \in \mathbf{C}$ that hold:

$$\Delta u + \omega^2 u = 0 \quad \text{for } r > a, \quad (4.13)$$

$$\frac{\partial u}{\partial r} = c \quad \text{for } r = a, \quad (4.14)$$

$$\frac{\partial u}{\partial r} - i\omega u = o\left(\frac{1}{r}\right) \quad \text{for } r \rightarrow \infty, \quad (4.15)$$

with some constant c and $r^2 = x^2 + y^2 + z^2$, $\phi = \arctan \frac{y}{x}$ and $\theta = \arctan \frac{\sqrt{x^2+y^2}}{z}$ the spherical coordinates. Solutions of the exterior Helmholtz problem that satisfy the Sommerfeld condition are called *radiating* solutions.

The Laplacian operator in spherical coordinates has the form

$$\Delta u(r, \phi, \theta) = \frac{1}{r^2} \left\{ \frac{\partial}{\partial r} \left(r^2 \frac{\partial u}{\partial r} \right) + \frac{1}{\sin \theta} \frac{\partial}{\partial \theta} \left(\sin \theta \frac{\partial u}{\partial \theta} \right) + \frac{1}{\sin^2 \theta} \frac{\partial^2 u}{\partial \phi^2} \right\} \quad (4.16)$$

Again separation of variables $u(r, \phi, \theta) = R(r)\Phi(\phi)\Theta(\theta)$ is applied and

$$0 = 2r \frac{R'}{R} + r^2 \frac{R''}{R} + \frac{1}{\Theta} \left(\frac{1}{\sin(\theta)} \frac{\partial}{\partial \theta} (\sin(\theta)\Theta') \right) + \frac{1}{\sin^2 \theta} \frac{\Phi''}{\Phi} + r^2 \omega^2, \quad (4.17)$$

is the result. With the same argument as in the cartesian case, the following system of separated ordinary differential equation is obtained

$$0 = r^2 R'' + 2r R' + R(r^2 \omega^2 + \nu), \quad (4.18)$$

$$0 = \sin(\theta) \frac{\partial}{\partial \theta} (\sin(\theta)\Theta') - (\nu \sin^2 \theta + \mu)\Theta, \quad (4.19)$$

$$0 = \Phi'' + \mu\Phi, \quad (4.20)$$

with ν and μ constants. The function $R(r)$ is defined on $r > a$, whereas $\Phi(\phi)$ and $\Theta(\theta)$ are defined on $[0, 2\pi]$ respectively on $[-\pi, \pi]$. Furthermore R satisfies the Sommerfeld condition. Since the sphere S is a closed surface, the function $\Phi(\phi)$ is periodic, that is $\Phi(0) = \Phi(2\pi)$. Therefore equation (4.20) has the solutions $\sin m\phi$ and $\cos m\phi$ with $\mu = m^2$, $m = 0, 1, 2, \dots$. To solve equation (4.19) it is divided by $\sin^2 \theta = 1 - \cos^2 \theta$ and then transformed with $t := \cos \theta$ to

$$0 = (1 - t^2) \frac{\partial^2 \Theta}{\partial t^2} - 2t \frac{\partial \Theta}{\partial t} + \left(\nu - \frac{\overbrace{\mu}^{m^2}}{1 - t^2} \right) \Theta. \quad (4.21)$$

For $\nu = n(n+1)$, $n = 0, 1, \dots$ this is a Legendre's equation. Its solutions are the so-called *Legendre functions* P_n^m that are defined with the Legendre polynomials P_n

$$\Theta_{mn}(\theta) = P_n^m(\cos \theta) \quad \text{for } 0 \leq m \leq n, \quad (4.22)$$

$$P_n^m(t) := (1 - t^2)^{m/2} \frac{\partial^m P_n(t)}{\partial t^m}, \quad (4.23)$$

and these *Legendre polynomials* P_n are defined by the following recurrence relation

$$\begin{aligned} P_0(t) &= 1, \\ P_1(t) &= t, \\ P_{n+1}(t) &= \frac{2n+1}{n+1} t P_n(t) - \frac{n}{n+1} P_{n-1}(t). \end{aligned} \quad (4.24)$$

At last equation (4.18) is a Bessel's differential equation for $\nu = n(n+1)$, $n = 0, 1, \dots$. For

each n it has the independent solutions

$$h_n^1(\omega r) = \frac{1}{i^{n+1}} \frac{e^{i\omega r}}{\omega r} \sum_{j=0}^n (-2i\omega r)^{-j} \frac{(n+j)!}{j!(n-j)!}, \quad (4.25)$$

$$h_n^2(\omega r) = i^{n+1} \frac{e^{-i\omega r}}{\omega r} \sum_{j=0}^n (2i\omega r)^{-j} \frac{(n+j)!}{j!(n-j)!}, \quad (4.26)$$

that are called the *spherical Hankel* functions, see [20]. In the far field, where r is large, the Hankel functions depend on the r as $h_n^1(\omega r) \approx \frac{e^{ir}}{r}$ respectively $h_n^2(\omega r) \approx \frac{e^{-ir}}{r}$ and thus the Hankel functions of the second kind represent the incoming waves, which are eliminated by the Sommerfeld condition. So only the Hankel functions of the first kind are taken. To summarize the results u now looks the following

$$u(r, \phi, \theta) = \sum_{n=0}^{\infty} \sum_{m=0}^n h_n^1(\omega r) P_n^m(\cos \theta) (A_{nm} \cos m\phi + B_{nm} \sin m\phi), \quad (4.27)$$

dependent on the eigenvalue ω . The series (4.27) converges absolutely and uniformly in every closed and bounded domain that is contained in $|\vec{x}| > a$, if u is a radiation solution of the Helmholtz equation in the domain exterior to the spherical surface $|\vec{x}| = a$.

This can be written more compactly by use of the de Moivre identity $(\cos \phi + i \sin \phi)^n = \cos n\phi + i \sin n\phi$

$$u(r, \phi, \theta) = \sum_{n=0}^{\infty} h_n^1(\omega r) \sum_{m=-n}^n c_{mn} y_{mn}(\theta, \phi), \quad (4.28)$$

with c_{mn} complex coefficients and the *spherical harmonics* y_{mn}

$$y_{mn}(\theta, \phi) = P_n^{|m|}(\cos \theta) e^{im\phi} \quad \text{with } -n \leq m \leq n. \quad (4.29)$$

These spherical harmonics are the eigenfunctions of the Laplace operator Δ for constant r . The harmonics y_{0n} are not dependent of ϕ and represent the axisymmetric modes (axisymmetric in regard to the z -axis).

The spherical harmonics have three special properties:

1. For each n there are $2n+1$ linearly independent spherical harmonics y_{mn} , $m = -n, \dots, n$.
2. The spherical harmonics are orthogonal with respect to the inner L_2 product over the surface S of the unit sphere, i.e. $(u, v)_{L_2} = \int_S u \bar{v} dS$. They can be orthonormalized.
3. Each function $f(\theta, \phi) \in L_2$ can be expanded into a series of spherical harmonics

$$f(\phi, \theta) = \sum_{n=0}^{\infty} \sum_{m=-n}^n f_{mn} y_{mn}(\phi, \theta), \quad (4.30)$$

with coefficients $f_{mn} = \int_0^{2\pi} \int_{-\pi}^{\pi} f(\phi', \theta') \overline{y_{mn}}(\phi', \theta') d\theta d\phi$.

The properties 2. and 3. can be used to determine the unknown coefficients c_{mn} from the boundary condition 4.14. Just expand c into such a series as in 3. and compare left side with the right side (after derivation).

4.1.3 Cylindrical Coordinates

Problems of scattering from infinite cylinder can be reduced to two-dimensional scattering from a "circle". Then radiating solutions of the Helmholtz equation in polar coordinates $r^2 = x^2 + y^2$ and $\phi = \arctan \frac{y}{x}$ are looked for. The Laplacian operator in polar [cylindrical] coordinates is

$$\Delta u = \frac{1}{r} \frac{\partial}{\partial r} \left(r \frac{\partial u}{\partial r} \right) + \frac{1}{r^2} \frac{\partial^2 u}{\partial \phi^2} \left[+ \frac{\partial^2 u}{\partial z^2} \right]. \quad (4.31)$$

Separation of variables for the cylindrical case leads to the following two equations

$$rR' + r^2 R'' + (\omega^2 r^2 - \nu)R = 0, \quad (4.32)$$

$$\Phi'' + \nu \Phi = 0. \quad (4.33)$$

The first of these two is a Bessel differential equation, if $\nu = n^2$ and its solution is the Bessel function of third kind, also called *Hankel function of first kind*, see [20]. These functions are defined the following way

$$H_n^1(z) := J_n(z) + iY_n(z), \quad (4.34)$$

with J_n the cylindrical Bessel functions of the first kind and Y_n those of the second kind. Both kind of Bessel functions in comparison to either the real or the imaginary part of e^{iz}/z are shown in Figure 4.2.

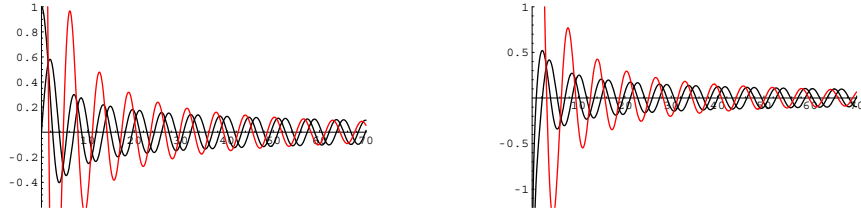


Figure 4.2: The Bessel functions $J_n(z)$, $n = 0, 1$ compared with $\text{Re}(\exp(iz)/z)$ (left picture) and $Y_n(z)$, $n = 0, 1$ compared with $\text{Im}(\exp(iz)/z)$ (right picture)

The solution of the second equation is the same as with spherical coordinates, therefore the whole solution is

$$u(r, \phi) = \sum_{n=0}^{\infty} H_n^1(\omega r) (A_n \cos n\phi + B_n \sin n\phi). \quad (4.35)$$

Since $H_n^1 = H_{-n}^1$ for all $n = 1, 2, \dots$ the solution u can be written as

$$u(r, \phi) = \sum_{n=-\infty}^{\infty} u_n H_n^1(\omega r) e^{in\phi}, \quad (4.36)$$

with u dependent from ω and u_n unknown coefficients. For inserting the Neumann boundary condition $\partial_r u = c$ at $r = a$, the same procedure as before applies, but the spherical harmonics are replaced by Fourier expansion around a unit circle. Hence

$$u_n = \frac{1}{2\pi} \int_0^{2\pi} u(\phi) e^{-in\phi} d\phi, \quad (4.37)$$

and comparison will give u_n dependent from ω .

More about new methods (with Laplace transformation and Pole condition instead of Sommerfeld condition) to get analytical and numerical solutions is described in [28],[29],[30] and [23].

4.2 Problems in Variational Formulation

The variational formulation of the exterior Helmholtz problem is more complicated, especially the choice of the test and trial spaces. This is because it is integrated over an unbounded, infinite domain Ω_∞ . From the analysis before it is expected that the solution u depends asymptotically on r as

$$u \approx \frac{e^{i\omega r}}{r}. \quad (4.38)$$

The L_2 product

$$\left(\frac{e^{i\omega r}}{r}, \frac{e^{i\omega r}}{r} \right)_{L_2} = \int_{\Omega_\infty} \frac{e^{i\omega r}}{r} \frac{e^{-i\omega r}}{r} dV = 4\pi \int_a^\infty \frac{1}{r^2} r^2 dr = \infty, \quad (4.39)$$

is not finite (with a the radius, where the exterior Ω_∞ begins). Thus the solution u is not in L_2 or any other Sobolev space and the trial space must not be L_2 . One way out of this dilemma is to work with weighted products that terminate these integrals. The other is to find methods that terminate the domain Ω_∞ .

Here the latter approach is pursued.

Chapter 5

The Perfectly Matched Layer

The Perfectly Matched Layer (PML) was first introduced by Jean Pierre Bérenger in 1994 (see [5], improvements in [6]). He showed how to modify a Maxwell system to provide a perfectly matched absorbing layer for an electromagnetic scattering problem. His approach constructs an absorbing half-space such that any waves from the standard Maxwell medium are not reflected independent of their frequency and direction of propagation. In the PML, the wave is absorbed and decays exponentially with distance into the layer. The perfectly matched layer can be seen as a sponge layer to terminate Finite Element approximations of scattering problems.

There are two methods to construct the PML: One is the classical approach of Bérenger (see [5]) and the other is complex variable transformation described in [9]. For optimization see [8]. For more information about PML, see [12], [14], [13] and for analysis see [1], [3]. Applications of PML in aeronautics are described in [18] and [24].

Here, the PML absorbing boundary conditions are derived for the 1D Helmholtz case by a complex change of variables. Furthermore the same is done in variational form for the two or three dimensional case.

5.1 Sketch of the PML Method in 1D

Consider the one-dimensional Helmholtz equation on the semi-infinite interval $[-1, \infty)$:

$$-\partial_{xx}u - \omega^2 u = 0 \quad x \in [-1, \infty), \quad (5.1)$$

$$u(-1) = 0, \quad (5.2)$$

$$\partial_n u = i\omega u \text{ for } x \rightarrow \infty, \quad (5.3)$$

The "boundary" condition at infinity is the Sommerfeld condition (5.3), which states that all waves are outgoing. See Chapter 2.2 for more.

The aim is to restrict the Helmholtz equation (5.1) to the interval $[-1, 0]$. Thus the exterior is $(0, \infty)$. The idea of the PML-method is to bend the wave into the complex domain. This is done by complex coordinate transformation $x \rightarrow \bar{x} = \gamma(x)$ on the exterior.

For example γ is defined as follows: $\gamma(x) := (1 + i\alpha)x$ in the exterior $(0, \infty)$ and $\gamma(x) := x$ in the interior $[-1, 0]$. Since $\gamma(0) = 0$ and $\gamma'(0) = (1 + i\alpha)$ the solution of the transformed equation $\tilde{u}_{PML}(x) := u(\gamma(x))$ coincides with u at 0. Assuming that ω is constant, the solution

of the Helmholtz equation (5.1) can be extended analytically to the complex plane, since the normal derivative at 0 is $\partial_n u(0)(1 + i\alpha) = \partial_n \tilde{u}_{PML}(0)$ and the solution \tilde{u}_{PML} is given by

$$-\partial_{xx}\tilde{u}_{PML} - (1 + i\alpha)^2\omega^2\tilde{u}_{PML} = 0, \quad (5.4)$$

$$\tilde{u}_{PML}(0) = u(0), \quad (5.5)$$

$$\partial_n \tilde{u}_{PML}(0) = \partial_n u(0)(1 + i\alpha), \quad (5.6)$$

$$\partial_n \tilde{u}_{PML} = i\omega(1 + i\alpha)\tilde{u}_{PML}. \quad (5.7)$$

Equation (5.5) and (5.6) are interface conditions to get continuous solutions.

There are two fundamental solutions of the partial differential equation 5.4:

1. $x \mapsto \exp(i\omega(1 + i\alpha)x)$, decreasing and
2. $x \mapsto \exp(-i\omega(1 + i\alpha)x)$, increasing.

Only the first obeys the radiation condition $\partial_n u = i\omega(1 + i\alpha)u$ and is exponentially decreasing, so at infinity this solution is 0. Replacing condition (5.7) by $u_{PML}(\delta) = 0$ leads to the following equations

$$-\partial_{xx}u_{PML} - (1 + i\alpha)\omega^2u_{PML} = 0, \quad (5.8)$$

$$u_{PML}(0) = u(0), \quad (5.9)$$

$$\partial_n u_{PML}(0) = \partial_n u(0)(1 + i\alpha), \quad (5.10)$$

$$u_{PML}(\delta) = 0. \quad (5.11)$$

The error by replacing \tilde{u}_{PML} with u_{PML} decreases exponentially with the thickness δ of the PML. The final solution u should fulfill equation (5.1) on the interior, equation (5.8) on

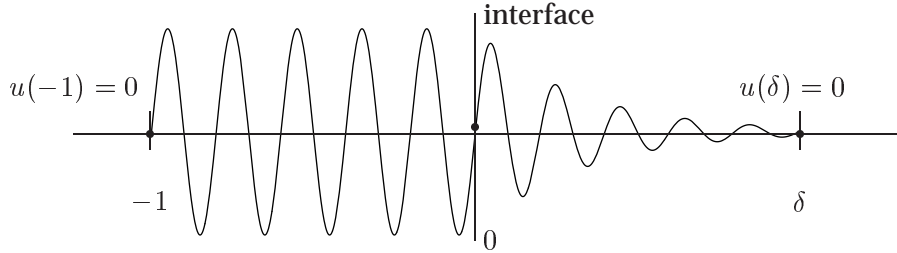


Figure 5.1: Model of the behavior of the final solution

the exterior, the interface conditions (5.5) and (5.6), and the boundary conditions (5.2) and (5.11), as can be seen in Figure 5.1.

In the PML the oscillations decays very fast (exponentially). So the PML need not to be very thick.

All steps above can be done similar in the weak formulation, see the next Section.

The variable transformation is easy to perform and gives the same result as the originally

proposed way. In the two- or three-dimensional case the coordinate transformation can be applied on rectilinear or curvilinear coordinates, see Figure 5.2. Here all numerical examples use curvilinear coordinates.

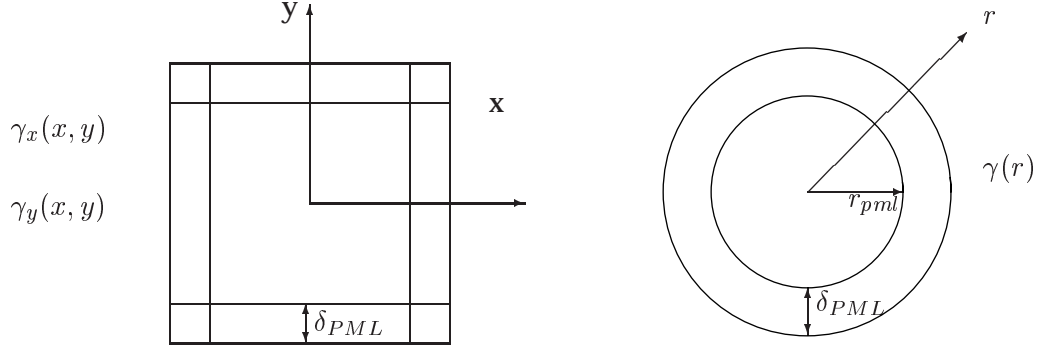


Figure 5.2: Rectilinear and curvilinear coordinates with PML of thickness δ_{PML}

Here the following formula for γ (curvilinear) with the PML parameter α is used.

$$\gamma(\vec{x}) = \begin{cases} \vec{x}(1 + i\alpha) - i\alpha r_{pml} \frac{\vec{x}}{|\vec{x}|} & \text{in the PML,} \\ \vec{x} & \text{else.} \end{cases} \quad (5.12)$$

In curvilinear coordinates the radius from the origin to the PML is called r_{pml} . In rectilinear this reads as

$$\gamma(\vec{x}) = \begin{cases} \vec{x}(1 + i\alpha) - i\alpha \begin{pmatrix} x_{pml} \frac{x}{\max\{|x|, |y|\}} \\ y_{pml} \frac{y}{\max\{|x|, |y|\}} \end{pmatrix} & \text{in the PML,} \\ \vec{x} & \text{else,} \end{cases} \quad (5.13)$$

with $\vec{x} = (x, y)$ and x_{pml} the length from the boundary to the PML in x -direction and y_{pml} the length from the boundary to the PML in y -direction. The function γ can easily be extended to the \mathbb{R}^3 .

Remark:

If low frequencies ω are of interest it is preferred to work with a large PML parameter α . A small α gives better results for high frequencies.

Bérenger's PML formulation is equivalent to complex variable transformation, which can be interpreted as an analytic continuation of the governing equations into the complex domain. Therefore this formulation can easily be implemented into existing finite element codes. For all examples the high order finite element code NGSolve and its mesh generator NETGEN of Joachim Schöberl [25] is used.

If PML is applied on symmetric bilinearforms, the resulting matrices become complex symmetric after FEM-discretization. This property has no advantages except memory saving as can be seen in Chapter 5.4.

5.2 Variational Derivation

Here the PML method is derived for the variational formulation in general and afterwards tested on examples in the one and two dimensional case.

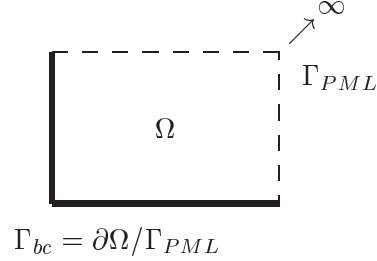


Figure 5.3: A semi-infinite domain $\Omega \subset \mathbf{R}^2, \mathbf{R}^3$ analogous

Consider a semi-infinite domain Ω as seen in Figure 5.3 (it need not be rectangular, just any (semi-)infinite domain can be taken). The initial Problem (3.17) is an eigenvalue problem on Ω with the Sommerfeld condition at infinity and a usual boundary condition at $\Gamma_{bc} = \partial\Omega/\Gamma_{PML}$.

$$-\Delta u(x) - \omega^2 u(x) = 0 \text{ for } x \in \Omega, \quad (5.14)$$

$$|x|^{(d-1)/2} (\partial_n u(x) - i\omega u) \longrightarrow 0 \text{ for } |x| \rightarrow \infty, \quad (5.15)$$

$$\text{homogeneous Dirichlet-, Neumann- or Robin-b.c. at } \Gamma_{bc} = \partial\Omega/\Gamma_{PML}, \quad (5.16)$$

with ω the acoustic resonance. Multiplication with a test function v , integration over Ω and integration by parts gives

$$\text{Find } u \in H_{loc}^1(\Omega) : \int_{\Omega} \nabla u \nabla v - \int_{\Gamma} \frac{\partial u}{\partial n} v = \omega^2 \int_{\Omega} uv \text{ for } v \in V_c(\Omega), \quad (5.17)$$

$$V_c(\Omega) = \{v \in H^1(\Omega) : \text{supp}(v) \text{ compact}\}. \quad (5.18)$$

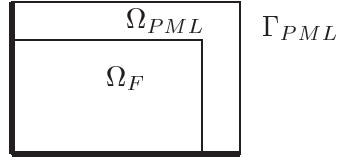
Here the Neumann or Robin-boundary condition on Γ_{bc} can be inserted. The homogeneous Neumann boundary condition $\frac{\partial u}{\partial n} = 0$ on $\Gamma_{bc} = \Gamma_N = \partial\Omega/\Gamma_{PML}$ is taken, since it means that at Γ_N there is no change of air pressure u in normal direction. To eliminate the boundary integral on Γ_{PML} the test functions v are members of the space $V_0 = \{v \in H_{loc}^1(\Omega) : v = 0 \text{ on } \Gamma_{PML}\}$. This leads to the following problem:

$$\text{Find } u \in V = H_{loc}^1(\Omega), \omega \in \mathbf{C} : \int_{\Omega} \nabla u \nabla v = \omega^2 \int_{\Omega} uv \text{ for } v \in V_0, \quad (5.19)$$

$$|x|^{(d-1)/2} (\partial_n u(x) - i\omega u) \longrightarrow 0 \text{ for } |x| \rightarrow \infty. \quad (5.20)$$

Still the Sommerfeld condition is not yet inclined into (5.19). For this PML is used. The semi-infinite Domain Ω is terminated to a finite domain Ω_F and the sponge layer Ω_{PML} as seen in Figure 5.4.

To get to the PML formulation variable transformation ($u(x) \rightarrow u(\gamma(x)), \nabla u \rightarrow J^{-t} \nabla u$, with J the Jacobi-Matrix of γ) is applied.



$$\Gamma_N = \partial\Omega/\Gamma_{PML}$$

Figure 5.4: The finite domain Ω_F and its PML Ω_{PML}

If a rectangular domain in \mathbb{R}^2 as in Figure 5.4 is considered then γ as in (5.13) is taken. The measures x_{pml} and y_{pml} are the lengths from the boundary Γ_N to the PML (to Ω_{PML} and not to Γ_{PML}) in x - and y -direction.

Otherwise curvilinear coordinates with a γ as in (5.12) are the choice.

In the Perfectly Matched Layer u decreases exponentially, so at the boundary Γ_{PML} the solution u should be very small. Therefore a Dirichlet boundary $u = 0$ on Γ_{PML} can be used without getting high errors.

Finally (after variable transformation and termination of the infinite domain Ω) $u \in V_0$ and $\omega \in \mathbb{C}$ are searched so that

$$\int_{\Omega} \nabla u J^{-1} J^{-t} \nabla v \det(J) = \omega^2 \int_{\Omega} uv \det(J) \text{ for } v \in V_0, \quad (5.21)$$

holds with

$$V_0 = \{u \in H^1(\Omega) : u = 0 \text{ on } \Gamma_{PML}\}. \quad (5.22)$$

This problem is a general eigenvalue problem with $\lambda = \omega^2$ the eigenvalue and u the eigenfunctions. In short it can be written as

Find $u \in V_0, \lambda \in \mathbb{C}$:

$$a(u, v) = \lambda b(u, v) \quad \text{for } v \in V_0, \quad (5.23)$$

with $a(u, v) = \int_{\Omega} \nabla u J^{-1} J^{-t} \nabla v \det(J)$ and $b(u, v) = \int_{\Omega} uv \det(J)$ bilinearforms, $\lambda = \omega^2$ and V_0 as above.

Discretization with the Finite Element Method gives a generalized Eigenvalues Problem $Au = \lambda Bu$ where the matrices A, B are complex symmetric but not hermite. Complex symmetric matrices have the single advantage that right eigenvectors are also left eigenvectors. They may not even be diagonalizable, so complex symmetry is a purely algebraic property (see Chapter 5.4).

5.3 Examples

This Chapter presents three examples where and how to use PML. The first is analogous to the String eigenvalue problem from Section 3.3, but PML is applied. The second is a similar one dimensional problem with the difference that the PML and the domain where the material parameter is not one, have distinct intervals. Finally a two dimensional eigenvalue problem is computed.

5.3.1 The Oscillating String Problem with PML

Take the unbounded string problem as in Section 3.3 and apply the PML method. Notice that the Dirichlet boundary condition is not yet inclined. The interface points are $x_0 = 1/3$ and $x_1 = 2/3$. The computational domain is the interval $[0, 1]$.

$$\text{Find } u \in X, \omega \in \mathbf{R} : \quad u''(x) + \rho\omega^2 u(x) = 0 \quad \text{in } (x_0, x_1), \quad (5.24)$$

$$u''(x) + (\gamma')^2 \omega^2 u(x) = 0 \quad \text{in } (0, x_0) \cup (x_1, 1), \quad (5.25)$$

$$\frac{\partial u}{\partial n} = i\omega\gamma'(x)u \quad \text{at } x = 0, 1, \quad (5.26)$$

$$u(x_{0-}) = u(x_{0+}) \quad \text{and} \quad u(x_{1-}) = u(x_{1+}), \quad (5.27)$$

$$\partial_n u(x_{0-}) = \partial_n u(x_{0+})\gamma'(x_0) \quad \text{and} \quad \partial_n u(x_{1-})\gamma'(x_1) = \partial_n u(x_{1+}), \quad (5.28)$$

$$\text{with } X = C^2((0, x_0) \cup (x_0, x_1) \cup (x_1, 1)) \cap C^1[0, 1]. \quad (5.29)$$

The complex Helmholtz equation (5.25) represents the analytic continuation of the Helmholtz equation (5.24) into the complex ($\gamma' = (1 + i\alpha)$) domain. Solutions of (5.25) are $\{\exp(i\omega\gamma'x), \exp(-i\omega\gamma'x)\}$. The Sommerfeld conditions (5.26) limit this set of solutions to one each.

The material parameter

$$\rho(x) = \begin{cases} 0.1 & \text{for } x \in [\frac{1}{3}, \frac{2}{3}], \\ 1 & \text{else,} \end{cases} \quad (5.30)$$

is inclined because in the one dimensional case there are only simply connected domains. This would give only trivial solutions, therefore a material parameter ρ is used. The PML function is

$$\gamma(x) = \begin{cases} x & \text{for } x \in [\frac{1}{3}, \frac{2}{3}], \\ (1 + i\alpha)x - i\alpha/3 & \text{for } x \in [0, \frac{1}{3}], \\ (1 + i\alpha)x - 2i\alpha/3 & \text{for } x \in [\frac{2}{3}, 1], \end{cases} \quad (5.31)$$

with a positive PML parameter α . Thus the solution pair (u, ω) is

$$u(x) = c \begin{cases} -i(c_1 \sin(\omega\sqrt{\rho}/3) + \cos(\omega\sqrt{\rho}/3)) \exp(i\omega(1 + i\alpha)(1/3 - x)) & x \in [0, \frac{1}{3}], \\ -ic_1 \sin(\sqrt{\rho}\omega x) - i \cos(\sqrt{\rho}\omega x) & x \in [\frac{1}{3}, \frac{2}{3}], \\ -i(c_1 \sin(2\omega\sqrt{\rho}/3) + \cos(2\omega\sqrt{\rho}/3)) \exp(i\omega(1 + i\alpha)(x - 2/3)) & x \in (\frac{1}{3}, 1], \end{cases} \quad (5.32)$$

$$\text{with } c_1 = \frac{\sin(\omega\sqrt{\rho}/3) - \frac{i(1+i\alpha)}{\sqrt{\rho}} \cos(\omega\sqrt{\rho}/3)}{\cos(\omega\sqrt{\rho}/3) + \frac{i(1+i\alpha)}{\sqrt{\rho}} \sin(\omega\sqrt{\rho}/3)} \quad (5.33)$$

$$\text{and } \omega = \frac{3n\pi}{\sqrt{\rho}} - 2\pi i, \quad (5.34)$$

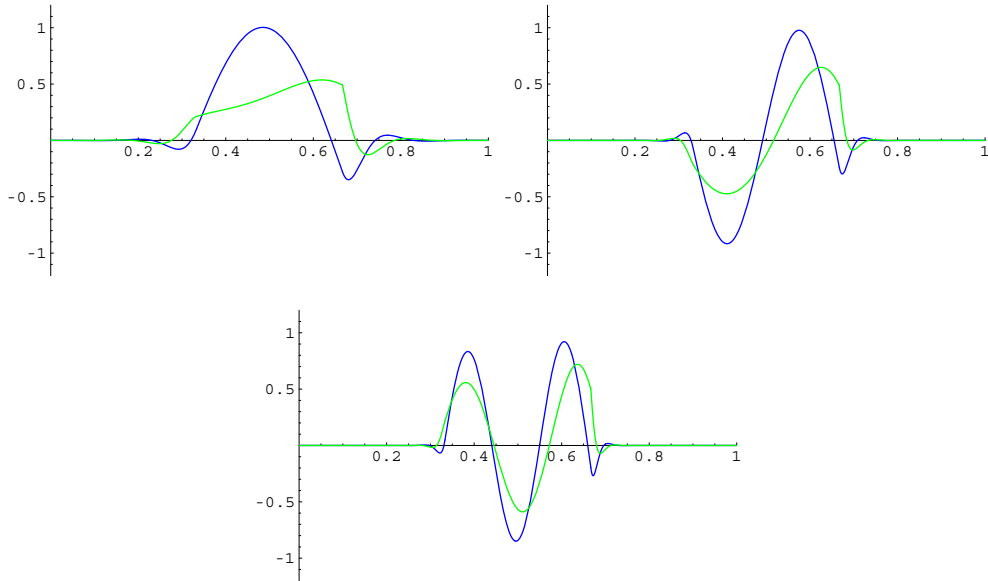


Figure 5.5: $Re(u)$ and $Im(u)$ with $n = 1, 2, 3$ and $\alpha = 1$ of the unbounded eigenvalue problem and $\rho = 0.1$.

with c any real constant value and $n = 1, 2, \dots$. This solution decays exponentially as can be seen in Figure 5.5.

The material parameter ρ is 0.1 in this example. The solution u with $n = 1, 2$ and the PML parameter $\alpha = 1$ satisfies the homogeneous Dirichlet boundary conditions at $x = 0, 1$ (see the both pictures in Figure 5.5). Thus replacing the Neumann condition $\partial_x u = i\omega\gamma' u$ by the Dirichlet boundary condition results only in small error if α is large enough or the PML is thick enough. In any case absorption of all waves is achieved.

Now all above is computed numerically with the Finite Element method. The eigenfrequencies obtained with order $p = 5$ and $\alpha = 1$ are shown in Figure 5.6.

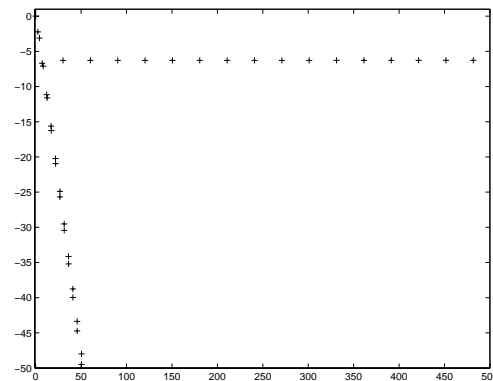


Figure 5.6: Eigenfrequencies obtained with Finite Element method

These eigenvalues ω have imaginary part -2π and their real part is approximately the analytical eigenvalue $3n\pi/\sqrt{\rho} = 3n\pi/\sqrt{0.1} \approx 30n$, $n = 1, 2, \dots$.

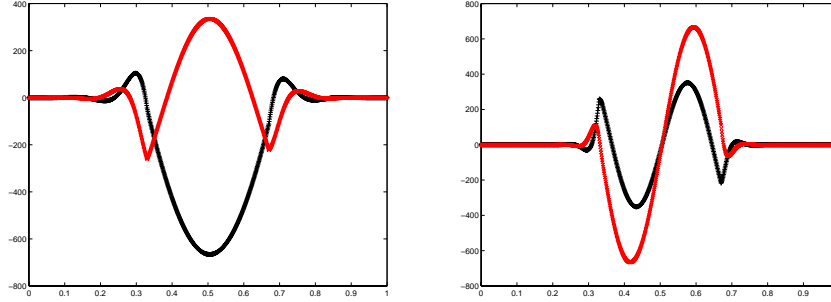


Figure 5.7: Eigenfunctions (real part in black, imaginary in red) belonging to the above eigenfrequencies

The eigenfunctions to the first two eigenvalues in Figure 5.6 are shown in Figure 5.7. Their scaling is different to those of the analytical solution but that does not matter, since the solution is unique up to a constant factor.

Minimizing the thickness of the PML results in a more complicated problem.

5.3.2 Unbounded Eigenvalue Problem

Take the following problem.

Find $u \in V_0, \omega \in \mathbf{C}$:

$$\int_{\Omega} \frac{u'v'}{\det(\gamma')} = \omega^2 \int_{\Omega} \rho uv \det(\gamma') \text{ for } v \in V_0, \quad (5.35)$$

$$\text{with } \gamma(x) = \begin{cases} x & \text{for } x \in [1/6, 5/6] \\ (1+i\alpha)x - i\alpha/6 & \text{for } x \in [0, 1/6] \\ (1+i\alpha)x - i5\alpha/6 & \text{for } x \in [5/6, 1] \end{cases}, \quad (5.36)$$

with the Hilbert space $V_0 = \{v \in H^1(\Omega) : v = 0 \text{ at } \Gamma_D\}$, the domain Ω the interval $[0, 1]$, $\Gamma_N = \emptyset$ and $\Gamma_{PML} = \{0, 1\}$. Note that the thickness of the PML is reduced by half compared with the last example.

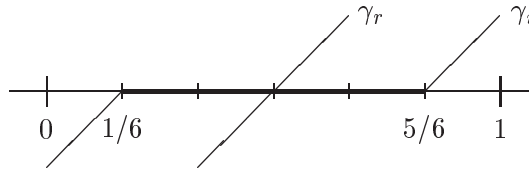


Figure 5.8: The PML function $\gamma(x) = \gamma_r(x) + i\gamma_i(x)$

Inserting both γ as in (5.36) and ρ as defined in (5.30) gives the following problem.

Find $u \in V_0 = \{u \in H^1([0, 1]) : u(0) = 0 = u(1)\}$ and $\omega \in \mathbf{C}$:

$$\int_0^1 \frac{u'(x)v'(x)}{\det(\gamma')} dx = \omega^2 \int_0^1 \rho(x)u(x)v(x) \det(\gamma') dx \text{ for } v \in V_0. \quad (5.37)$$

After discretization the problem is solved with an Arnoldi-algorithm (see Section 8.1). Figure 5.9 shows all frequencies ω computed with order $p = 5$ and $\alpha = 1$. The frequencies

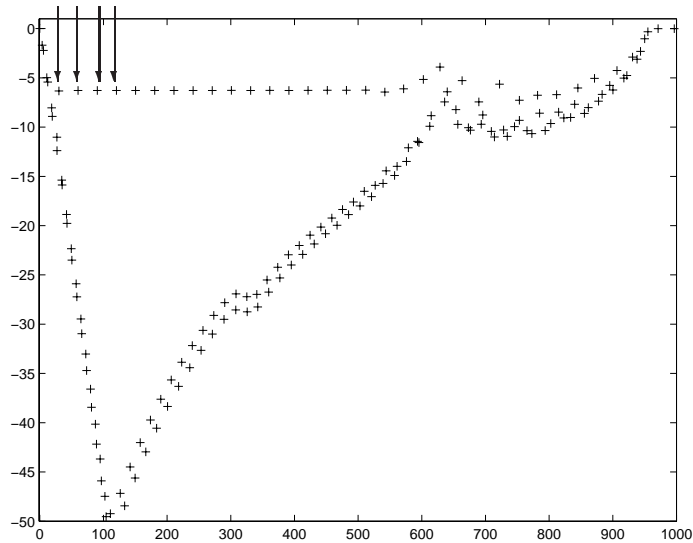


Figure 5.9: Frequencies obtained with PML parameter $\alpha = 1$ and order $p = 5$

with imaginary part ≈ -6 lying at the horizontal line at top of the picture with distance ≈ 30 to each other are the desired eigenvalues. Those on the left nearly vertical line are dependent of the PML. To be more precisely if the PML parameter α changes the gradient of the line with those frequencies change as well. All other eigenvalues depend on the Finite Element (FE) approximation respectively on the material parameter ρ . As already mentioned the PML and the domain where $\rho = \rho_1$ are only overlapping, but not equal.

With the PML method there are still eigenvalues coming from the FE noise (see Figure 5.9). This can be avoided if Reduced Integration (see Section 6.1.1) is used.

For the eigenfunctions belonging to the first four eigenvalues (pointed at with arrows in Figure 5.9) see Figure 5.10. In the middle $[1/3, 2/3]$ the eigenfunctions behave the same as in the example before.

The PML method gives good results in the one dimensional case. Consider now a two dimensional problem.

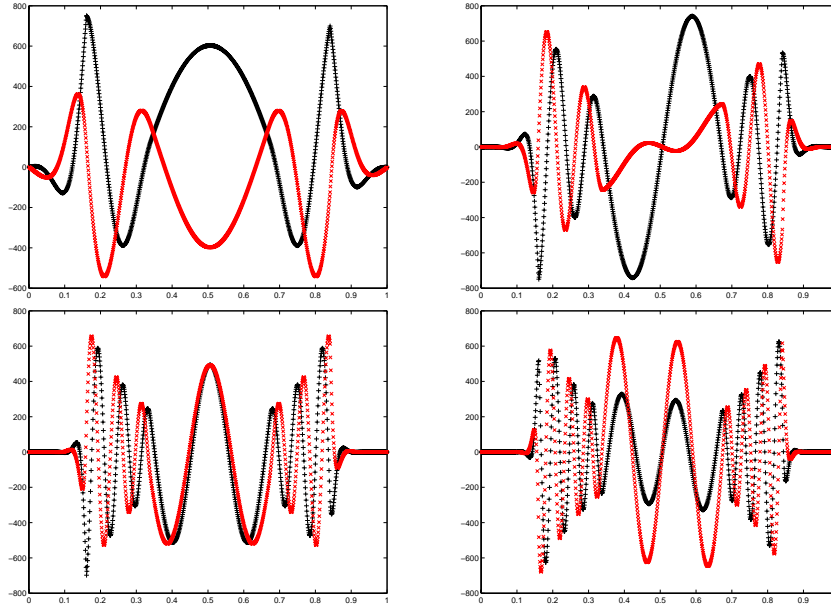


Figure 5.10: Eigenfunctions (real part in black, imaginary in red) belonging to the above eigenfrequencies

5.3.3 Unbounded two dimensional Eigenvalue Problem

The domain is partitioned in the PML, that is called Ω_{PML} and the interior, that is Ω_F , see Figure 5.11. Assume homogeneous Neumann boundary conditions at Γ_N and homogeneous Dirichlet boundary conditions at Γ_D .

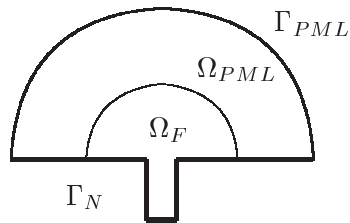


Figure 5.11: Computational domain in 2D

The PML function $\gamma(x)$ is chosen for curvilinear coordinates, see declaration (5.12). Discretization of the problem (5.21) and solving the discrete problem with the Arnoldi method, see Section 8.1, gives eigenfrequencies ω that are all shown in Figure 5.12.

Again the desired eigenfrequencies ω are those with similar imaginary part and those that lie with the same distance to each other, see top of Figure 5.12. In the one dimensional case the desired eigenfrequencies had all the same imaginary part. In 2D, there are three groups of ω 's with similar imaginary part, that lie in the same distance to each other.

The eigenvalues dependent of the PML are those on the left nearly vertical line. Those not

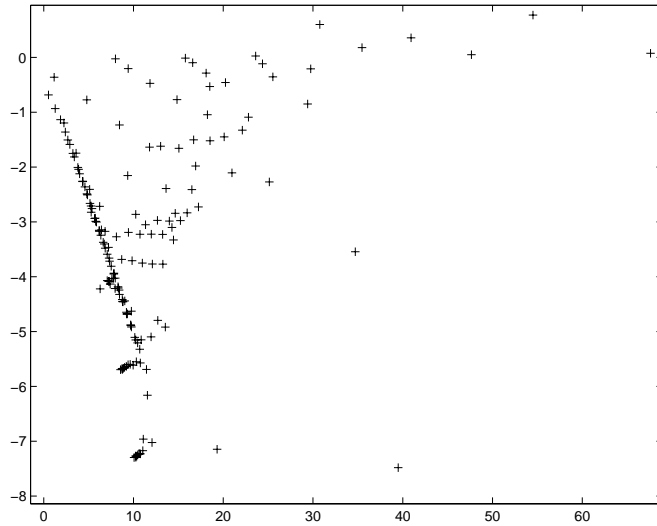


Figure 5.12: Frequencies obtained with PML parameter $\alpha = 1$ and order $p = 4$

mentioned yet depend on the Finite Element approximation.

In general the PML method is a very good method to approximate absorbing boundary conditions. Nevertheless trouble happens when using them on eigenvalue problems, see Chapter 6.

5.4 Properties of Complex Symmetric Matrices

Complex symmetry is a purely algebraic property and has no effect on the spectrum of a matrix, unlike hermite matrices. A complex symmetric matrix may not even be diagonalizable and if it is, then it has an eigendecomposition that reflects the complex symmetry.

Definition:

A matrix $Z \in \mathbf{R}_n^n$ that satisfies $Z^T Z = I_n$ is called complex orthogonal.

Lemma:

A complex symmetric matrix $A \in \mathbf{R}_n^n$ is diagonalizable if and only if its eigenvector matrix $Z \in \mathbf{R}_n^n$ can be chosen such that $Z^T A Z = \text{diag}(\lambda_1, \lambda_2, \lambda_3, \dots, \lambda_n)$ and $Z^T Z = I_n$ (Z is complex orthogonal).

For the proof see [32].

The complex orthogonality of Z reflects the complex symmetry.

In the hermitian case (if A is hermite, $A = A^*$) the eigenvector matrix Z can always be chosen to be the unitary $Z^* A Z = \text{diag}(\lambda_1, \lambda_2, \dots, \lambda_n)$ and $Z^* Z = I_n$. The unitariness of Z reflects the fact that A is hermite.

The reason why an eigendecomposition for complex symmetric matrices does not always exist is that there are complex vectors z with

$$z^T z = 0 \text{ but } z \neq 0. \quad (5.38)$$

Suppose A has an eigenvalue with a one-dimensional eigenspace and the vector z spanning the space satisfies condition (5.38). Then one of the columns of any eigenmatrix Z of A would be of the form $z_k = \gamma z$, where $\gamma \neq 0$ is a scalar. Then $z_k^T z_k = \gamma^2 z^T z = 0$, while the complex orthogonality condition ($Z^T Z = I_n$) would imply $z_k^T z_k = 1$.

Chapter 6

Methods of Discretization/Modelling

We want to solve equations the unbounded Helmholtz problem (3.17) respectively its variational formulation (3.18). Since (except in the one-dimensional case) the Sommerfeld condition can't be applied as a Dirichlet-, Neumann- or Robin-boundary condition, it is necessary to apply some method that changes the Sommerfeld condition into a boundary condition which is easier to handle and that terminates the infinite domain.

One approach to do so is the *PML Method*, that was first introduced by Berénger in 1994 [5]. The other is a newly developed method called *wavefactorization*. Both methods and their combination are discussed and tested in this chapter.

6.1 PML: Problems and Fixes

The same problem as in 5.37 investigated. Solving it with order $p = 5$ gives very good results, as was already seen in Figure 5.9. Now a lower order $p = 1$ is chosen.

Figure 6.1 shows all frequencies ω computed with order $p = 1$ and $\alpha = 1$. The frequencies ω that are on a nearly vertical line starting from zero depend on the Perfectly Matched Layer (on α) and are artificial. The above ω 's are better, but still not the best. The physically interesting eigenvalues should have zero imaginary part, a positive real part and nearly the same distance to one other. In Figure 6.1 only those with real part > 350 fulfill this, but more eigenvalues (with smaller real part) are needed!!

In fact four ω 's (arrows above) are good to distinguish, one has a red circle around and the other three lie with the same distance next to each other. Their imaginary part is around -6 . The eigenvectors to one interesting and one artificial ω (red circled in Figure 6.1) are shown in Figure 6.2.

The Eigenvector which belongs to the interesting (good) eigenvalue oscillates regularly in the middle (the interval $[1/3, 2/3]$ where $\rho = \rho_0 = 0.1$), decreases exponentially in the PML (the intervals $[0, 1/6]$ and $[5/6, 1]$) and goes to zero at the boundary. But the eigenvector belonging to the PML-dependent eigenvalue has no oscillation in the middle but high one in the left PML, where it should already decrease.

Figure 6.3 shows a comparison of different orders p of this 1D PML-example. The higher the order the better the distinction between good and bad eigenvalues. With order $p = 1$ only 4 good eigenfrequencies can be seen, with order 2 even 9 and with order 5 already 20 good eigenvalues. So increasing the order gives better results. If the order is p , the number

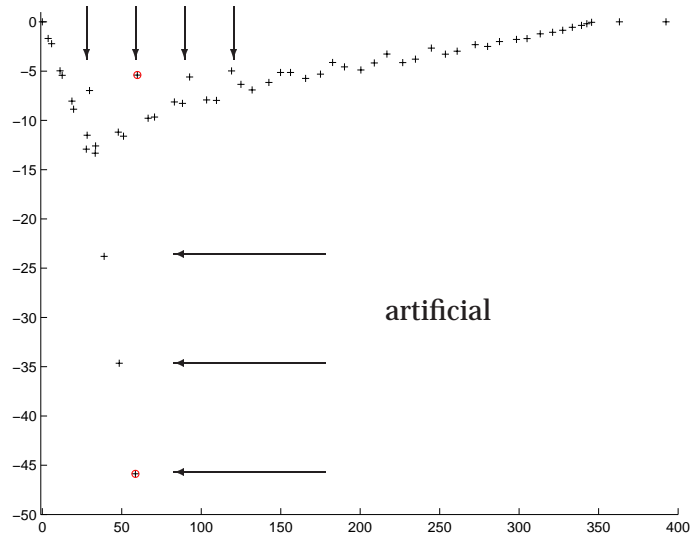


Figure 6.1: Eigenfrequencies ω of the eigenvalue problem in 1D (x-axes: $Re(\omega)$, y-axes: $Im(\omega)$)

of eigenvalues should be around $4 * p$.

Although this is an acceptable result, the imaginary part of the first eigenvalues is not even close to zero, as it is in physics. Another disadvantage is that the higher the finite element order p the more computational work. Therefore some changes in discretization are suggested.

6.1.1 Reduced Integration

In the eigenvalue problem (5.37) u and v were discretized with polynomials of order p . The mass integral $\int uv$ is computed with an integration rule of order $2p$ while the stiffness integral $\int u'v'$ is computed with a rule of order $2p - 2$.

This might cause some problems, e.g. assume u to be a linear, continuous polynomial on each interval, then u' is constant on each interval, but not continuous. Therefore the Sommerfeld condition $u' = i\omega u$ can never be fulfilled, unless u is zero.

With reduced integration or L_2 projections this problem can be avoided.

Assuming polynomial order $p = 1$ for u and the test functions v gives a stiffness integral with a function ($= u'v'$) of polynomial order 0 and a mass integral with a function ($= uv$) of order 2. Instead of full assembling with an exact integration rule of order 2 an integration rule of order 1, as in

$$\text{middle point rule: } \int_a^b f(x)dx \approx (b - a)f\left(\frac{b - a}{2}\right), \quad (6.1)$$

$$\text{trapeze rule: } \int_a^b f(x)dx \approx \frac{(b - a)}{2} (f(a) + f(b)), \quad (6.2)$$

is taken.

In general an integration rule of order p computes the integral of polynomials up to order p

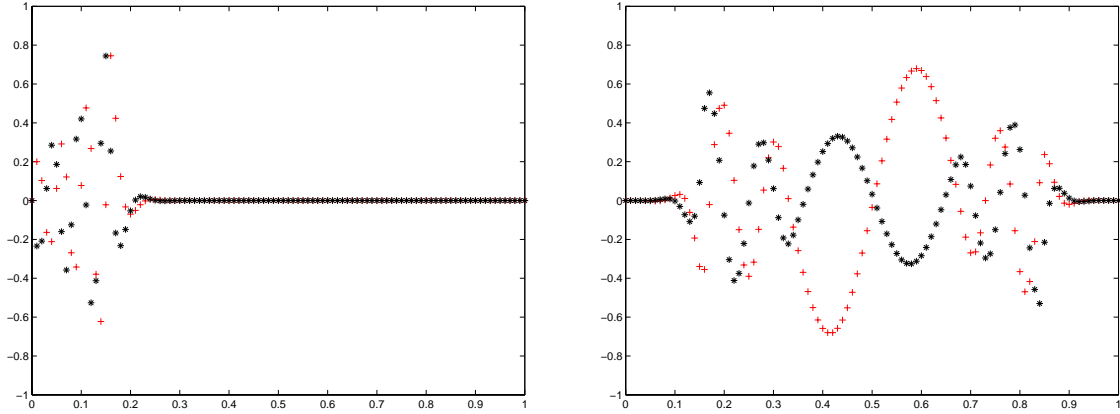


Figure 6.2: Eigenvectors of PML-dependent (left) and interesting (right) eigenvalue, real part ... *, imaginary part ... +

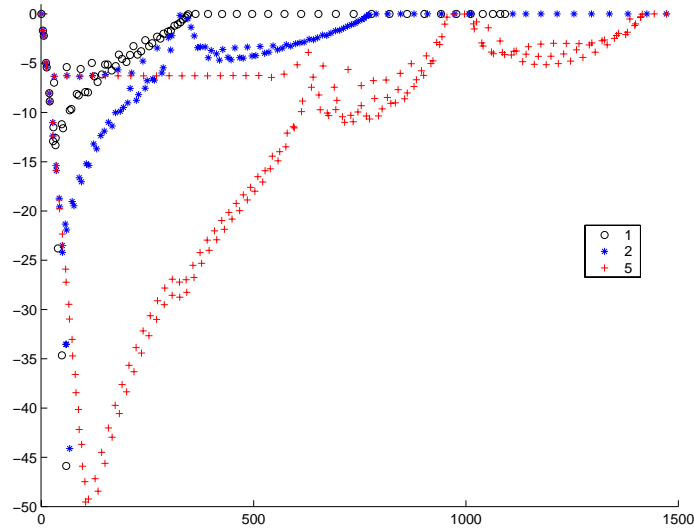


Figure 6.3: comparison of different orders $p = 1, 2, 5$

exact. For higher polynomials a local error is introduced. In the one dimensional case this is defined the following way:

Let $Q_n(f)$ be a formula for numerical integration of the form

$$Q_n(f) := (b - a) \sum_{i=1}^n w_i f(x_i) \approx \int_a^b f(x) dx, \quad (6.3)$$

with n points $x_i \in [a, b]$ and weights w_i satisfying $\sum_{i=1}^n w_i = 1$.
 $Q_n(f)$ is of order p if it is exact for polynomials ϕ of order p :

$$\int_a^b \phi(x) dx = Q_n(\phi) \text{ for } \phi \in \mathcal{P}^p. \quad (6.4)$$

Q_n is then called Q_n^p . If a polynomial of any order is computed with an integration rule the local error is

$$E_n(\phi) := \int_a^b \phi(x) dx - Q_n(\phi) = O(h^{p+1}), \quad (6.5)$$

with $h = \max_i(x_i - x_{i-1})$.

Both integration rules (trapeze and middle point rule) are of order 1, but the middle point integration rule has better approximation property as the trapeze rule.

The different integration rules are applied only at the mass matrices and Figure 6.4 shows the eigenvalues belonging to the different approximations.

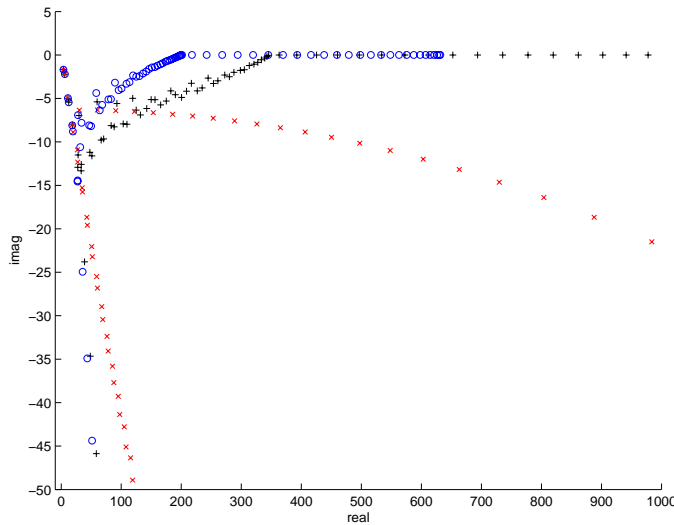


Figure 6.4: x ... middle point rule, o ... trapeze rule, + ... full assembling

Here the middle point integration rule applied onto the mass integrals gives the better results. The eigenvalues lie with the same distance to each other and are easy to distinguish. The artificial eigenvalues are those on the nearly vertical line and the interesting eigenvalues are situated on this horizontal arc in Figure 6.4.

One reason why the middle point rule gives better results than the trapeze rule although they are both of the same order might be that its approximation error is half of the error of the trapeze rule. The other reason is that the middle point rule can be seen as a L_2 projection of u from \mathcal{P}^1 to \mathcal{P}^0 .

$$P_{L_2}^1(I) : \mathcal{P}^1 \rightarrow \mathcal{P}^0, \quad (6.6)$$

$$\text{m.p.r.} \left(\int_I uv dx \right) = \int_I \underbrace{(P_{L_2}^1 u)}_{\in \mathcal{P}^0} v dx, \quad (6.7)$$

with I an interval $\subset \mathbf{R}$. This projection $P_{L_2}^1$ is a self adjoint projection ($\langle P_{L_2}^1 u, v \rangle = \langle u, P_{L_2}^1 v \rangle$) with $(P_{L_2}^1)^2 = P_{L_2}^1$.

The same results are obtained if u and v are of order p and the mass integral $\int uv$ is assembled with an integration rule of order $2p - 1$ or $2p - 2$ instead of $2p$. Figure 6.5 shows the result with u and v of order $p = 5$ respectively $p = 10$ and some lower integration rules applied onto the mass integral.

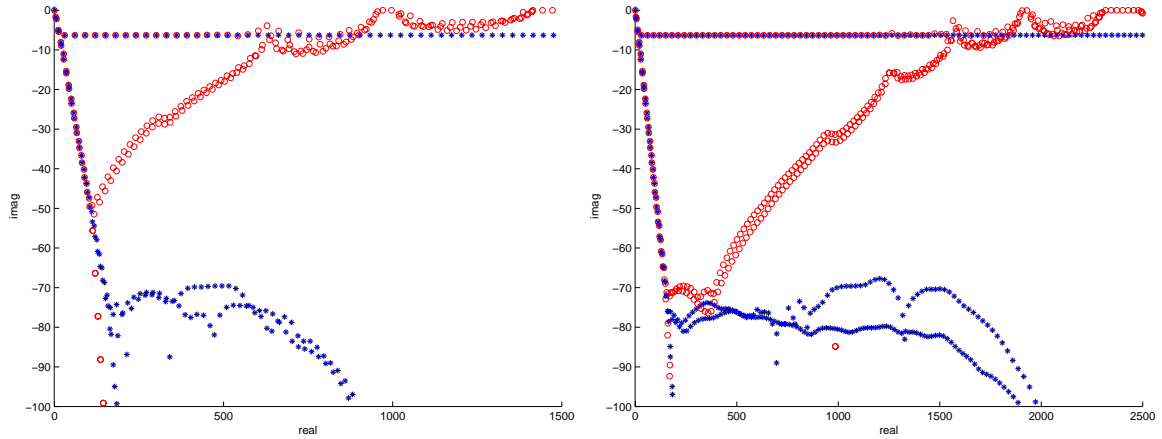


Figure 6.5: u and v of order $p = 5$ (left) and $p = 10$ (right); \circ ... full assembling with an integration rule of order $2p$, \times ... assembling with a rule of order $2p - 1$, $+$... assembling with a rule of order $2p - 2$

What is interesting about Figure 6.5 is that the lower integration rules of order $2p - 1$ and $2p - 2$ onto the mass integral give exactly the same result, although uv is a polynomial of order $2p$ and an exact integration rule (of order $2p$) should be the best choice.

In Figure 6.5 the first 20 eigenvalues of the PML-method with full assembling correspond with the eigenvalues of the PML-method with lower integration rule. The lower order approaches give even more eigenvalues, which are better to distinguish and the finite element order p need not to be as high as with full assembling to get enough good eigenvalues. Furthermore no mathematical computation is needed to select the interesting from the artificial eigenvalues, it can be seen.

So less computational work and easy distinction are the advantages of applying lower integration rules onto the mass integrals.

Integration rules with order $2p - 3$ or lower give different (worse) results. Only if u and v are of order p , if $\int u'v'$ is integrated with an exact integration rule of order $2p - 2$ and $\int uv$ with a lower integration rule of order $2p - 1$ or $2p - 2$ the best results are obtained.

But why does this approach work that good???

One reason as above mentioned is that the integration rules are L_2 projections. For general

p the L_2 -projections for an interval $I \subseteq \mathbb{R}$ look the following way:

$$P_{L_2}^{1,p}(I) : \mathcal{P}^p \rightarrow \mathcal{P}^{p-1}, \quad (6.8)$$

$$P_{L_2}^{2,p}(I) : \mathcal{P}^p \rightarrow \mathcal{P}^{p-2}, \quad (6.9)$$

$$\langle P_{L_2}^{1,p} u, v \rangle_{L_2} = \int_I \underbrace{(P_{L_2}^{1,p} u)}_{\in \mathcal{P}^{2p-1}} v \, dx := Q_n^{2p-1}(uv), \quad (6.10)$$

$$\langle P_{L_2}^{2,p} u, v \rangle_{L_2} = \int_I \underbrace{(P_{L_2}^{1,p} u)}_{\in \mathcal{P}^{2p-2}} (P_{L_2}^{1,p} v) \, dx := Q_n^{2p-2}(uv), \quad (6.11)$$

with Q_n^p a formula for numerical integration as defined in (6.3) and (6.4).

Another reason might be that if the integration rules onto the mass integral and the stiffness integral are both of the same order, there is no further approximation error.

The integral $\int u'v'$ can only be computed with an integration rule of order $2p-2$ (with u and v of order p), whereas the integral $\int uv$ can be computed more exactly. This leads to some discrepancy of the approximation precision. Whether this is the reason for worse results with exact integration rules is left open.

In order to avoid this discrepancy the mass integral is computed with lower integration rules of order $2p-1$ and $2p-2$ instead of $2p$. Indeed this approach gives better results as Figure 6.5 suggests.

In the one dimensional case the L_2 projection is easy to choose (it's a lower integration rule), but there are problems in the higher dimensional case. Already in \mathbb{R}^2 an appropriate mesh has to be chosen. In this case a lower order integration rule on triangles gives no L_2 projection but applied on squares a L_2 projection is obtained.

Therefore Reduced Integration is a good approach in the one-dimensional case but it's no longer pursued for higher dimensions.

6.1.2 Dispersion Analysis for the FE-Solution

Reduced integration gives interesting results in 1D. Why this is the case is investigated by methods of spectral analysis.

Assume equidistant partition of the interval $[0, 1]$, with n the number of partitions and $h = \frac{1}{n}$ the distance between neighbour points. The stiffness matrix K and the mass matrices M_{mid} , $M_{t.r}$ and $M_{f.a.}$ that are obtained by using the middle point rule (*mid*), the trapeze rule

(*t.r.*) and full assembling (*f.a.*) look the following way (outside the PML, with order $p = 1$):

$$K = \frac{1}{h} \begin{pmatrix} 2 & -1 & & \\ -1 & 2 & \ddots & \\ & \ddots & 2 & -1 \\ & & -1 & 2 \end{pmatrix}, \quad (6.12)$$

$$M_{f.a.} = \frac{h}{6} \begin{pmatrix} 4 & 1 & & \\ 1 & 4 & \ddots & \\ & \ddots & 4 & 1 \\ & & 1 & 4 \end{pmatrix}, \quad (6.13)$$

$$M_{mid} = \frac{h}{4} \begin{pmatrix} 2 & 1 & & \\ 1 & 2 & \ddots & \\ & \ddots & 2 & 1 \\ & & 1 & 2 \end{pmatrix}, \quad (6.14)$$

$$M_{t.r.} = h I_m, \quad (6.15)$$

with I_m the identity matrix $\in \mathbf{C}^{m \times m}$ and m the number of knots in the interior (all knots that are not in the PML).

Except for the first and last lines and those with complex entries (inside the PML), each line of these matrices (the stiffness matrix plus one of the mass matrices) corresponds to the homogeneous difference equation

$$-u(x_{j-1}) + 2u(x_j) - u(x_{j+1}) = \lambda h^2 \begin{cases} \frac{1}{6}(u(x_{j-1}) + 4u(x_j) + u(x_{j+1})), & \text{f.a.} \\ \frac{1}{4}(u(x_{j-1}) + 2u(x_j) + u(x_{j+1})), & \text{mid} \\ u(x_j). & \text{t.r.} \end{cases} \quad (6.16)$$

Since a solution of the form $u(x_j) = \exp(i\pi k x_j)$ is looked for with a discrete wave number $k \in \mathbf{C}$ and an eigenvalue λ_k , equation (6.16) transforms (with $x_j = jh$ and some trigonometric sum rules) into:

$$2 - 2 \cos \pi k h = \lambda(k, h) h^2 \begin{cases} \frac{1}{6}(4 + 2 \cos \pi k h), & \text{f.a.} \\ \frac{1}{4}(2 + 2 \cos \pi k h), & \text{mid} \\ 1. & \text{t.r.} \end{cases} \quad (6.17)$$

Now it is possible to compute the eigenvalues $\lambda(k, h)$ for the various mass matrices

$$\lambda_{f.a.}(k, h) = \frac{12 \sin^2 \frac{k\pi h}{2}}{h^2 (2 + \cos k\pi h)}, \quad (6.18)$$

$$\lambda_{mid}(k, h) = \frac{4}{h^2} \tan^2 \frac{k\pi h}{2}, \quad (6.19)$$

$$\lambda_{t.r.}(k, h) = \frac{4}{h^2} \sin^2 \frac{k\pi h}{2}. \quad (6.20)$$

As is easy to verify the orthogonal eigenfunctions $u(x) = \mu(x)$ of (6.16) are the same for the different mass matrices, namely

$$\mu(x) = \sqrt{2} \sin k\pi x. \quad (6.21)$$

These eigenfunctions are orthogonal with respect to the usual L_2 product $(\cdot, \cdot)_{L_2}$. The eigenvalues λ depend on k and h . For a fixed h and $k \rightarrow \frac{1}{h}$ the eigenvalues λ behave the following way

$$\lambda_{f.a.}(k, h) = \frac{12}{h^2} \frac{\sin^2 \frac{k\pi h}{2}}{2 + \cos k\pi h} \in \frac{12}{h^2} [0, 1], \quad (6.22)$$

$$\lim_{k \rightarrow \frac{1}{h}} \lambda_{mid}(k, h) = \lim_{k \rightarrow \frac{1}{h}} \frac{4}{h^2} \tan^2 \frac{k\pi h}{2} = \infty, \quad (6.23)$$

$$\lambda_{t.r.}(k, h) = \frac{4}{h^2} \sin^2 \frac{k\pi h}{2} \in \frac{4}{h^2} [0, 1]. \quad (6.24)$$

Their behaviour is plotted in Figure 6.6 for $h = 0.1$ and $k \rightarrow 1/h$. The inverse eigenvalues of the middle point rule $\frac{1}{\lambda_{mid}}$ accumulate in zero, while the others have no limit at all.

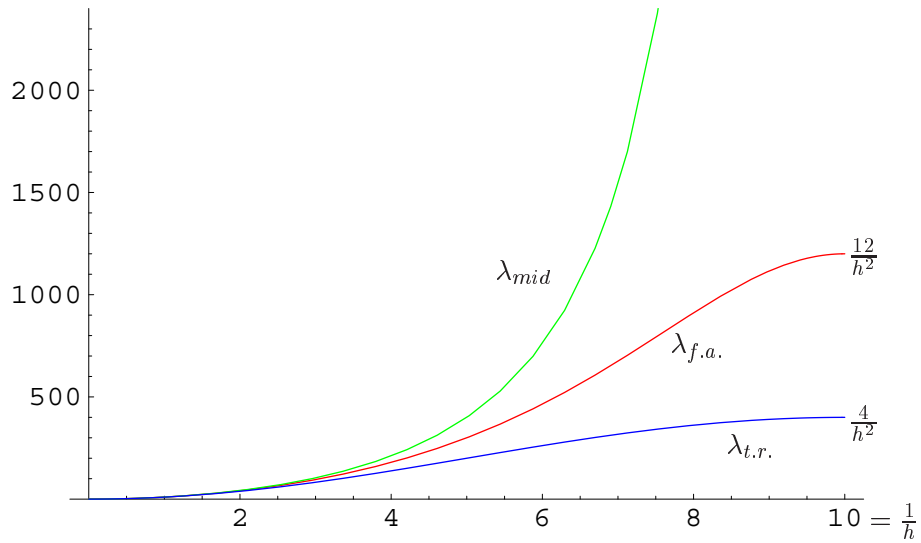


Figure 6.6: λ_{mid} , $\lambda_{f.a.}$ and $\lambda_{t.r.}$ and their behavior for $h = 0.1$ and $kh \rightarrow 1$

If the middle point rule is seen as an operator M onto u , the eigenvalue problem has the structure $Ku = \lambda Mu$ (K the stiffness operator), then the inverse problem is

$$\frac{1}{\lambda}u = K^{-1}Mu. \quad (6.25)$$

Note that this is the problem that the Arnoldi method 8.1 solves!! The operator $\mathcal{K} := K^{-1}M$ is a compact operator, since these operators have the special quality that their eigenvalues accumulate in zero as 3. of the next theorem shows.

Theorem:

Let \mathcal{K} be a compact operator in a normed space X . Then the following characteristics hold:

1. If $\dim(X) = \infty$, then zero is an eigenvalue of \mathcal{K} , i.e. $0 \in \sigma(\mathcal{K})$.
2. If $\lambda \in \sigma(\mathcal{K}) / \{0\}$, then λ is an eigenvalue of \mathcal{K} with finite geometric manifold, that is: $\dim N(\lambda I - \mathcal{K}) < \infty$, with $N(\lambda I - \mathcal{K})$ the null space of the operator $\lambda I - \mathcal{K}$.

3. *The spectrum $\sigma(\mathcal{K})$ of \mathcal{K} is at best countable with zero the only possible accumulation point in $(C) \cup \{\infty\}$.*

For the proof of this theorem see [15].

In 1D with order $p = 1$ applying the middle point rule results in a compact operator. This is also the case for higher orders p , if the mass operator M is a projection $P_{L_2}^{1,p}$ or $P_{L_2}^{2,p}$ and the stiffness operator K also the $P_{L_2}^{2,p}$ projection.

6.1.3 Derivatives and Sensitives

Consider a two-dimensional domain $\Omega := \Omega_F \cup \Omega_{PML}$ which models the cove of the landing gear and its surrounding of an aeroplane. For details of modelling see Figure 6.7. On this domain $u \in V_0 := \{v \in H^1 : v = 0 \text{ on } \Gamma_{PML}\}$ and $\omega \in \mathbf{C}$ are searched so that equation (5.21) with $V = V_0$ holds on Ω .

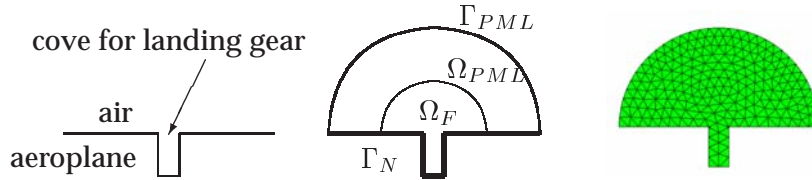


Figure 6.7: model, geometry and mesh

For the finite element discretization and its solution NETGEN/NGSolve [25] is used. The discretized equation $Au = \lambda Bu$ is solved with an Arnoldi solver on the eigenvalue Problem $A^{-1}Bu = \frac{1}{\lambda}u$, see Section 8.1.

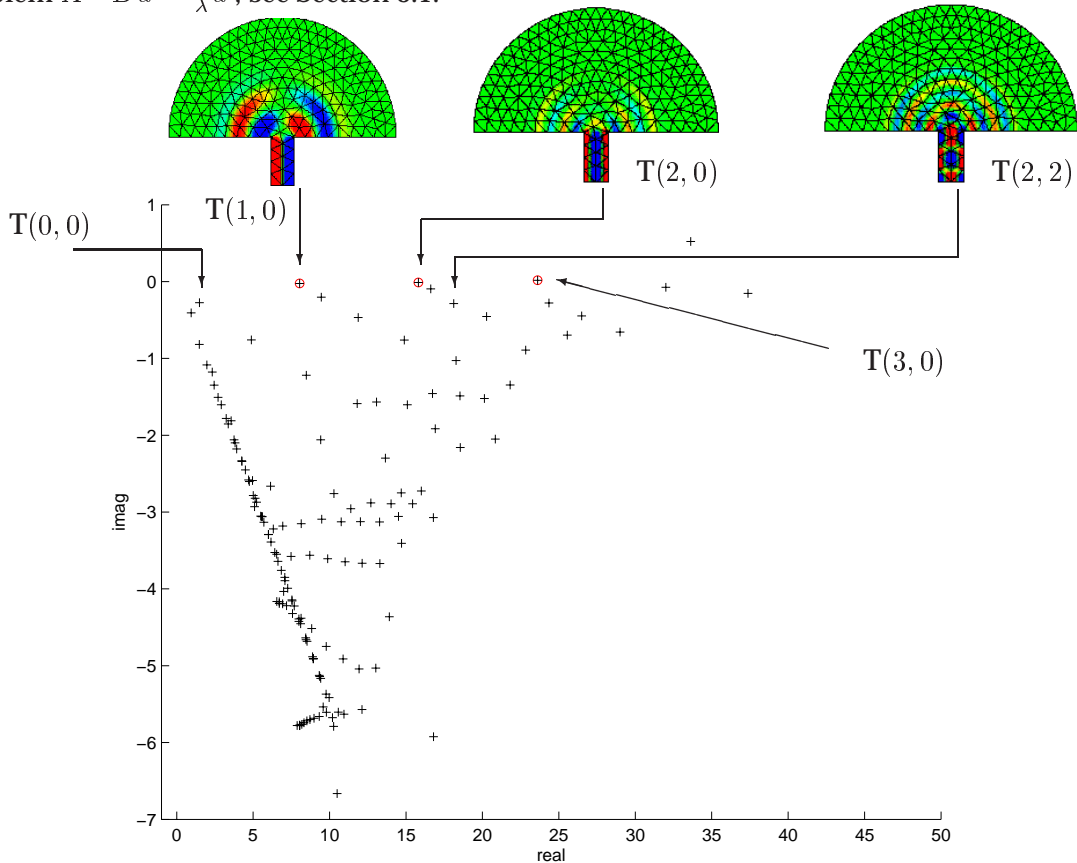


Figure 6.8: Eigenfrequencies of the 2D problem and some T modes

Figure 6.8 shows all the eigenvalues, and obviously all along the PML line are artificial and therefore useless. Some physically interesting eigenvalues and their eigenfunctions

(T-modes) are on top of Figure 6.8. The redcircled eigenfunctions are the T-modes with $T(i, 0), i = 1, 2, 3$. The interesting eigenvalues are those pointed to with an arrow and those on the diagonal lines below them.

What is needed is a method to distinguish between artificial and important eigenvalues in some mathematical respectively computational way. To get such a strategy α is changed slightly, see Figure 6.9.

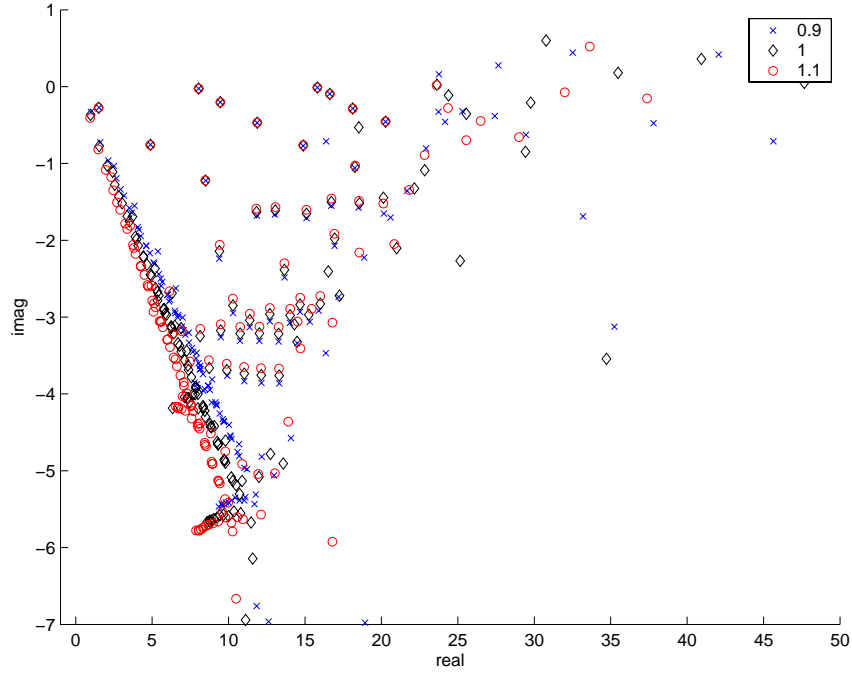


Figure 6.9: eigenvalues with different α 's

Obviously the important eigenvalues stay the same, even with different α 's and the artificial eigenvalues change. So the approach to get α -independent eigenvalues is to derive them. With

$$(A - \lambda B)u = 0, \quad (6.26)$$

$$u^t B u = 1, \quad (6.27)$$

and the Theorem of Implicit Functions

$$\begin{aligned} f_1(u, \alpha, \lambda) &= u^t(A - \lambda B)u = 0 \\ f_2(u, \alpha, \lambda) &= u^t B u - 1 = 0 \end{aligned} \quad \Rightarrow \quad \begin{aligned} 0 &= \frac{\partial f_1}{\partial \alpha} + \frac{\partial f_1}{\partial \lambda} \frac{\partial \lambda}{\partial \alpha} + \frac{\partial f_1}{\partial u} \frac{\partial u}{\partial \alpha} \\ 0 &= \frac{\partial f_2}{\partial \alpha} + \frac{\partial f_2}{\partial \lambda} \frac{\partial \lambda}{\partial \alpha} + \frac{\partial f_2}{\partial u} \frac{\partial u}{\partial \alpha} \end{aligned} \quad (6.28)$$

the following equations are obtained:

$$0 = u^t \left(\frac{\partial A}{\partial \alpha} + \lambda \frac{\partial B}{\partial \alpha} \right) u - u^t B u \frac{\partial \lambda}{\partial \alpha} + 2(A - \lambda B)u \frac{\partial u}{\partial \alpha} \quad (6.29)$$

$$0 = u^t \frac{\partial B}{\partial \alpha} u + 0 \cdot \frac{\partial \lambda}{\partial \alpha} + 2B u \frac{\partial u}{\partial \alpha} \quad (6.30)$$

In equation (6.29) the last part $(A - \lambda B)u$ is zero, if λ is an eigenvalue. Thus $\frac{\partial \lambda}{\partial \alpha}$ is computed as

$$\frac{\partial \lambda}{\partial \alpha} = \frac{-u^t (\partial_\alpha A - \lambda \partial_\alpha B) u}{u^t B u}. \quad (6.31)$$

At first numerical differentiation of the matrices A and B

$$\frac{\partial \lambda_z}{\partial \alpha} = \frac{-u^t (z(A, \alpha, \Delta\alpha) - \lambda z(B, \alpha, \Delta\alpha)) u}{u^t B u}, \quad (6.32)$$

with the central differential quotient

$$z(M, \alpha, \Delta\alpha) = \frac{M(\alpha + \Delta\alpha) - M(\alpha - \Delta\alpha)}{2\Delta\alpha}, \quad (6.33)$$

is used. Similar results are obtained if $z(M, \alpha, \Delta\alpha)$ is the backward or forward differential quotient.

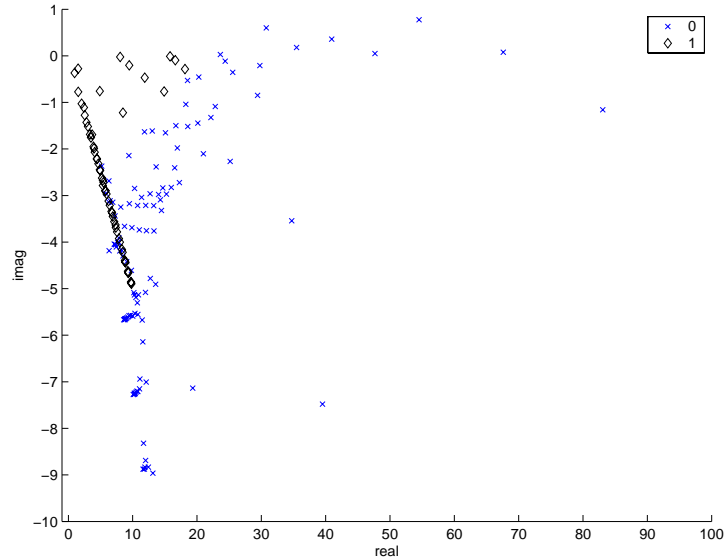


Figure 6.10: parameters: $\alpha = 1$ and $\Delta\alpha = 0.01$

Figure 6.10 shows those ω 's which $\frac{\partial \lambda_z}{\partial \alpha}$ is small in comparison to $\Delta\alpha$ in black \diamond and the others in blue \times . There are still some artificial ω 's that fulfill this condition and so it might be better to compute the exact derivatives $\partial_\alpha A, \partial_\alpha B$ instead of only the central differential quotient. With exact differentiation more artificial eigenvalues, see Figure 6.11, can be picked out, nevertheless there are enough artificial left.

As a condition $|\frac{\partial \lambda}{\partial \alpha}| < c$ with $\frac{\partial \lambda}{\partial \alpha}$ computed as in (6.31) and c the value $c = 8$ is taken.

If shifts are used, even better results are obtained, see Figure 6.12. The right picture in Figure 6.12 shows the eigenfrequencies ω obtained with a shift that is 900. This shift gives interesting ω 's around 30, whereas the shift 400 (left picture in Figure 6.12) gives interesting eigenfrequencies near 20. As above the same condition $|\frac{\partial \lambda}{\partial \alpha}| < 8$ has been taken.

Finally automatic differentiation combined with shifting of the eigenvalues is a good method to get some interesting eigenvalues around the special shifts.

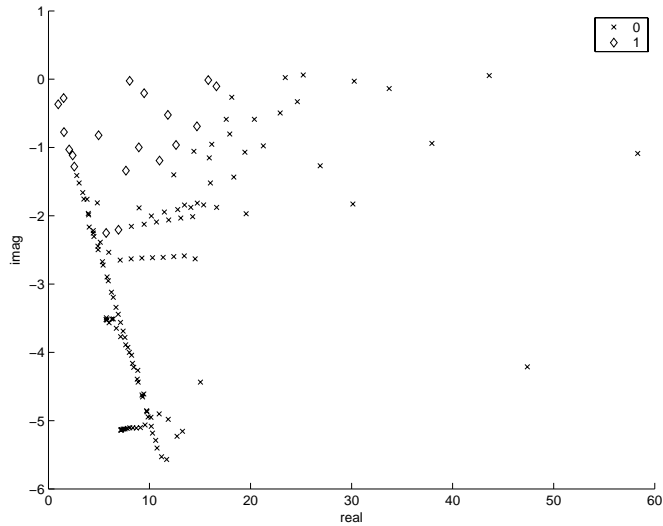


Figure 6.11: Exact differentiation, \times ... artificial, \diamond ... good

Shifting alone is not enough for the distinction of artificial and interesting eigenvalues, as can be seen in Figure 6.13. Using shifts computes only the eigenvalues near those shift more exact, but no further distinction is obtained.

Therefore a totally different approach, which is called *wavefactorization* is discussed and tested in the next section.

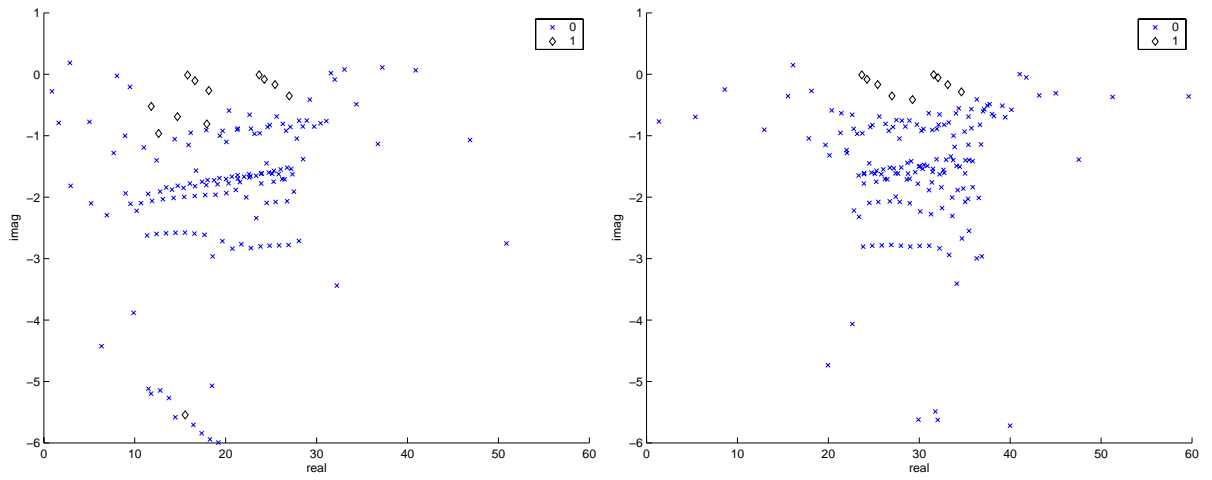


Figure 6.12: Exact differentiation with different shifts (left: shift = 400, right: shift = 900) and the obtained interesting ω 's (\diamond)

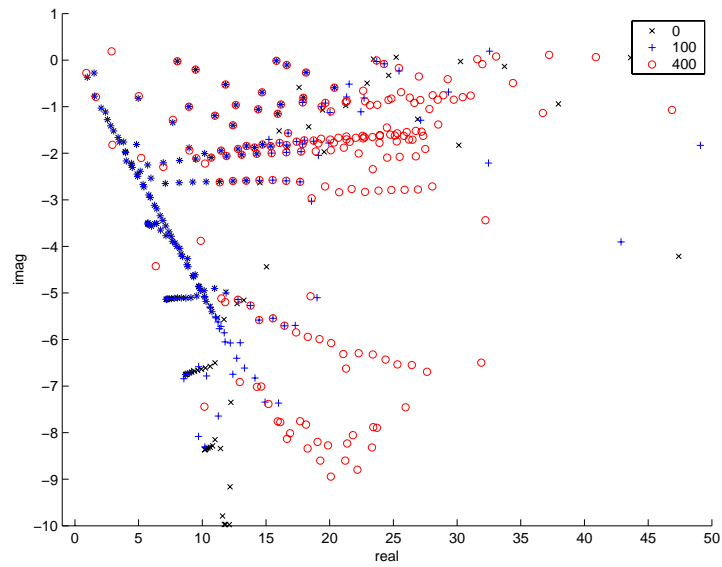


Figure 6.13: Computation of the eigenvalues without shift (\times) and with different shifts ($+$... shift=100 and o ... shift=400)

6.2 Wavefactorization

The Sommerfeld condition (2.10) states that at infinity the waves are outgoing, but consider all waves are outgoing (not only at infinity), which means u is set as $u(x) = \tilde{u} \exp(i\omega|x|)$. The wave is factorized into an exponential-term and a wave \tilde{u} . So u fulfills the Sommerfeld condition and the spherical wave is built in. As test functions all incoming waves are taken and so the exp -term vanishes. Only \tilde{u} has to be computed.

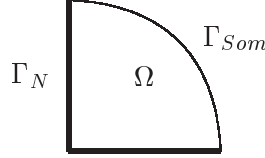


Figure 6.14: The domain Ω and its division of its boundary $\Gamma = \Gamma_{Som} \cup \Gamma_N$

The approach

$$u(\vec{x}) = \tilde{u}e^{i\omega|\vec{x}|} \Rightarrow \nabla u = (\nabla \tilde{u} + i\omega n \tilde{u})e^{i\omega|\vec{x}|}, \quad (6.34)$$

$$v(\vec{x}) = \tilde{v}e^{-i\omega|\vec{x}|} \Rightarrow \nabla v = (\nabla \tilde{v} - i\omega n \tilde{v})e^{-i\omega|\vec{x}|}, \quad (6.35)$$

is inserted in equation (5.17) and results into

$$\int_{\Omega} (\nabla \tilde{u} \nabla \tilde{v} - i\omega (\nabla \tilde{u} n \tilde{v} - \nabla \tilde{v} n \tilde{u})) + \omega^2 n^T n \tilde{u} \tilde{v} - \int_{\Gamma} \frac{\partial u}{\partial n} v = \omega^2 \int_{\Omega} \tilde{u} \tilde{v}. \quad (6.36)$$

The integral $\int_{\Gamma} \frac{\partial u}{\partial n} v$ vanishes at Γ_N (homogeneous Neumann boundary condition) and transforms into $\int_{\Gamma_{Som}} (\frac{\partial \tilde{u}}{\partial n} \tilde{v} + i\omega n^T n \tilde{u} \tilde{v})$ elsewhere. Its right part stays (with $n^T n = 1$) and its left vanishes because of the Sommerfeld condition (2.10) at Γ_{Som} which is (without limes)

$$(\partial_n u - i\omega u) = (\partial_n \tilde{u} + i\omega n^T n \tilde{u} - i\omega \tilde{u})e^{i\omega|x|} = \partial_n \tilde{u} e^{i\omega|x|} = 0. \quad (6.37)$$

So if the normal derivative $\frac{\partial \tilde{u}}{\partial n} = \partial_n \tilde{u} = \nabla \tilde{u} \vec{n}$ is zero at Γ_{Som} the Sommerfeld condition is fulfilled.

Finally the integral $\omega^2 \int_{\Omega} n^T n \tilde{u} \tilde{v}$ vanishes with the right hand side of (6.36).

Thus the final problem is

Find $\tilde{u} \in V_0 = H^1(\Omega)$ and $\omega \in \mathbf{C}$:

$$\int_{\Omega} \nabla \tilde{u} \nabla \tilde{v} = i\omega \left(\int_{\Omega} \left(\tilde{v} \frac{\partial \tilde{u}}{\partial n} - \tilde{u} \frac{\partial \tilde{v}}{\partial n} \right) + \int_{\Gamma} \tilde{u} \tilde{v} \right) \text{ for } \tilde{v} \in V = H^1(\Omega). \quad (6.38)$$

In this formulation two natural and no essential boundary condition are included. Nevertheless \tilde{u} is uniquely determined in $H^1(\Omega)$, because equation (6.38) compels \tilde{u} to be unique.

Because of $\partial_n \tilde{u} = 0$, the spherical wave \tilde{u} is constant at the boundary Γ_{Som} respectively at infinity. This fits well to the approach $u = \tilde{u}e^{i\omega|\vec{x}|}$ of the wavefactorization. The exponential term prevents reflection and is responsible for the oscillation whereas the spherical wave \tilde{u} depends on material properties and is constant at infinity.

Instead of $|\vec{x}|$ a potential $a(\vec{x})$ can be taken. For example this can look like $a(x) = \sqrt{\rho}|x - x_0|$, with ρ a material parameter and x_0 the origin (in 1D). If $a(\vec{x}) = |\vec{x}|$, then $\nabla a = \frac{\vec{x}}{|\vec{x}|} = \vec{n}$ and therefore $\nabla \tilde{u} \nabla a = \nabla \tilde{u} \vec{n} = \frac{\partial \tilde{u}}{\partial n}$. Generally the potential $a(\vec{x})$ should fulfill two conditions:

$$\nabla a^T \nabla a = \rho \quad \text{at} \quad \Omega, \quad (6.39)$$

$$(\nabla a)^T n = \sqrt{\rho} \quad \text{at} \quad \Gamma, \quad (6.40)$$

depending on the material parameter ρ , whose default value is 1. A material parameter $\rho \neq 1$ is only used if there are (at least two) different materials/fluids. The first condition erases the integral $\omega^2 \int \nabla a^T \nabla a \tilde{u} \tilde{v}$ with $\omega^2 \int \rho \tilde{u} \tilde{v}$, the second turns $i\omega \int \nabla a^T n \tilde{u} \tilde{v}$ into $i\omega \int \sqrt{\rho} \tilde{u} \tilde{v}$. These conditions can be summed up into one: $\nabla a = \sqrt{\rho} \vec{n}$ at $\bar{\Omega}$. The parameter ρ is continuous or constant in the material/fluid but jumps if two materials/fluids come together. With this condition the potential a is nearly fully determined. It has to be a positive, linear and continuous function of an absolute value of a linear function of \vec{x} . This makes $a(\vec{x}) = c_1 |c_2 \vec{x} + c_3| + c_4$ with $c_1 \cdot c_2 = \sqrt{\rho}$ and $c_1, c_2, c_3, c_4 \in \mathbf{R}$. Only three degrees of freedom are left.

Discretization gives a generalized eigenvalue problem $Au = i\omega Bu$ but with real matrices instead of complex ones. B is not symmetric but A .

For better understanding an example.

6.2.1 Wavefactorization: one-dimensional case

Assume the potential $a(x)$ with ρ as defined in equation (5.30). Both a and ρ are shown

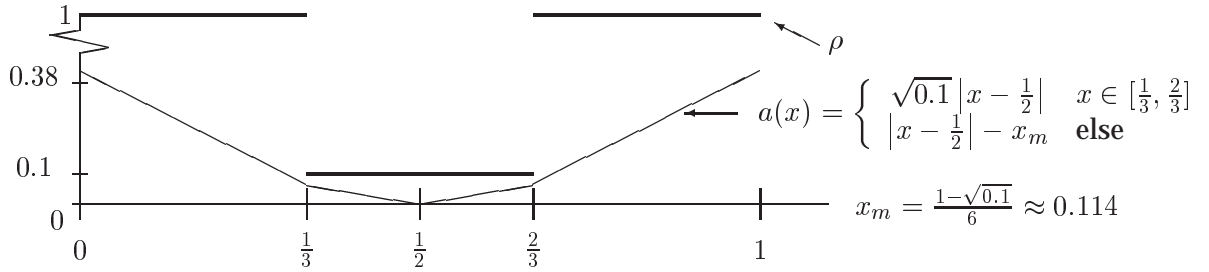


Figure 6.15: The material parameter $\rho(x)$ and the potential $a(x)$

in Figure 6.15. The potential a has to be continuous (thus the x_m), but not differentiable although $\nabla a = \sqrt{\rho} \vec{n}$ is known. The jumping ρ prevents the continuity of ∇a .

With the above definition of a and ρ the eigenvalue problem has the following structure:

Find $\tilde{u} \in H^1(\Omega)$ and $\omega \in \mathbf{C}$:

$$\int_{\Omega} \nabla \tilde{u} \nabla \tilde{v} = i\omega \left(\int_{\Omega} \sqrt{\rho} \left(\tilde{v} \frac{\partial \tilde{u}}{\partial n} - \tilde{u} \frac{\partial \tilde{v}}{\partial n} \right) + \int_{\Gamma} \sqrt{\rho} \tilde{u} \tilde{v} \right) \quad \forall \tilde{v} \in H^1(\Omega), \quad (6.41)$$

with Ω the interval $[0, 1]$, Γ the boundary points $\{0, 1\}$ and $\Gamma_{Som} = \Gamma$. To be more precise this equals

$$\int_0^1 \nabla \tilde{u} \nabla \tilde{v} = i\omega \left(\int_0^1 \sqrt{\rho} \left(\tilde{v} \frac{\partial \tilde{u}}{\partial n} - \tilde{u} \frac{\partial \tilde{v}}{\partial n} \right) + \tilde{u}(1)\tilde{v}(1) + \tilde{u}(0)\tilde{v}(0) \right). \quad (6.42)$$

Finite-Element-discretization with an equidistant partition of the interval $[0, 1]$ gives a generalized eigenvalue problem $Au = i\omega Bu$ with A, B real matrices. Again it is solved with the Arnoldi method 8.1.

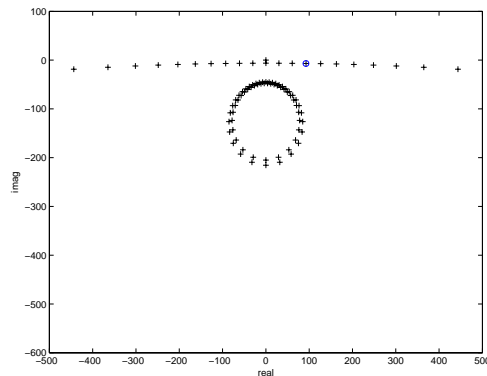


Figure 6.16: Eigenvalues ω of the on dimensional problem

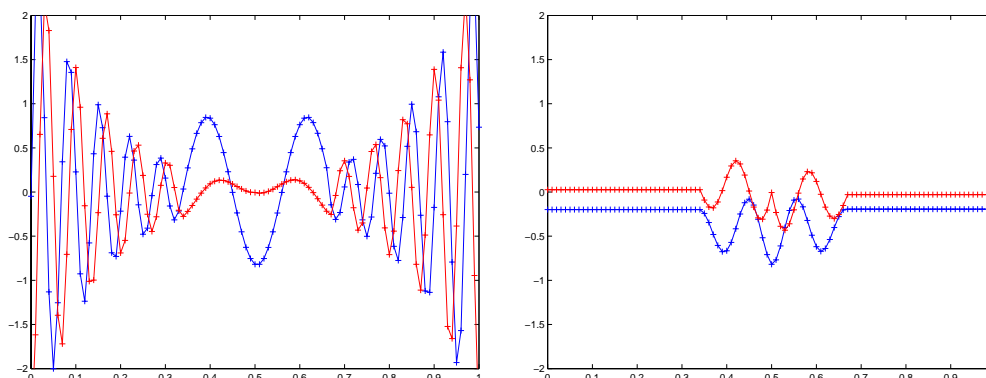


Figure 6.17: u (left) and \tilde{u} (right) belonging to the bluecircled eigenvalue of Figure 6.16

In Figure 6.16 all eigenfrequencies ω are shown. All interesting eigenvalues are those which don't belong to the circle but to the line. So in 1D it's easy to distinguish. In Figure 6.17 $u = \tilde{u} \exp(i\omega a(x))$ and \tilde{u} belonging to the bluecircled ω (of Figure 6.16) is shown. It is seen very clearly that \tilde{u} is constant in the outer domain, as the Sommerfeld condition demands. In the interior $[1/3, 2/3]$ the real part of the wave u is the sine curve $\sin(9\pi x)$.

The eigenvectors \tilde{u} from artificial ω 's (i.e. from eigenvalues in the circle) are not so regularly respectively continuous. The u belonging to them have higher amplitude and frequency.

Remark:

Recall that $u = \tilde{u} \exp(i\omega a(x))$ decays not, but increases the more, the farther from the origin.

The above problem is discretized with an equidistant mesh respectively an equidistant partition $h = \frac{1}{n}$ of the interval $[0, 1]$. A slight disturbance of this equidistant mesh gives different

eigenvalues. The eigenvalue solver cannot solve it correctly since 0 respectively $\frac{1}{h}$ (with numerical computation) are multiple eigenvalues λ with an infinite eigenspace. A different partition, e.g. a harmonic partition, near the boundary gives different artificial eigenvalues, as can be seen in Figure 6.18 in black. Again those on the horizontal line are interesting eigenvalues and those on the vertical line are artificial ones. The first eigenvalues in the center of the top stay exactly the same, but the farther from the center the wider the distance between the eigenvalues computed with different partition.

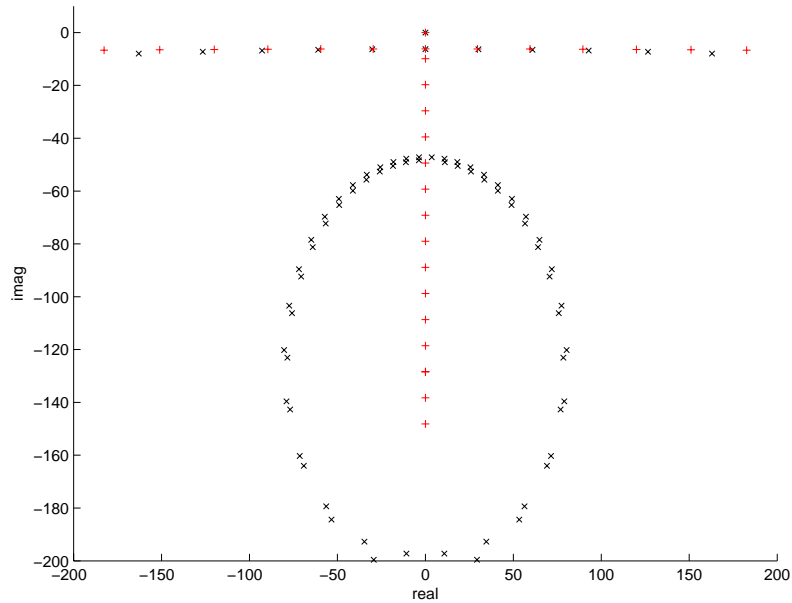


Figure 6.18: equidistant (×) and harmonic partition (+)

Here h is harmonic ($h_j = \frac{c}{j}, j = 1, 2, \dots$ with c a constant depending on the last $h_k = c/k \approx 1/n$ that is harmonic) only near the boundaries and not in the middle of the interval, there equal $h = \frac{1}{n}$ are taken. After the computation of h and the coordinates of the points $x_i = x_{i-1} + h_{i-1}$, it is necessary to rescale the domain to the interval $[0, 1]$.

6.2.2 Wavefactorization in higher dimensions

The same domain as in the PML example in Section 6.1.3 is taken but now with radius $r = 0.6$ and it's searched an $\tilde{u} \in H^1$ so that equation (6.38) holds. Here Γ is the outer round boundary. NETGEN gives the eigenvalues as shown in figure 6.19.

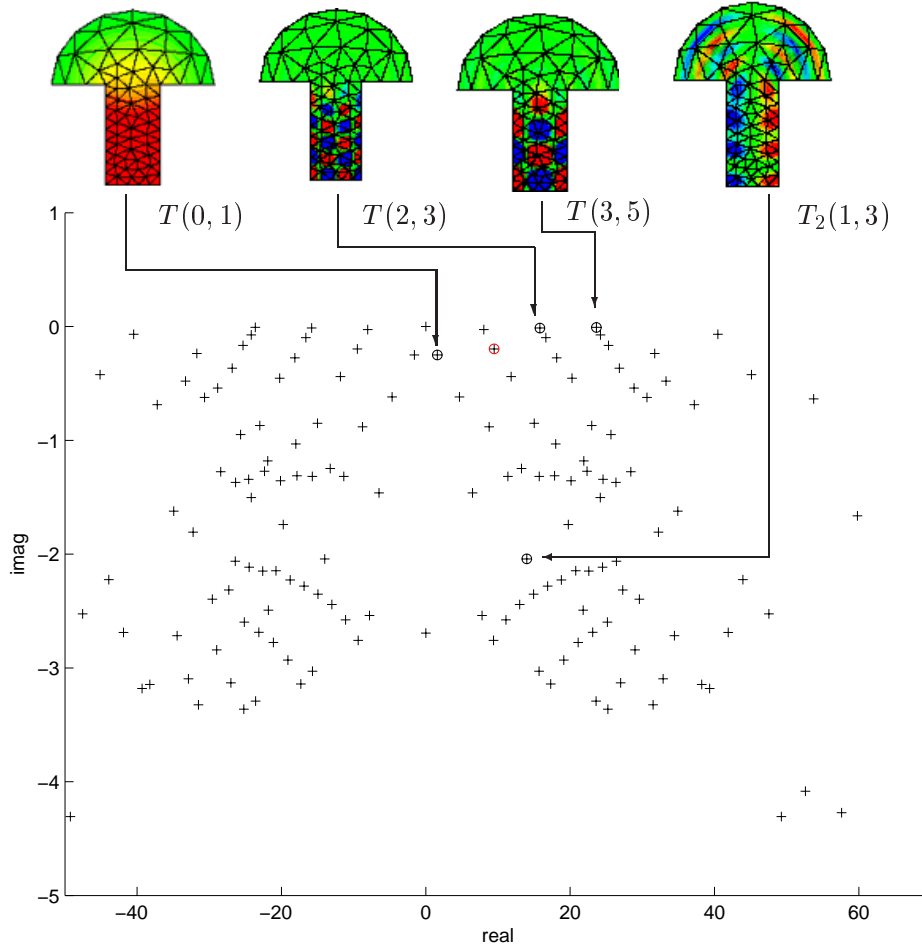


Figure 6.19: On top the eigenvectors \tilde{u} : $T(0, 1)$, $T(2, 3)$, $T(3, 5)$ and $T_2(1, 3)$ belonging to the blackcircled eigenvalues down under

The eigenvalues which are circled in black belong to the eigenvectors on top of Figure 6.19, as the arrows show. The eigenvalue $T_2(1, 3)$ differs a little bit from the other mentioned eigenvectors. It oscillates in the outer domain, where the others are already constant (here zero). There exists a $T(1, 3)$ which has this desired behavior (no oscillation near the boundary) and it's circled in red.

The question is now: Is this $T_2(1, 3)$ a physical interesting eigenvalue? In some mathematical sense it is, because \tilde{u} is constant (zero) at Γ , but not even a little bit before. It just happened that $T_2(1, 3)$ is zero at Γ , because \tilde{u} completes a wavelength λ : $\tilde{u}(r) = \tilde{u}(n\lambda) = 0, n \in \mathbf{N}$. If there would be some disturbance of the radius $r \rightarrow r + \epsilon$, the wavelength λ would not be complete $\tilde{u}(r + \epsilon) = \tilde{u}(n\lambda + \epsilon) \neq 0$.

To avoid such coincidences some change of radius is proposed. The idea is now that the interesting eigenvalues do not change if the radius is changed, at least not as much as all the other artificial eigenvalues.

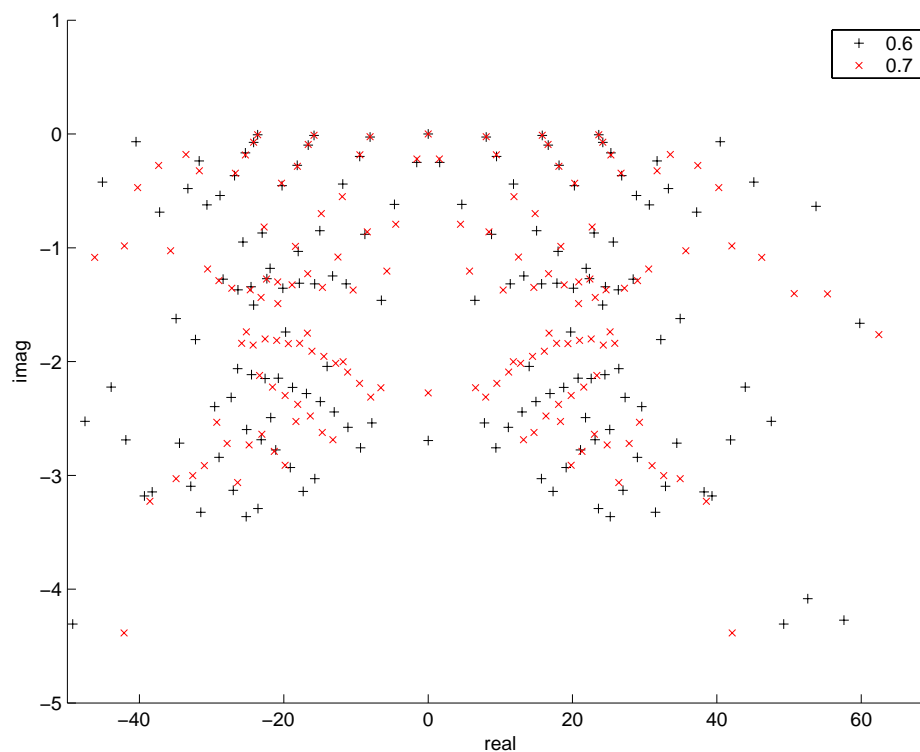


Figure 6.20: Change of radius from $r = 0.6$ to 0.7

Figure 6.20 shows what happens if the radius is changed slightly. Only the eigenvalues on top stay the same, so these are really interesting ones. The artificial ones change a lot (look for the eigenvalues arranged in arcs in the lower half of the picture) but some like $T_2(1, 3)$ not as much as the artificial ones.

At least we can suppose that the eigenvalues on top are those we are looking for. Nevertheless no mathematical strategy is obtained to pick out the artificial eigenvalues from those of physical use.

In addition changing the radius disturbs the mesh a little and so the two situations are to compare with each other carefully.

6.3 Combination of Wavefactorization and PML method

Neither PML nor wavefactorization gives sufficient results so what happens if they are combined?

First wavefactorization and then the coordinate transformation ($\tilde{u}(x) \rightarrow \tilde{u}(\gamma(x))$), with γ as defined in (5.12) is applied and the following problem is obtained.

Find $\tilde{u} \in V_0 = H^1(\Omega)$ and $\omega \in \mathbf{C}$:

$$\int_{\Omega} \nabla \tilde{u} J^{-1} J^{-t} \nabla \tilde{v} \det(J) = i\omega \int_{\Omega} \left(\tilde{v} J^{-t} \frac{\partial \tilde{u}}{\partial n} - \tilde{u} J^{-t} \frac{\partial \tilde{v}}{\partial n} \right) \det(J) + i\omega \int_{\Gamma_{PML}} \tilde{u} \tilde{v} \det(J) \quad \forall \tilde{v} \in V = H^1(\Omega) \quad (6.43)$$

The domain Ω should be the same as in Figure 5.4, where the boundary Γ_{PML} equals Γ_{Som} .

Here the integral $\int_{\Gamma_{PML}} \tilde{u} \tilde{v} \det(J)$ has to stay and vanishes not by inclining the Dirichlet boundary condition $\tilde{u} = 0$. In the latter case \tilde{u} would get zero and is not a constant value at infinity, which is demanded by the Sommerfeld condition.

With the finite element discretization a generalized eigenvalue problem $Au = i\omega Bu$ has to be solved with A a complex symmetric and B a complex matrix. To be more precisely B is a sum of a complex symmetric matrix (coming from the boundary integral) and an antisymmetric matrix (coming from the domain integral). This structure is of no use.

So the advantages of both further approaches are lost: the matrices are not (complex) symmetric (as with the PML approach) and not real (as with the wavefactorization) any more.

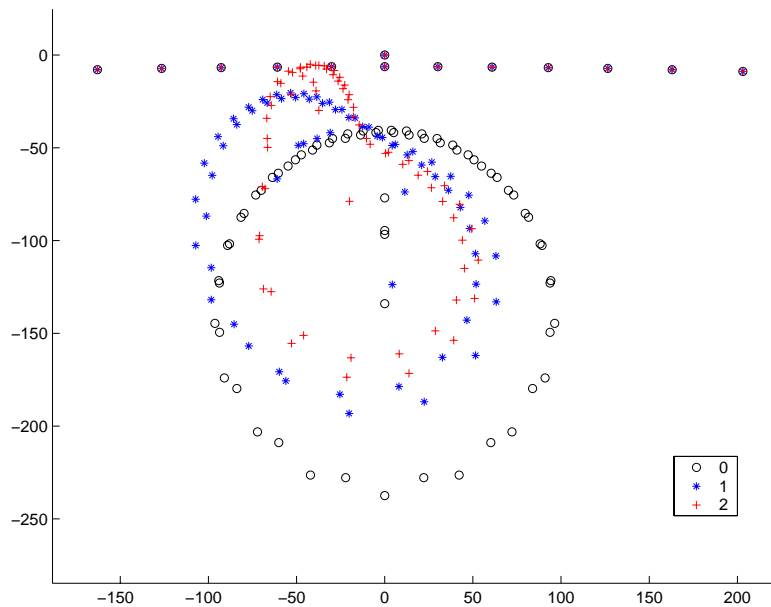


Figure 6.21: Wavefactorization alone ($\alpha = 0$, o) and wavefactorization with PML, $\alpha = 1$ (*), $\alpha = 2$ (+)

6.3.1 The One Dimensional Case

The same problem as in (6.41) is taken, but now with an additional PML and a function γ as in (5.36). The problem is as follows:

$$\text{Find } \tilde{u} \in V_0 = V \text{ and } \omega \in \mathbf{C} : \quad (6.44)$$

$$\int_{\Omega} \nabla \tilde{u} \nabla \tilde{v} \frac{1}{\det \gamma} = i\omega \left(\int_{\Omega} \sqrt{\rho} \left(\tilde{v} \frac{\partial \tilde{u}}{\partial n} - \tilde{u} \frac{\partial \tilde{v}}{\partial n} \right) + \int_{\Gamma} \sqrt{\rho} \tilde{u} \tilde{v} \det \gamma \right) \quad \forall \tilde{v} \in V,$$

with $V_0 = V = H^1(\Omega)$, Ω the interval $[0, 1]$, the PML the intervals $[0, \frac{1}{6}]$ and $[\frac{5}{6}, 1]$ and ρ defined as in (5.30). The PML function $\gamma(x)$ is $(1 + i\alpha)x$ in the PML and x else.

In the one dimensional case without PML Figure 6.16 gives the result, now α is not zero any more but 1 respectively 2, see Figure 6.21.

The circle moves away from the interesting ω 's which are on the line on the right ($Re(\omega) > 0$, $Im(\omega) < 0$). Since in 1D there is already some good (clearly seen) distinction between good and artificial eigenvalues the circle moving away gives no further information. If a different partition is used, i.e. the harmonic partition as with wavefactorization alone, some more information is received, see Figure 6.22. There the first two or three vertical eigenval-

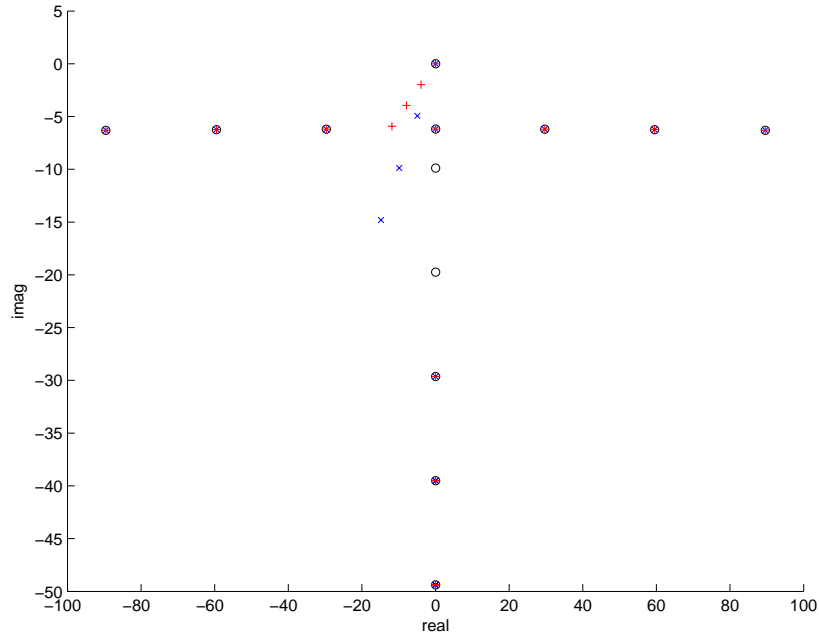


Figure 6.22: Wavefactorization (o ... $\alpha = 0$) and PML (\times ... $\alpha = 1$; $+$... $\alpha = 2$) combined with a harmonic partition

ues move to the left, all the others stay the same. So here a combination of wavefactorization and the PML method gives us a hint which eigenvalues are interesting, namely those that do not move and are not dependent from the eigenvalue solver, which are those on the horizontal line.

What is most interesting now is whether such behaviour (the artificial eigenvalues moving away) can be achieved in higher dimensions. If this is the case is checked in the next Section.

6.3.2 Higher Dimensions

The domain is the same as in Figure 6.7 and a $\tilde{u} \in V_0 = V = H^1(\Omega)$ is searched that holds equation (6.43) for all $\tilde{v} \in V$.

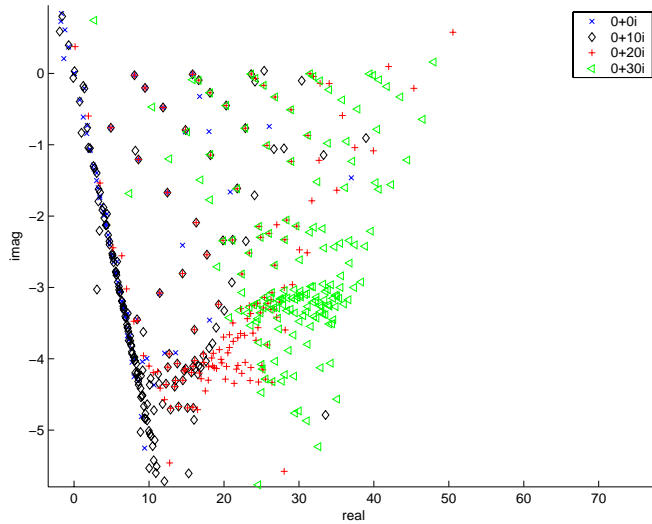


Figure 6.23: Eigenvalue computation with different complex shifts

Figure 6.23 shows that it is necessary to work with complex shifts. So for the following two figures 6.24 and 6.25 a shift of $30i$ is taken. The eigenvalue solver is an Arnoldi solver onto $(A - \text{shift}.B)^{-1}Bu = i\omega u = \lambda u$. The Inverse matrix is computed with the sparse solver PARDISO (see [22]). For Figure 6.23 the polynomial order of the Finite Element basis functions is 8 and the dimension of the Krylov space (for the Arnoldi) is 200.

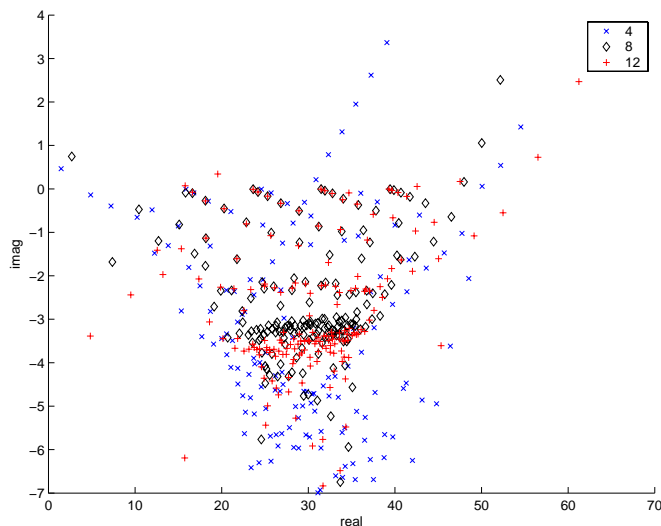


Figure 6.24: Different orders p of the FE basis functions

In Figure 6.24 the Finite Element basis functions of polynomial order $p = 4, 8$ and 12

are compared. With lower order (here 4) there are artificial PML lines, which vanish with higher order. Order 8 gives already good results, but if α increases while the order p stays the same, these artificial eigenvalues appear again, see the left picture in Figure 6.25.

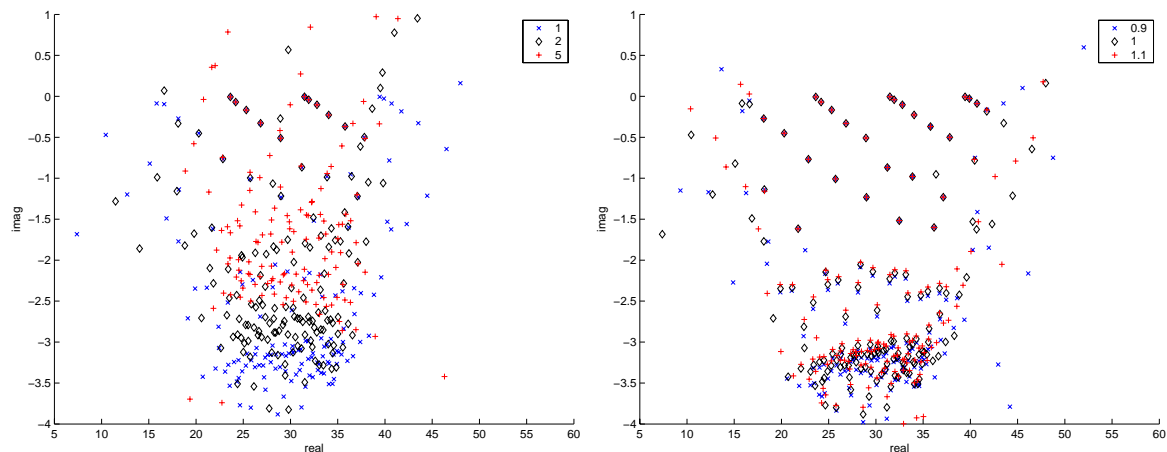


Figure 6.25: Different α , $s = 30i$

Changing α a little bit, see second picture in Figure 6.25, gives a really good distinction of artificial and physical relevant eigenvalues. All interesting eigenvalues do not change with a varying α , the others do. So exact mathematical derivation seems to be a good strategy for the distinction between artificial and relevant eigenvalues.

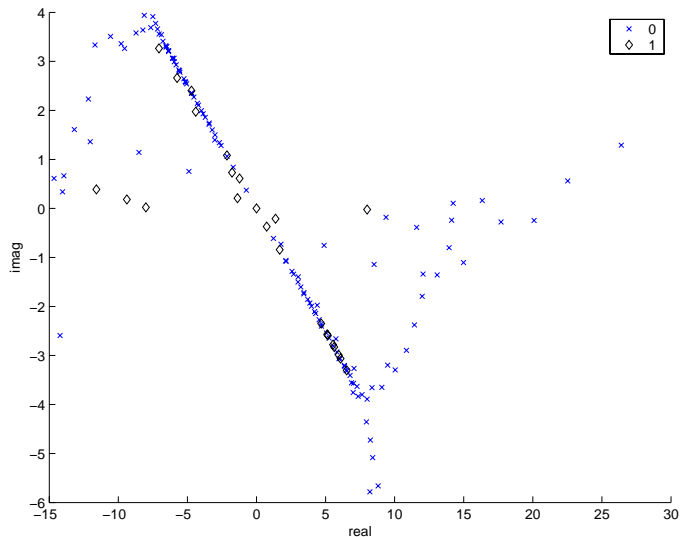


Figure 6.26: Exact differentiation with $\alpha = 1$ and no shift

Unfortunately even exact differentiation does not work well here, see Figure 6.26. Here very high values for

$$\frac{\partial \lambda}{\partial \alpha} = \frac{u^T (\partial_\alpha A - \lambda \partial_\alpha M) u}{u^T M u}, \quad (6.45)$$

distort the result.

The reason for these high values is that $u^T M u$ is very small $\approx 10^{-20}$, $u^T A' u$ rather large $\approx 10^{-3} - 10^{-5}$ and $u^T M' u$ is around $\approx 10^{-23}$, and therefore $\lambda u^T M' u \approx 10^{-20} - 10^{-23}$. So $\frac{\partial \lambda}{\partial \alpha}$ depends mainly on $\partial_\alpha A$.

As a condition

$$\left| \frac{\partial \lambda}{\partial \alpha} \right| < \epsilon, \quad (6.46)$$

with ϵ the huge value $4 \cdot 10^{15}$ is taken. Remember that with the PML method alone only an $\epsilon = 8$ has to be needed. The eigenvalues fulfilling this condition (\diamond) are not always the interesting ones. But it helps a lot to apply shifts, see Figure 6.27. There are still some artificial eigenvalues fulfilling this condition but less than before.

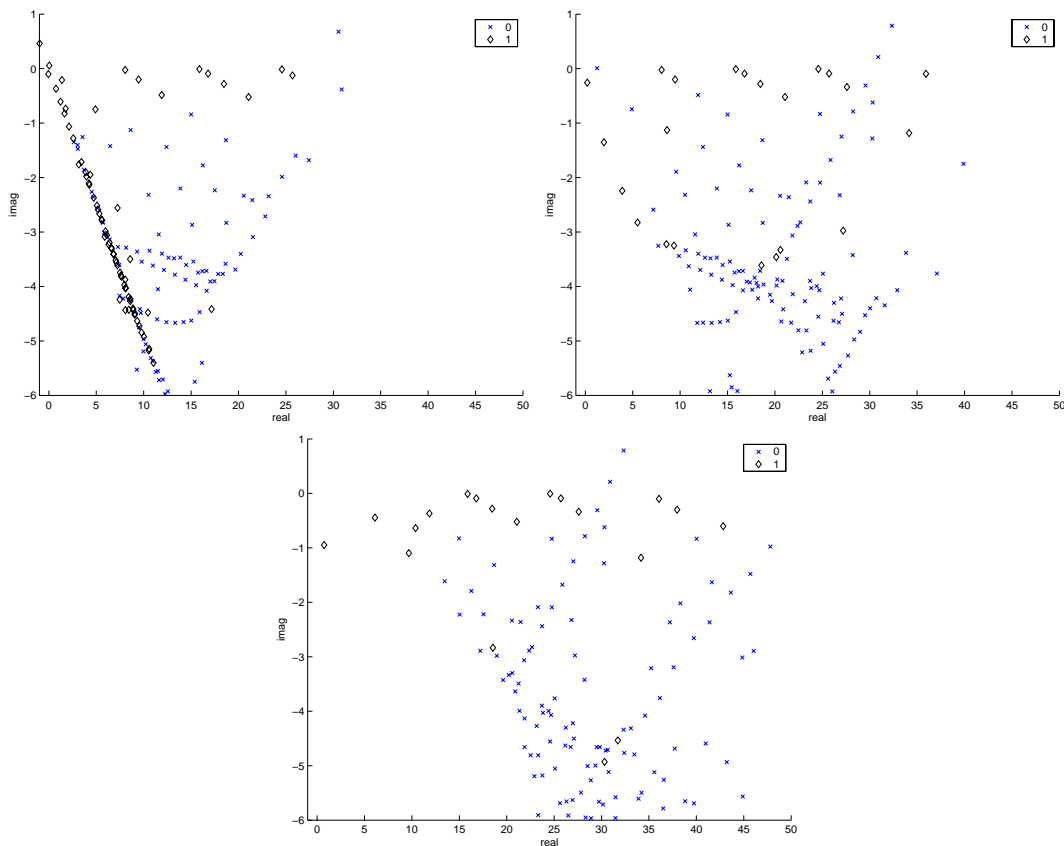


Figure 6.27: Exact differentiation with $\alpha = 1$ and some shifts $s = 10i$ (on the left top), $s = 20i$ (on the right top) and $s = 30i$ (on bottom) and order $p = 4$

Finally it can be said that the above condition (6.46) combined with shifting results in a rather good method to distinguish between artificial and interesting eigenvalues. In this case (with this special geometry) nothing more can be attained, but see the next Chapter - especially the last Section - for more interesting results.

Chapter 7

Example: Slat Cove of an Aeroplane

In this Chapter a special geometry is regarded. The PML method, wavefactorization and its combination are tested and discussed on this special geometry, which is provided by DLR, see also [18], [24].

7.1 Geometry

Consider the wing of an aeroplane (cut lengthwise to make it two dimensional) with a slat cove as shown on the left in Figure 7.1.

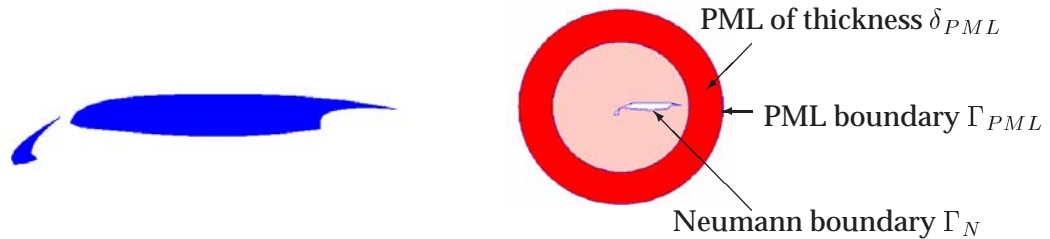


Figure 7.1: Geometry of the wing and the surrounding PML

This object is inside a circle of the radius r_{PML} , from where the PML begins. The thickness of the PML is δ_{PML} . All in all, the whole computational domain is a circle with radius $r_{PML} + \delta_{PML}$, where the slat cove is arranged as shown in the right picture of Figure 7.1.

7.2 PML Method

For derivation of the method see Chapter 4 and the last chapter for the exact equations. The only difference to the problem in Chapter 6 is now that the Neumann boundary is the boundary of the slat cove and the PML Dirichlet boundary is placed at the circle with radius $r_{PML} + \delta_{PML}$.

Meshing with NETGEN and solving with NGSolve gives eigenfrequencies ω as shown in Figure 7.2. There are different PML parameters α used, and it is seen that a large α make a better distinction between artificial and interesting eigenvalues possible. The interesting ones are those on the horizontal line on top of the picture.

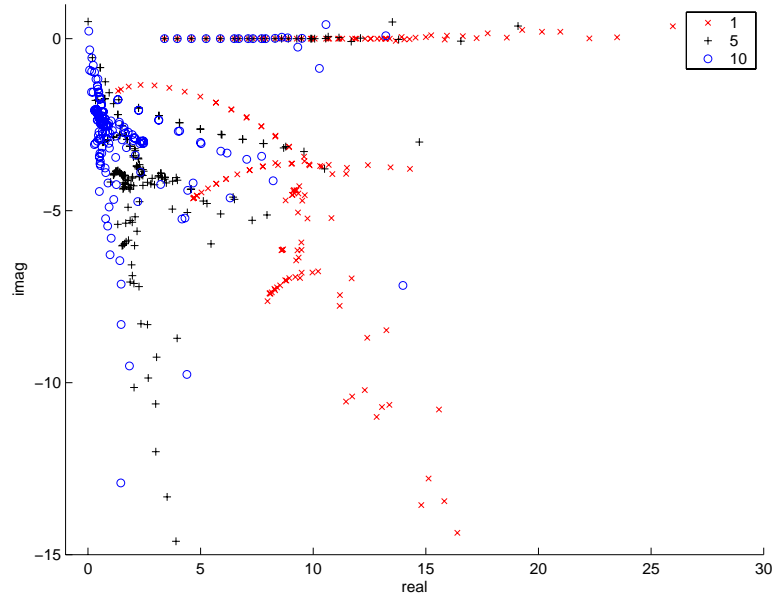


Figure 7.2: Eigenvalues obtained with order $p = 8$ and various $\alpha = 1, 5, 10$

Shifting alone without changing α gives no distinction but more eigenvalues on top, see Figure 7.3.

Finally exact differentiation is used. Those eigenvalues fulfilling $\frac{\partial \lambda}{\partial \alpha} < \epsilon = 0.01$ are marked with a diamond (\diamond) in Figure 7.4. It is clearly seen that this condition works very good here, unlike in Section 6.3.2.

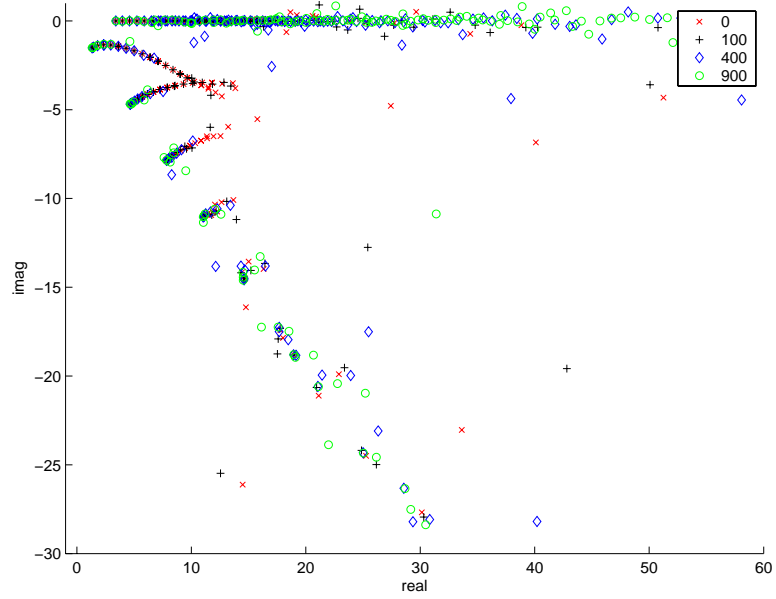


Figure 7.3: Eigenvalues obtained with various shifts

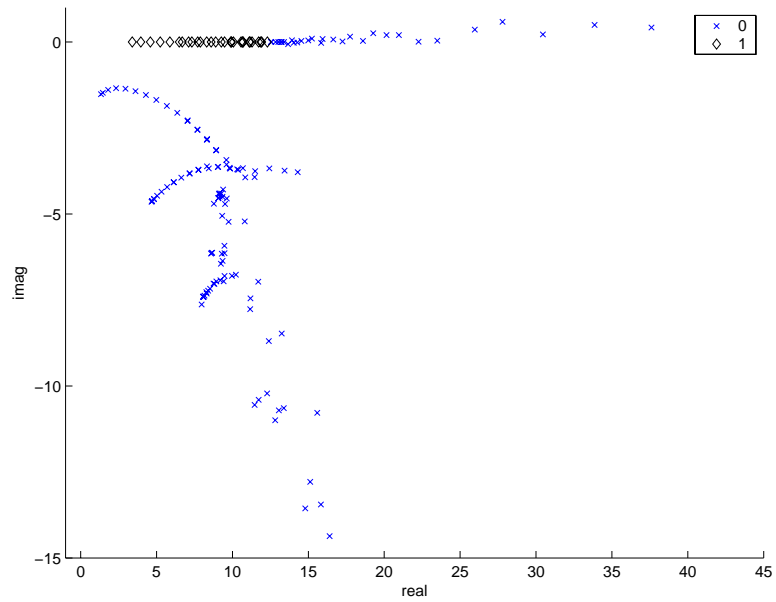


Figure 7.4: Interesting eigenvalues (\diamond) with $\epsilon = 0.01$

7.3 Wavefactorization

The domain is the same as before, but $\Gamma_{PML} = \Gamma_{Som}$ and no PML is needed. The following Figure 7.5 shows the eigenfrequencies ω obtained by wavefactorization and some interesting eigen modes.

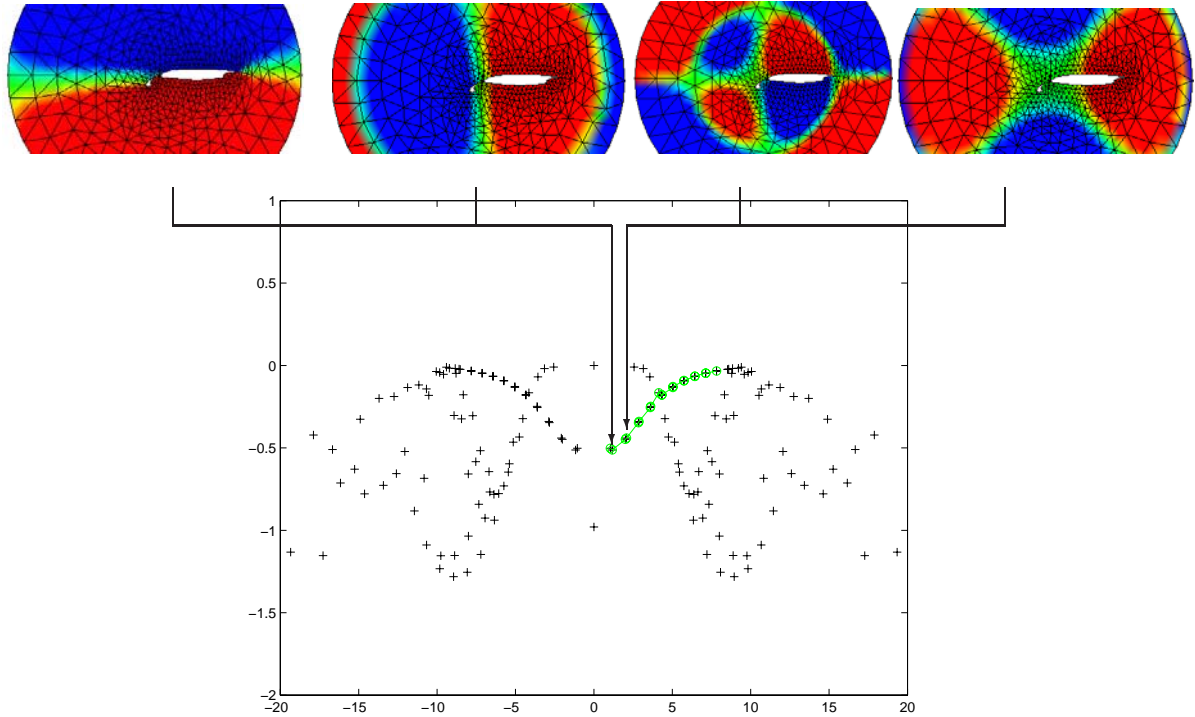


Figure 7.5: ω 's and some modes obtained by wavefactorization

The interesting eigenvalues are those pairs circled in green. They have positive real part ($Re(\omega) > 0$) and negative imaginary part ($Im(\omega) < 0$). The first two pairs are shown in the above modes. Clearly the connection between each mode of one pair is seen.

As seen in Chapter 6 changing the radius slightly gives some kind of distinction, so let's try this. Here only δ_{PML} is changed, not r_{PML} . For the results see Figure 7.6.

Obviously the double eigenfrequencies on the curved lines are interesting, which is true. Still there are some artificial eigenvalues that don't change if the radius is changed, i.e. look at $\omega = 0$ or $\omega = -i$ or those on top with nearly zero imaginary part, near the origin. Thus other approaches have to be tried.

At last the mesh is refined at an edge, see the right picture of Figure 7.7. Here the boundary has been refined and thus the mesh touching this boundary part is also refined. The left picture in 7.7 shows the computed ω 's. The refined mesh has consequences on those eigenfrequencies ω with the absolute value of their real part bigger than 15 and their imaginary part bigger than zero. In short only the ω 's on the outside are affected.

So wavefactorization alone results in no mathematical strategy to distinguish between important and artificial eigenvalues. Therefore it is combined with the PML method, see the next Chapter.

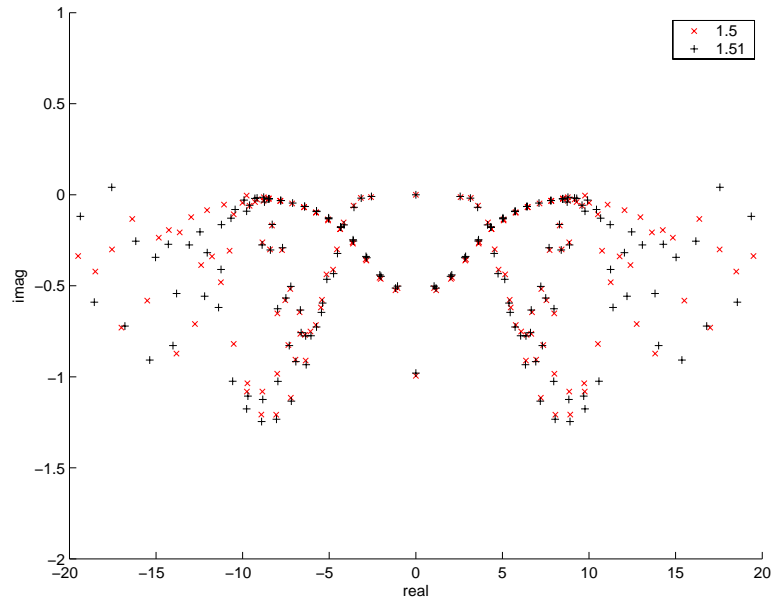


Figure 7.6: ω 's obtained with different radius $r_{PML} + \delta_{PML} = 1.5$ and 1.51

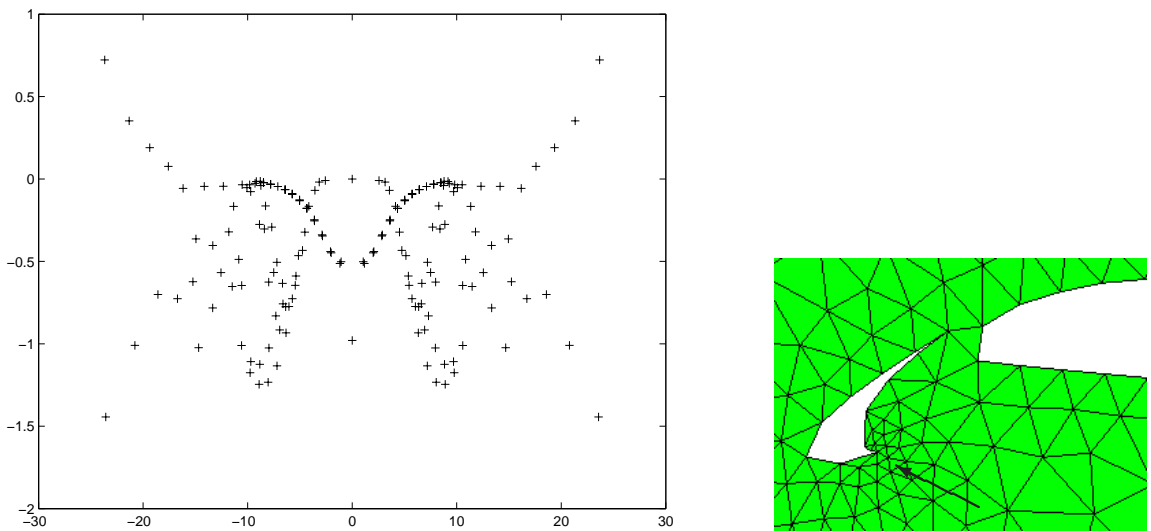


Figure 7.7: Eigenvalues computed with a refined mesh (left) and the edge that is refined (right)

7.4 Wavefactorization and PML Method combined

The same domain as with the PML method is taken.

First various values for the PML parameter α are tested, see Figure 7.8. A large α moves the PML dependent eigenvalues away from the interesting ones. So different α 's are responsible for the distinction.

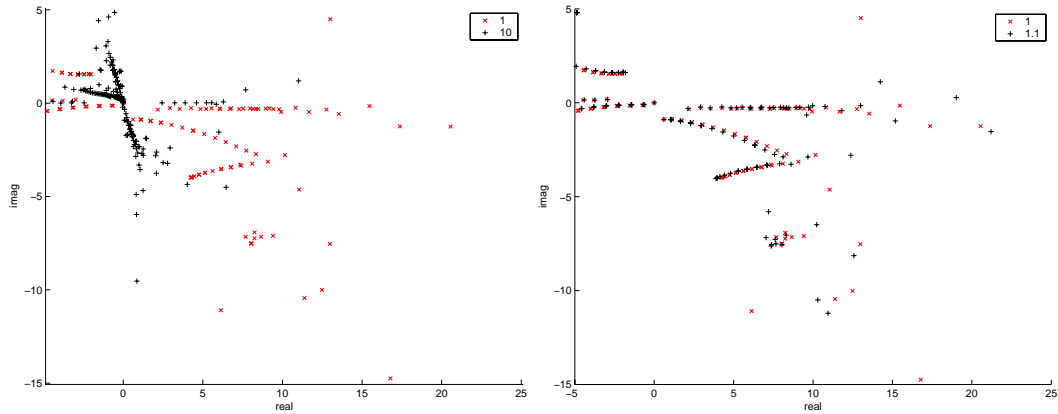


Figure 7.8: Eigenfrequencies ω computed with $\alpha = 1, 10$ (left) and $\alpha = 1, 1.1$ (right)

Evidently those eigenfrequencies on the horizontal line on top of the picture are the interesting ones, see Figure 7.9 for the eigen modes. At the above pictures order $p = 4$ is used. Increasing the order up to $p = 8$ affects the ω 's not much, see Figure 7.9.

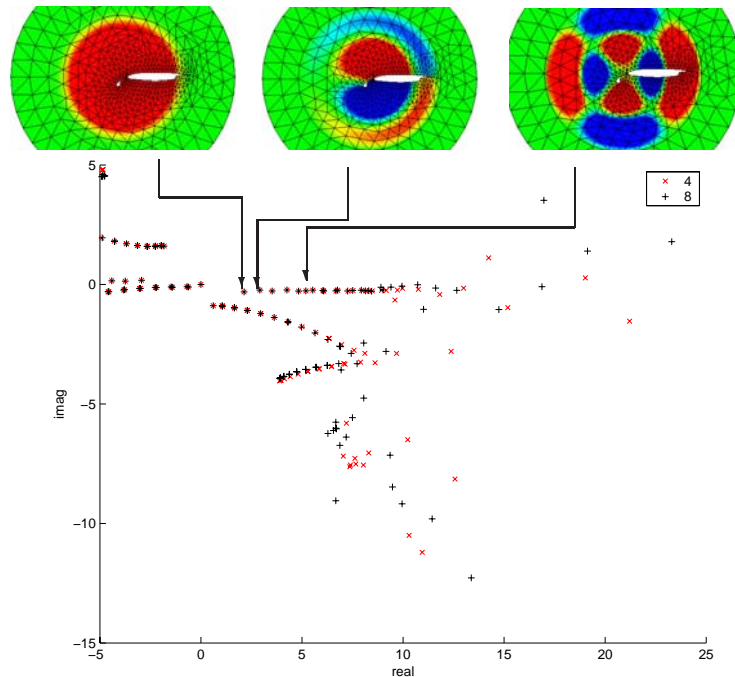


Figure 7.9: ω 's computed with order $p = 4$ and $p = 8$ and some interesting eigen modes

Since increasing the order gives no further interesting eigenvalues complex shifts are suggested, for the result see Figure 7.10.

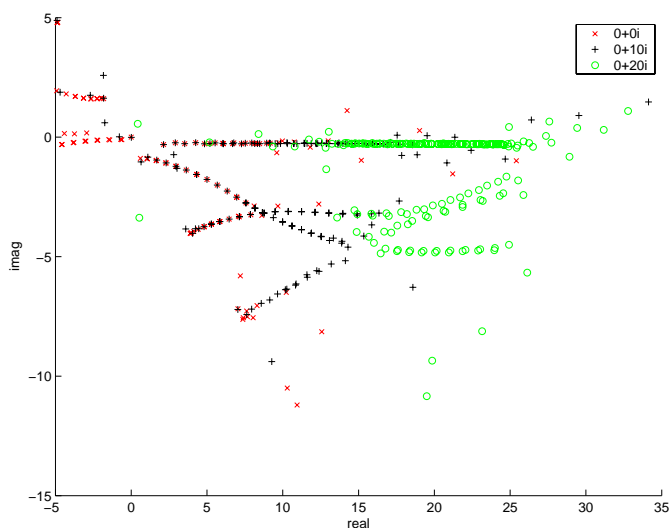


Figure 7.10: Eigenfrequencies computed with various shifts $s = 0, 10i$ and $s = 20i$ ($\alpha = 1.1$)

Shifting increases the number of interesting ω 's computed. Let's see what happens if a large α and shifting is applied. The first should affect onto the distinction quality, the latter on the number of eigenvalues obtained, see Figure 7.11.

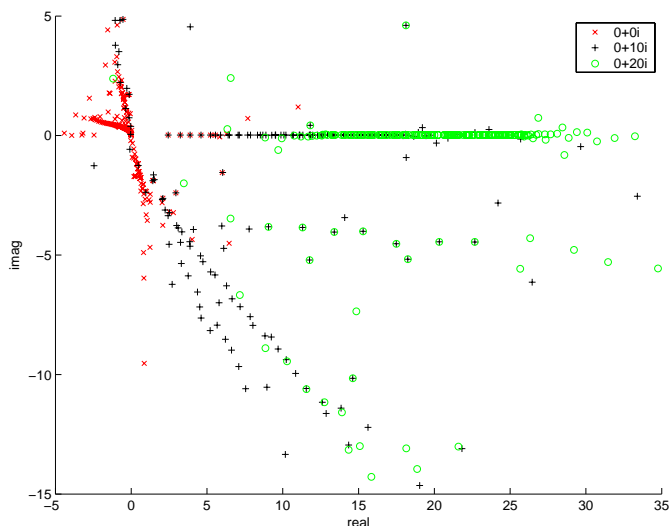


Figure 7.11: Eigenfrequencies computed with various shifts $s = 0, 10i$ and $s = 20i$ and $\alpha = 10$

As above mentioned shifting combined with some large PML parameter α provides the best results.

Finally test if the condition

$$\left| \frac{\partial \lambda}{\partial \alpha} \right| < \epsilon, \quad (7.1)$$

for some ϵ is fulfilled. Here the eigenvalue λ is the imaginary unit multiplied with the eigenfrequency ω , i.e. $\lambda = i\omega$.

At first no shift is applied and $\frac{\partial \lambda}{\partial \alpha}$ is computed for the various $\alpha = 1$ and $\alpha = 10$, see Figure 7.12. Those eigenfrequencies that fulfill condition (7.1) with an $\epsilon = 5$ are marked with a diamond (\diamond).

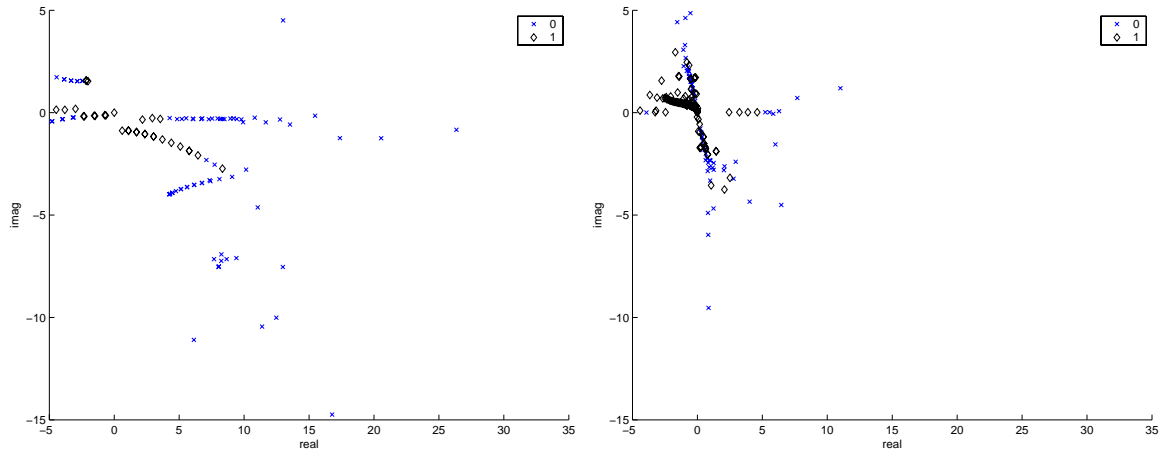


Figure 7.12: Exact differentiation $\alpha = 1$ (left) and $\alpha = 10$ (right) without shifts

Remember that the limit ϵ is far smaller than in Chapter 6, where ϵ was huge.

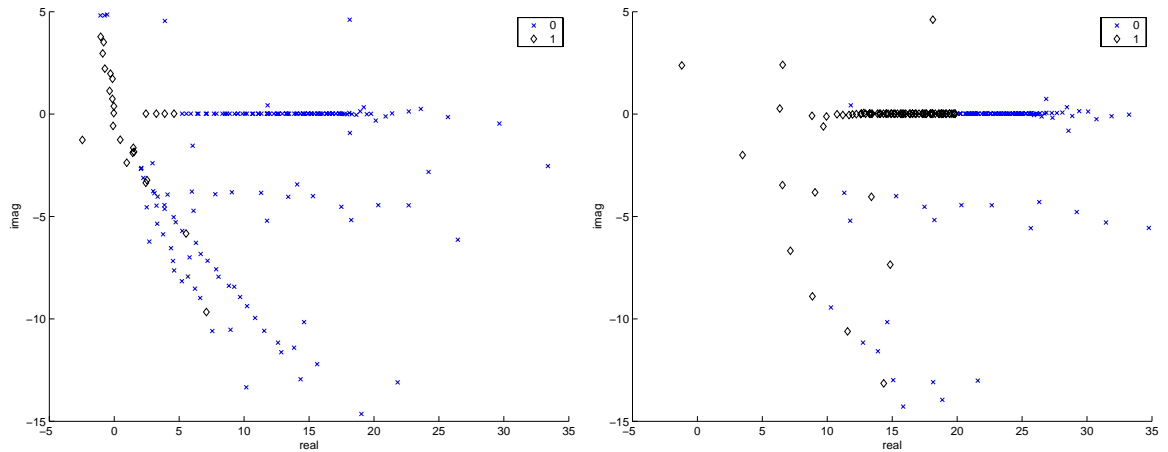


Figure 7.13: Exact differentiation $\alpha = 10$, shift $s = 10i$ ($\epsilon = 5$) and $s = 20i$ ($\epsilon = 20$)

Picking out those eigenvalues that fulfill the above condition (6.46) might not be the best idea. In Figure 7.13 and in Figure 7.12 it seems as if the interesting eigenvalues depend on ϵ , if shifts are used. Only those ω 's with real part smaller than ϵ are declared as interesting eigenvalues.

Is it possible that for the interesting eigenvalues the derivative $\frac{\partial \lambda}{\partial \alpha}$ is approximately ω ??

As the next Figure 7.14 shows the derivative is not ω , but the absolute values of both are similar. Now take the condition

$$\left| \left| \frac{\partial \lambda_j}{\partial \alpha} \right| - |\omega_j| \right| < \epsilon, \quad \text{for all } j = 1, \dots, m, \quad (7.2)$$

with m is the size of the Hessenberg matrix H_m . Finally the limit ϵ is a really small value, for the following pictures $\epsilon = 0.01$.

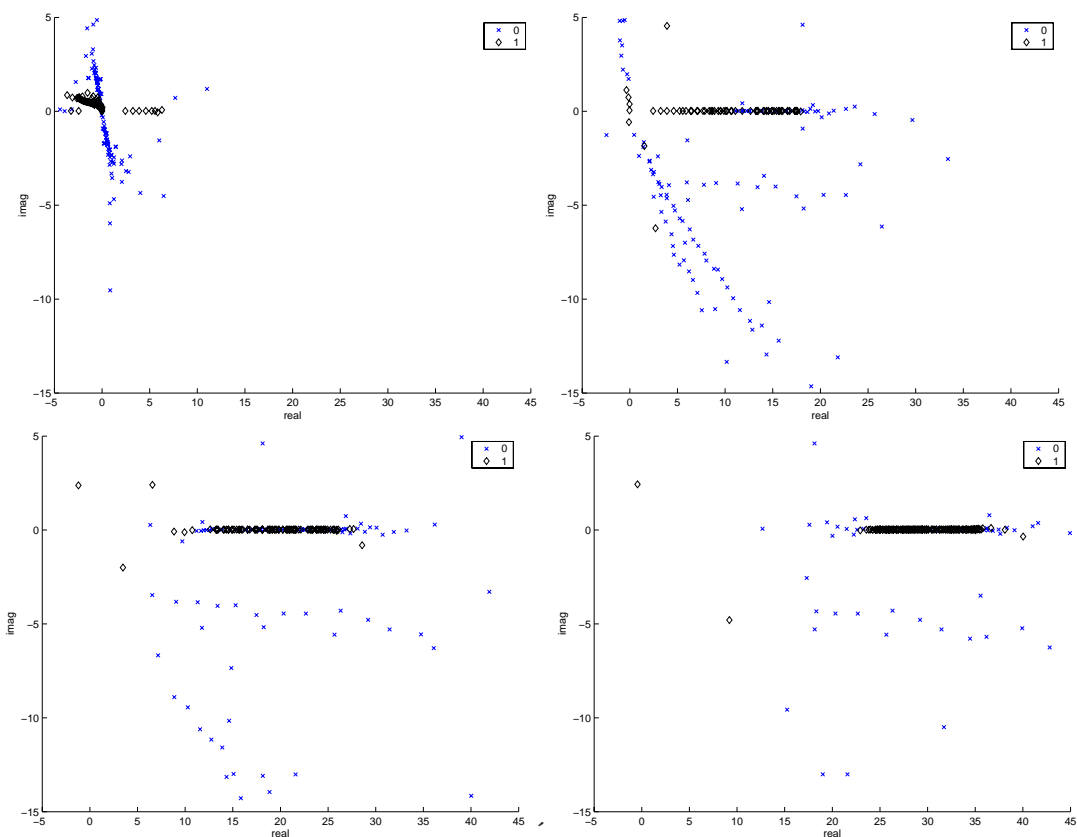


Figure 7.14: Eigenfrequencies satisfying condition (7.2) are marked \diamond , shifts $s = 0$ (left top), $s = 10i$ (right top), $s = 20i$ (left bottom) and $s = 30i$ (right bottom).

The second condition (7.2) works very good here with this special geometry. In Chapter 6 no connection between the derivative and ω has been found. Thus condition (7.2) works only with this special geometry and with the approach of using wavefactorization combined with PML.

Finally a mathematical strategy, i. e. condition (7.2), to pick out the interesting eigenvalues has been found (for this special problem). This is very important for further work, as can be seen in the next Chapter.

Chapter 8

The Eigenvalue Solver

This chapter gives a short summary over the Arnoldi eigenvalue solver, its advantages, which other solvers work in the special cases and about some deflation strategies, where the latter two topics are future work.

The start problem is a Generalized Eigenvalue Problem:

Find $u \in \mathbf{C}^n$ and $\lambda \in \mathbf{C}$:

$$Au = \lambda Bu, \quad (8.1)$$

with A, B matrices in $\mathbf{C}^{n \times n}$.

Since the Arnoldi procedure can only be applied on eigenvalue problems of the form $Mx = \mu x$, the above generalized eigenvalue problem has to be transformed.

The Matrix A from 8.1 is the stiffness matrix and therefore diagonal dominant. The Inverse of A should exist and can be applied on B . The problem is as follows.

Find $u \in \mathbf{C}^n$ and $\lambda \in \mathbf{C}$:

$$\underbrace{A^{-1}B}_M u = \frac{1}{\lambda} u, \quad (8.2)$$

with A, B as above.

If the PML-method is used both matrices A and B are complex symmetric. In case of wave-factorization those matrices are real and A is symmetric. Applying the combination of both methods gives complex matrices with A complex symmetric.

The inverse A^{-1} of a symmetric matrix A is symmetric but multiplied with another symmetric matrix B the result $A^{-1} B$ need not to be symmetric any more.

If some shift s is used then the following eigenvalue problem has to be solved

$$\underbrace{(A - sB)^{-1}B}_M u = \mu u, \quad (8.3)$$

and the eigenvalues λ are computed as $\lambda = \frac{1}{\mu} + s$.

Now the use of PARDISO [22] and LAPACK [19] are described. The package PARDISO (Parallel Sparse Direct Linear Solver) is needed to compute the inverse matrices $(A - sB)^{-1}$, $s \neq$

0, which is not symmetric if B is non symmetric. Otherwise the Linear Algebra Package LAPACK is able to compute the inverse matrix. Furthermore LAPACK computes the eigenvalues of the Hessenberg matrix H_m , which is obtained by the Arnoldi algorithm. Two routines in special are used: `zhseqr`, which computes the eigenvalues and Schur factorization of an upper Hessenberg matrix, using the multishift QR algorithm and `zhsein`, which computes specified right and/or left eigenvectors of an upper Hessenberg matrix by inverse iteration.

Both packages are provided by the Intel Math Kernel Library [21] for Windows. Here the MKL evaluation version 8.0 is used.

8.1 The Arnoldi Method

The Arnoldi method was first introduced as a direct algorithm for reducing a general matrix into upper Hessenberg form. It was later discovered that this algorithm leads to a good iterative technique for approximating eigenvalues of large sparse matrices.

The algorithm works for non-Hermitian matrices. It is most useful for cases when the matrix is large but matrix-vector products are relatively inexpensive to perform. This is the situation, for example, when M of problem (8.2) or (8.3) is large and sparse.

8.1.1 The algorithm

The Arnoldi method is an orthogonal projection method onto a Krylov subspace. The procedure can be essentially viewed as a modified Gram-Schmidt process for building an orthogonal basis of the Krylov subspace $\mathcal{K}^m(M, v)$.

The Arnoldi procedure reduces M to a Hessenberg matrix $H_m \in \mathbf{C}^{m \times m}$ with $m \ll n$ and then the LAPACK [19] routines compute the eigenvalues and -vectors of H_m .

The Arnoldi algorithm is as follows:

```

 $v_1 = v / \|v\|_2$            define start vector
for  $j = 1, 2, \dots, m$ 
   $w := Mv_j$ 
  for  $i = 1, 2, \dots, j$ 
     $h_{ij} = w^T v_i$        compute  $j$ 'th column of  $H_m$ 
     $w := w - h_{ij}v_i$      orthogonalize against previous vectors
  end for
   $h_{j+1,j} = \|w\|_2$ 
  if  $h_{j+1,j} < \epsilon$  then stop   breakdown
   $v_{j+1} = w / h_{j+1,j}$ 
end for

```

Table 8.1: The Arnoldi algorithm

The vectors $v_j, j = 1, \dots, m$ that form (by construction) an orthonormal basis of the Krylovsubspace $\mathcal{K}^m(M, v)$ are called the *Arnoldi vectors*.

After a look at the algorithm is it clearly seen that

$$Mv_j = \sum_{i=1}^{j+1} h_{ij}v_i, \quad j = 1, \dots, m. \quad (8.4)$$

Therefore if V_m denote the $n \times m$ matrix with the vectors v_1, \dots, v_m as columns and H_m the Hessenberg matrix with entries h_{ij} , the following relations hold

$$MV_m = V_m H_m + h_{m+1,m} v_{m+1} e_m^*, \quad (8.5)$$

$$V_m^* M V_m = H_m, \quad (8.6)$$

with V^* the complex conjugated matrix of V and e_m^* the m 'th canonical basis vector $e_m^* = (0, \dots, 0, 1)$. Now only the eigenvalues of the simpler matrix H_m have to be computed. This leads to the eigenvalue problem

$$H_m y = V_m^* M V_m y = \lambda y. \quad (8.7)$$

These eigenvalues λ_i are called the *Ritz (eigen)values*. The eigenvectors y_i of H_m that belong to the eigenvalues λ_i are transformed to the so called *Ritz approximate eigenvectors* by

$$u_i = V_m y_i. \quad (8.8)$$

The Ritz pairs $(\lambda_i, u_i), i = 1, \dots, m$ are approximations for eigenvalues λ and eigenvectors u of the original problem $Mu = \lambda u$.

If $h_{k+1,k}$ is smaller than ϵ (\approx zero) then v_{j+1} cannot be computed any more and the algorithm breaks down. But this is desirable, because in this case the subspace $\mathcal{K}^m(M, v)$ is invariant and the computed eigenvalues are exact. This does not happen often.

After reduction of M to a Hessenberg matrix H_m of size $m \times m$, LAPACK [19] computes all eigenvalues $\lambda_i, i = 1, \dots, m$ and eigenvectors $y_i, i = 1, \dots, m$ of H_m , transforms the eigenvectors to the Ritz vectors $u_i = V_m y_i$ and these u_i are the final eigenvectors, see Table 8.2.

This is different to the original Arnoldi eigenvalue solver, which computes the eigenpairs successively, one eigenpair after the other.

choose v_1

Arnoldi algorithm as in 8.1

store the arnoldi vectors in matrix $V_m = [v_1, \dots, v_m]$

$H_m y_i = \lambda_i y_i$ compute all eigenpairs $(\lambda_i, y_i), i = 1, \dots, m$ of H_m

$u_i = V_m y_i, i = 1, \dots, m$ transform the eigenvectors of H_m to those of M

Table 8.2: Computation of eigenvalues with Arnoldi algorithm

Now it is desirable that the interesting eigenvalues and their eigenvectors stay and the artificial eigenvalues are already picked out of the Krylov space during computation. Therefore some mathematical strategy is needed to distinguish between interesting and artificial

eigenvalues. Such a strategy has already been developed and tested if the PML method is used, see condition (7.1) or (7.2) . If

$$\left| \frac{\partial \lambda_j}{\partial \alpha} \right| < \epsilon, \quad (8.9)$$

holds for $\lambda_j = i\omega_j, j \in \Lambda$, then the eigenvalues of this set Λ of interesting eigenvalues and their eigenvectors $u_j, j \in \Lambda$ should not be computed any more. To avoid reconvergence to any eigenvalue of the desired subset Λ *deflation* is used, which is future work and will be described in the next Section.

8.2 Future Work on the Eigenvalue Solver

Here some suggestions how to improve the efficiency of the eigenvalue computation are discussed.

8.2.1 Deflation

There exist a variety of ways how to implement deflation, see [32], here only those useful in the above case are regarded.

Before any further explanation, some definitions have to be made.

Theorem

For any square Matrix $A \in \mathbb{C}^{n \times n}$ there exists a **Schur decomposition**

$$U^*AU = T = \begin{pmatrix} \lambda_1 & * & \dots & * \\ & \lambda_2 & \ddots & \vdots \\ & & \ddots & * \\ 0 & \dots & 0 & \lambda_n \end{pmatrix}, \quad (8.10)$$

with U a unitary matrix ($U^*U = I_n = UU^*$) and T an upper triangular matrix with the eigenvalues of A as diagonal entries. If A is hermite in addition, T is a diagonal matrix.

This well-known decomposition asserts that every square matrix A is unitarily similar to an upper triangular matrix T .

The Schur vectors u_j, j, \dots, n are the columns of U . They are not the eigenvectors, because

$$\sum_{j=1}^n A_{j,k}u_j = \sum_{j=1}^n T_{j,k}u_j = \lambda_k u_k + \sum_{j>k}^n T_{k,j}u_j, \quad k = 1, \dots, n. \quad (8.11)$$

Although Schur vectors are no eigenvectors they are important because they span an invariant subspace of A .

Definition: Invariant Subspace

X is a invariant subspace of the operator A if for all $x \in X$ holds that $Ax \in X$, i.e. AX is a subset of X .

For example: eigenvalues or Schur vectors span an invariant subspace.

If U_k represents the leading k columns of U (the first k Schur vectors), T_k the leading, principal $k \times k$ submatrix of T , then

$$AU_k = U_k T_k. \quad (8.12)$$

holds, which is called a *partial Schur decomposition*. Since the eigenvalues of A appear on the diagonal of T in any order, there exists always a partial Schur decomposition of A with the diagonal elements of T_k consisting of any specified subset of eigenvalues of A . Moreover, $\text{span}(U_k)$ is an invariant subspace of A for these eigenvalues.

Supposing c eigenpairs (λ_i, v_i) , $i \in \Lambda$ with v_i the corresponding Schur vectors have converged (are Ritz values and Ritz vectors) and fulfill condition (8.9).

One implementation, which fits in well with the Arnoldi procedure, is to work with a single basis v_i , $i = 1, \dots, m$ whose first c vectors are the above Schur vectors v_i , $i = 1, \dots, c$. Then choose a vector v_{c+1} which is orthogonal to v_i , $i = 1, \dots, c$ and of norm 1. Next $m - c - 1$ steps of an Arnoldi procedure are performed in which orthogonality of the vectors v_i , $i = c + 2, \dots, m$ against all previous vectors is enforced. This generates an orthogonal basis of the subspace

$$\text{span}(v_1, v_2, \dots, v_c, v_{c+1}, Av_{c+1}, \dots, A^{m-c-1}v_{c+1}). \quad (8.13)$$

Thus, the dimension of this modified Krylov subspace is constant and equal to m in general. Note that the Schur vectors associated with the eigenvalues v_i , $i = 1, \dots, c$ will not be touched in subsequent steps. They are sometimes referred to as *locked vectors*. Similarly, the corresponding upper triangular matrix corresponding to these vectors is also locked.

Another implementation is as follows:

Let

$$\Lambda_c = \text{diag}(\lambda_1, \dots, \lambda_c), \quad (8.14)$$

denote a quasi-diagonal matrix (a block diagonal matrix, whose blocks are of size 1×1 - corresponding to a real eigenvalue and 2×2 - corresponding to complex conjugate pair of eigenvalues) containing the converged eigenvalues and let

$$V_c = [v_1 | \dots | v_c], \quad (8.15)$$

be a matrix with the converged Schur vectors as columns. This deflation strategy requires to work with the matrix

$$M_c = M - V_c \Lambda_c V_c^*, \quad (8.16)$$

with $V_c \Lambda_c V_c^*$ the partial schur decomposition of M . Note that if $MU = UT$ is a Schur form of M , then

$$M_c U = MU - V_c \Lambda_c \underbrace{V_c^* U}_{E_c^*} = UT - V_c \Lambda_c E_c^* = U(T - E_c \Lambda_c E_c^*), \quad (8.17)$$

with $E_c = [e_1 | \dots | e_c]$ a matrix whose columns are the first c canonical basis vectors. From this it is evident that the eigenvalues of the deflated matrix M_c are related to those λ of M by

$$\{\lambda - \lambda_1, \lambda - \lambda_2, \dots, \lambda - \lambda_c, \lambda_{c+1}, \dots, \lambda_n\}. \quad (8.18)$$

Since the factor $(T - E_c \Lambda_c E_c^*)$ is a Schur form for A_c , the Schur vectors of the deflated matrix M_c are identical to those of M .

In fact there are two types of deflation:

1. **Locking**

If an eigenvalue λ is thought to be a member of the wanted set of eigenvalues, then it is wished to declare it so, to decouple the eigenpair (λ, u) and continue to compute the remaining eigenvalues with no further alteration of λ or u . This process is called locking.

2. **Purging**

If an eigenvalue is no member of the wanted set of eigenvalues, then it is wished to decouple and remove the eigenpair (λ, u) from the current subspace spanned by the Arnoldi vectors. This process is called purging.

8.3 Other Eigenvalue Solver

The computation and selection of interesting eigenvalues will require further work. Interesting methods are the *Block Arnoldi Method* described in [32], p. 185, or the *Shift and Invert Block Arnoldi method* proposed by D. L. Harrar [16], which is similar to the Arnoldi method with the difference that a block of Arnoldi vectors can be computed. This method is also highly favorable if there are clustered or multiple eigenvalues.

In the special case where PML (alone) is used, the complex symmetry of the resulting FE matrices can be exploited. Here the *Jacobi Davidson for complex symmetric Matrices* by P. Arbenz [2] is recommended.

Chapter 9

Conclusion and Future Work

In this thesis the Helmholtz eigenvalue problem on infinite domains has been discussed. Starting from the governing equations, a mathematical formulation has been derived and afterwards discretized with the Finite Element method.

Furthermore two methods (PML and wavefactorization) to terminate infinite domains, on which the Helmholtz problem is solved, have been discussed.

The aim was to find a strategy to pick out the important eigenvalues from the artificial ones.

Both PML and wavefactorization provide interesting results, although with the latter no strategy for the distinction between interesting and artificial eigenvalues of the problem is achieved. Additionally wavefactorization reacts sensitively onto the mesh partition (in the one dimensional case).

Thus they are combined and by this combination a condition for such a distinction has been found. This condition works good for the landing gear model, see Chapter 6 and perfectly well for the slat cove model, see Chapter 7.

Hence some future work is to incline this condition into the eigenvalue solver, as already said in the last Chapter.

Another promising method is *Reduced Integration* (if PML is used), see Section 6.1.1. Here only the one dimensional case has been considered, but this might be extended to higher dimensions.

Further more this work can be extended into solving the Helmholtz eigenvalue problem on *three dimensional* domains.

Appendix A

List of Notations

| | |
|--------------------------------------------------------------|---------------------------------------------------------------------------------------------------------|
| $v \cdot w = v^T w$ | dot product in \mathbf{C}^d , $v \cdot w = \sum_{i=1}^d v_i w_i$ |
| z^T | transposed vector of vector z |
| A^T | transposed matrix of matrix A |
| A^* | hermite (complex conjugated) matrix of matrix A ($a_{ij} = \overline{a_{ji}} \forall i, j$) |
| $\bar{v} = \overline{v_{re} + i v_{im}} = v_{re} - i v_{im}$ | complex conjugated number of v |
| $i = \sqrt{-1}$ | complex unity |
| I_n | Identity matrix $\in \mathbf{R}_n^n$ |
| $diag(\lambda_1, \dots, \lambda_n)$ | diagonal matrix $\in \mathbf{R}_n^n$ with entries $\lambda_1, \dots, \lambda_n$ in the diagonal row |
| ∂_k | short hand for $\frac{\partial}{\partial x_k}$ |
| ∇ | gradient, $\nabla u = \begin{pmatrix} \partial_1 u \\ \vdots \\ \partial_d u \end{pmatrix}$ |
| div | divergence, $\text{div } u = \sum_{i=1}^d \partial_i u_i = \nabla \cdot u$ |
| Δ | Laplacian operator, $\Delta u = \sum_{i=1}^d \frac{\partial^2 u}{\partial x_i^2} = \nabla \cdot \nabla$ |
| $\nabla \cdot n = \frac{\partial}{\partial n}$ | normal derivative, $\partial_n u = \nabla u \cdot n = \sum_{i=1}^d \frac{\partial u}{\partial x_i} n_i$ |
| n | normal unit vector, $n = \frac{\vec{x}}{ x }$ |
| $ x $ | absolute value of $x \in \mathbf{C}$ |
| $ v = \ v\ $ | euclidean norm of vector v |

| | |
|---------------------------|---------------------------------------------------------------------------------------------------------|
| $!$ | faculty, $n! = n \cdot (n - 1) \cdot \dots \cdot 2 \cdot 1$ |
| $\int_{\Omega} f dx$ | Lebesgue integral of a scalar field $f(x)$ over the domain Ω |
| $\int_{\Gamma} f ds_x$ | line or surface integral of a scalar field $f(x)$ over the manifold Γ |
| $\overset{\circ}{\Omega}$ | interior of Ω without boundary $\Gamma = \partial\Omega$ |
| $\overline{\Omega}$ | Ω with boundary $\Gamma = \partial\Omega$ |
| o, O | O and big O notation, Landau symbols |
| | $f(x) = o(g(x)) \Leftrightarrow \frac{f(x)}{g(x)} \rightarrow 0 \quad \text{for } x \rightarrow \infty$ |
| | $f(x) = O(g(x)) \Leftrightarrow \exists c \in \mathbf{R} : \frac{f(x)}{g(x)} < c \quad \forall x$ |

Appendix B

The Finite Element Method

A detailed introduction in Finite Element Methods can be found in [4] and [7].

The Eigenvalue Problem

Find $u \in V_0$:

$$a(u, v) = \lambda b(u, v) \text{ for } v \in V, \quad (\text{B.1})$$

with $a(u, v)$ and $b(u, v)$ bilinearform, V_0 the trial space (u the trial function) and V the test space (with test functions v) usually Hilbertspaces is considered.

If this problem is seen as a boundary value problem with fixed λ and zero right hand side, then the theory of Fredholm is needed to prove existence, uniqueness and stability of solutions u .

B.1 The Galerkin Ritz Method

Due to the Galerkin method, a sequence of finite dimensional subspaces $V_h \subset V$ is assumed and for each of it a discrete problem is associated:

Find $u_h \in V_h, \lambda \in \mathbf{C}$

$$a(u_h, v_h) = \lambda_h b(u_h, v_h). \quad (\text{B.2})$$

The index h stands for the discretization parameter and indicates that with $h \rightarrow 0$ the discrete solution pair (u_h, λ_h) converges against the exact solution pair (u, λ) .

The space V_h is of finite dimension and therefore has a finite basis. Let N_h denote the dimension of V_h and ϕ_i the basis functions, i.e. $V_h = \text{span}\{\phi_i : i = 1, \dots, N_h\}$. Consequently the solution u_h is of the following form

$$u_h(x) = \sum_{i=1}^{N_h} u^i \phi_i(x), \quad (\text{B.3})$$

with coefficients $u^i \in \mathbf{C}$. With some definitions

$$\underline{u}_h := (u^i)_{i=1}^{N_h} \in \mathbf{C}^{N_h}, \quad (\text{B.4})$$

$$A_{h \ i,j} := a(\phi_i, \phi_j), \quad A_h \in \mathbf{C}^{N_h \times N_h}, \quad (\text{B.5})$$

$$B_{h \ i,j} := b(\phi_i, \phi_j), \quad B_h \in \mathbf{C}^{N_h \times N_h}, \quad (\text{B.6})$$

the above variational eigenvalue problem transforms into a discrete eigenvalue problem of the form

$$\text{Find } \underline{u}_h \in \mathbf{C}^{N_h}, \lambda_h \in \mathbf{C} \quad A_h \underline{u}_h = \lambda B_h \underline{u}_h. \quad (\text{B.7})$$

This form is equivalent to the original discrete problem B.2. To get from B.2 to the Galerkin system B.7 the so-called *Ritz-Isomorphism*

$$u_h \in V_h \longleftrightarrow \underline{u}_h \in \mathbf{C}^{N_h}, \quad (\text{B.8})$$

is used. This isomorphism is a one-to-one function between the discrete variational problem and the Galerkin problem.

But how to construct these discrete spaces V_h to be conforming subspaces of some Hilbert spaces V . This will be discussed in the next Section.

B.2 Finite Elements - FE

Definition: *Triangulation*

Let $\Omega \in \mathbf{R}^d$ be an open, bounded domain with Lipschitz continuous boundary. \mathcal{T}_h is called a *Triangulation* of Ω , if it consists of subsets T which satisfy the following conditions:

1. $\bar{\Omega} = \bigcup_{T \in \mathcal{T}_h} T$
2. Each $T \in \mathcal{T}_h$ is a closed domain with a nonempty connected interior $\overset{\circ}{T}$.
3. Each $T \in \mathcal{T}_h$ has a Lipschitz continuous boundary ∂T .
4. Distinct $T_i, T_j \in \mathcal{T}_h$ have intersection of zero measure, i.e. $\overset{\circ}{T}_i \cap \overset{\circ}{T}_j = \emptyset$ for $i \neq j$.

The **Finite Element method** is a special case of Galerkin-Ritz with three major aspects:

1. A Triangulation \mathcal{T}_h in the above sense of the computational domain Ω is used.
2. The Finite Element space V_h is constructed such that for each $T \in \mathcal{T}_h$ the restriction $v_h \in V_h$ is a polynomial, i.e. $v_h|_T \in \mathcal{P}^p(T)$ for some polynomial order $p \in \mathbf{N}$.
3. It exists a canonical basis of V_h that has small support and can be easily described.

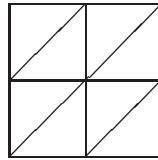


Figure B.1: A simple triangulation of a square

The Finite Elements $T \in \mathcal{T}_h$ should be simple. In the one dimensional case they are intervals of length h , in 2D they are triangles (see Figure B.1) or squares on any polygonal domain Ω and in 3D they are tetrahedrons and hexahedrons only.

B.3 Courant Elements

First the Courant elements are discussed in the one dimensional case and afterwards this is extended to higher dimensions.

B.3.1 Courant Elements on Intervals

Linear Courant Elements

Due to introduction of vertices (also called nodes) $x_j, j = 0, 1, \dots, N_h$ on the domain $\Omega = [0, 1]$ with $0 = x_0 < x_1 < \dots < x_{N_h} = 1$ a triangulation or partition \mathcal{T}_h of Ω is received. The subintervals $T_k = [x_{k-1}, x_k]$ for $k = 1, \dots, N_h$ are the elements. The precision h of the partition \mathcal{T}_h is given by

$$h = \max_{k=1, \dots, N_h} h_k \quad \text{with } h_k = |x_k - x_{k-1}|. \quad (\text{B.9})$$

Let P^k denote the set of one-dimensional polynomials of degree smaller or equal k . For the conforming finite element space V_h only linear polynomials are taken, extension to higher degrees will be discussed later. Now V_h is defined as

$$V_h = \{v \in C(\bar{\Omega}) : v|_T \in P^1 \text{ for all } T \in \mathcal{T}_h\}. \quad (\text{B.10})$$

For conforming finite element spaces holds $V_h \subset V = H^1(\Omega)$. The next step is to find basis functions that span V_h and have small support, e.g. the two surrounding elements. The nodal basis functions $\phi_i \in V_h, i = 0, \dots, N_h$ are defined by

$$\phi_i(x_j) = \delta_{ij} \quad \text{for } i, j = 0, \dots, N_h. \quad (\text{B.11})$$

Such a basis is called *nodal basis*. The functions ϕ_i are affine linear functions on elements $T_i, T_{i+1} \in \mathcal{T}_h$ (small support), they have the value 1 on the node x_i and are zero on the other nodes. They look like little hats, see Figure B.2 and are therefore also called *hat functions*.

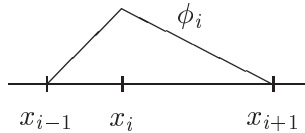


Figure B.2: Basis function ϕ_i of V_h

The basis functions ϕ_i are linearly independent and every function $v_h \in V_h$ has the special representation

$$v_h(x) = \sum_{i=0}^{N_h} v_i \phi_i(x) \quad \text{with } v_i = v_h(x_i). \quad (\text{B.12})$$

Here the expression *nodal basis* explains itself: the unknowns v_i are the function values on the nodes $v_i = v_h(x_i)$.

Since $a(\phi_i, \phi_j) = 0 = b(\phi_i, \phi_j)$ if the basis functions ϕ_i, ϕ_j have disjoint support, the stiffness matrix A and the mass matrix B are sparse. Both matrices are not computed by evaluating $a(\phi_i, \phi_j)$ or $b(\phi_i, \phi_j)$ (globally), but by assembling over the elements (locally). That means

that the integral of the bilinearforms a and b is split into the sum of all elements T of the triangulation \mathcal{T}_h

$$a(\phi_i, \phi_j) = \int_{\Omega} \nabla \phi_i \nabla \phi_j = \sum_{T \in \mathcal{T}_h} \int_T \nabla \phi_i \nabla \phi_j, \quad (\text{B.13})$$

$$b(\phi_i, \phi_j) = \int_{\Omega} \phi_i \phi_j = \sum_{T \in \mathcal{T}_h} \int_T \phi_i \phi_j. \quad (\text{B.14})$$

By iteration over all T the single integrals are computed and then added. These single integrals can be efficiently evaluated using the concept of *reference element*. In the course of this a *reference element* Δ has to be defined: $\Delta = [0, 1]$.

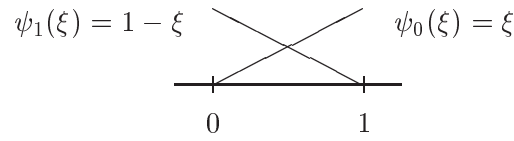


Figure B.3: Reference element $\Delta = [0, 1]$ with the local ansatz functions ψ_0, ψ_1

Every $T_k, k = 1, \dots, N_h$ can be written as an affine linear transformation f_k of Δ .

$$f_k : \Delta \rightarrow T_k, \quad f_k(\xi) = x_{k-1} + \xi(x_k - x_{k-1}), \quad (\text{B.15})$$

for the one dimensional case. The single integrals over the element T_k transform into

$$\begin{aligned} \int_{T_k} \nabla \phi_i(x) \nabla \phi_j(x) dx &= \int_{\Delta} \nabla \phi_i(f_k(\xi)) J^{-1} \nabla \phi_j(f_k(\xi)) J^{-T} \det(J) d\xi \\ &= \int_{\Delta} \nabla (\phi_i \circ f_k)(\xi) J^{-1} \nabla (\phi_j \circ f_k)(\xi) J^{-T} \det(J) d\xi \end{aligned} \quad (\text{B.16})$$

$$\begin{aligned} \int_{T_k} \phi_i(x) \phi_j(x) dx &= \int_{\Delta} \phi_i(f_k(\xi)) \phi_j(f_k(\xi)) \det(J) d\xi \\ &= \int_{\Delta} (\phi_i \circ f_k)(\xi) (\phi_j \circ f_k)(\xi) \det(J) d\xi \end{aligned} \quad (\text{B.17})$$

with J the Jacobi matrix of the function f_k . Only two local Ansatz functions $(\phi_k \circ f_k)$ respectively $(\phi_{k-1} \circ f_k)$ are not equal zero. Thus $\psi_0 := (\phi_k \circ f_k)$ and $\psi_1 := (\phi_{k-1} \circ f_k)$. In 2D already three and in 3D four linear ansatz functions are not equal zero.

Courant Elements of Order p

For Courant elements of higher degree only higher ansatz functions have to be provided (see figure B.4). In fact, $p + 1$ ansatz functions have to be provided for Courant elements of degree p : $\psi_i, i = 0, 1, 2, \dots, p$. Here *hierarchic* instead of *standard* reference elements are used, for details for both elements see [11]. In short the standard finite element shape functions are given by a set of Lagrange polynomials. For each degree p a separate set of polynomials have to be defined. For higher degree of hierarchic shape functions only polynomials have to be added.

The set of hierarchic one-dimensional shape functions on the reference element $\Delta = [-1, 1]$ was first introduced by Szabó and Babuška [27] and is given by

$$N_0(\xi) = \frac{1}{2}(1 - \xi), \quad (\text{B.18})$$

$$N_1(\xi) = \frac{1}{2}(1 + \xi), \quad (\text{B.19})$$

$$N_i(\xi) = \sqrt{\frac{2i-1}{2}} \int_{-1}^{\xi} P_{i-1}(x) dx = \frac{1}{\sqrt{4i-2}}(P_i(\xi) - P_{i-2}(\xi)), \quad i = 2, \dots, p, \quad (\text{B.20})$$

where P_i denote the *Legendre polynomials* that are defined by the following recurrence

$$P_0(x) = 1, \quad (\text{B.21})$$

$$P_1(x) = x, \quad (\text{B.22})$$

$$P_i(x) = \frac{2i-1}{i}xP_{i-1}(x) - \frac{i-1}{i}P_{i-2}(x). \quad (\text{B.23})$$

The *integrated Legendre polynomials*

$$L_i(\xi) = \int_{-1}^{\xi} P_{i-1}(x) dx, \quad (\text{B.24})$$

are zero on the boundary $\{-1, 1\}$ of the reference element, which makes the hierarchic nodal shape functions N_i , see B.20, also zero on the boundary. Because this quality N_i are also called *internal shape functions*. The L_2 orthogonality of the Legendre polynomials P

$$\int_{-1}^1 P_i(\xi)P_j(\xi) d\xi = \delta_{ij}, \quad (\text{B.25})$$

forces the hierarchic basis function N_i to be also orthogonal in H^1

$$\int_{-1}^1 \frac{\partial N_i(\xi)}{\partial \xi} \frac{\partial N_j(\xi)}{\partial \xi} d\xi = \delta_{ij}, \quad \text{for } i > 1, j > 3 \text{ or for } j > 1, i > 3. \quad (\text{B.26})$$

Figure B.4 shows some hierarchic one dimensional shape functions on the reference element $[-1, 1]$.

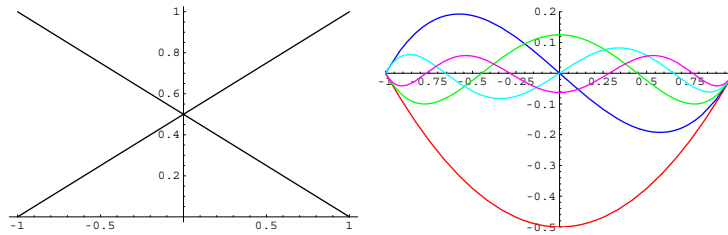


Figure B.4: Reference element $[-1, 1]$ and internal shape functions N_0, N_1 (left) and $N_i, i = 2, 3, 4, 5, 6$ (right)

A big advantage of using hierarchic instead of standard (which are not further considered here) nodal basis functions is that the condition number of the stiffness matrix is highly

improved. Furthermore the hierarchic basis has consequence on the structure of the stiffness matrix.

With ansatz functions of higher degree the u_j are not any longer $u_h(x_j)$ but $u_h(x_j) = \sum_{i=0}^{N_h} u_i \phi_i(x_j)$ has to be computed extra.

Everything above can be done in 2D or 3D, but some adaptations have to be made.

B.3.2 Linear Courant Elements on Triangles

The domain $\Omega \subset \mathbf{R}^2$ is decomposed into N_h triangles $T_k, k = 1, \dots, N_h$ that fulfill the conditions of a Triangulation. The nodes $\vec{x}_i = (x_i, y_i) \in \mathbf{R}^2$ are enumerated by an index set ω_h and are referred to by $\vec{x}_i, i \in \omega_h$. The precision h of \mathcal{T}_h is now defined as

$$h = \max_{k=1, \dots, N_h} h_k \quad \text{with } h_k = |\vec{x}_i - \vec{x}_j| = \sqrt{(x_i - x_j)^2 + (y_i - y_j)^2} \text{ with } \vec{x}_i, \vec{x}_j \in T_k. \quad (\text{B.27})$$

The finite element space V_h is defined as in B.10 with the same nodal basis functions as in B.11.

Assembling of the stiffness- or mass matrices works the same, but now integrals over some reference triangle Δ have to be computed. This reference triangle is defined as:

$$\Delta = \{(\xi, \eta) \in [0, 1]^2 : \xi + \eta \leq 1\}, \quad (\text{B.28})$$

and can be seen in Figure B.5. There the ansatz functions are shown as well.

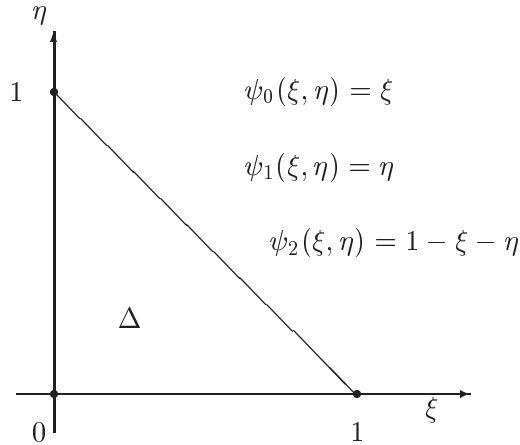


Figure B.5: Reference element Δ and local ansatz functions $\psi_i, i = 0, 1, 2$

For quadratic Courant elements (of order 2) on triangles there are 6 ansatz functions ψ_i needed. For cubic elements 10 ansatz functions and for elements of order p already

$$\frac{(p+1)(p+2)}{2} = \sum_{i=1}^{p+1} i, \quad (\text{B.29})$$

ansatz functions are needed. High order shape functions on triangles will be discussed later.

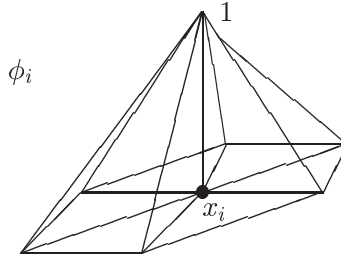


Figure B.6: Basis function (ansatz function) ϕ_i onto node x_i

The next Figure (B.6) shows a linear Courant ansatz function ϕ_i on the node x_i . The support of ϕ_i

$$\text{supp}(\phi_i) = \{T_k : x_i \in T_k \forall k = 1, \dots, N_h\}, \quad (\text{B.30})$$

are those triangles the node \vec{x}_i belongs to, see Figure B.6. The support is rather small and therefore the assembled matrices are sparse for some (optimal) numbering of the nodes or triangles.

B.3.3 High order ansatz functions in \mathbb{R}^2

Quadrilateral Elements

To construct high order shape functions on the quadrilateral $T = [-1, 1]^2$ is rather easy, only the tensor product of the one dimensional high order shape functions have to be formed

$$\psi_{i,j}(\xi, \eta) = N_i(\xi)N_j(\eta), \quad i, j = 0, \dots, p. \quad (\text{B.31})$$

Those shape functions can be classified into three groups:

1. Nodal modes:

The four nodal Modes

$$\psi_{i,j}^N(\xi, \eta) = N_i(\xi)N_j(\eta) = \frac{1}{4}(1 \pm \xi)(1 \pm \eta), \quad i, j = 0, 1, \quad (\text{B.32})$$

are the standard bilinear shape functions, see Figure B.7.

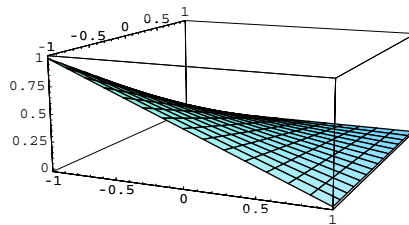


Figure B.7: Nodal mode $\psi_{0,0}^{N-1,-1}(\xi, \eta) = \frac{1}{4}(1 - \eta)(1 - \xi)$ on node $(-1, -1)$

2. Edge Modes:

These edge modes are defined separately for each edge

$$\psi_{i,j}^{E_v}(\xi, \eta) = \frac{1}{2}(1 \pm \xi)N_i(\eta), \quad j = 0, 1; i = 2, \dots, p, \quad (\text{B.33})$$

$$\psi_{i,j}^{E_h}(\xi, \eta) = \frac{1}{2}(1 \pm \eta)N_j(\xi), \quad i = 0, 1; j = 2, \dots, p, \quad (\text{B.34})$$

and they vanish at all the other edges, see Figure B.8. The edge $\psi_{i,j}^{E_v}$ describes the vertical and $\psi_{i,j}^{E_h}$ the horizontal edges, if it is looked from above onto the reference element T .

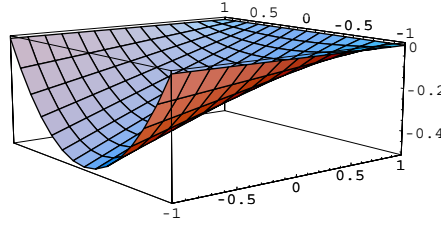


Figure B.8: Edge mode $\psi_{0,2}^{E_1}(\xi, \eta) = \frac{1}{2}(1 - \xi)N_2(\eta)$ on edge $\{-1\} \times [-1, 1]$

3. Internal Modes:

The internal modes

$$\psi_{i,j}^I(\xi, \eta) = N_i(\xi)N_j(\eta), \quad i, j = 2, \dots, p, \quad (\text{B.35})$$

are purely local and vanish at all the edges. They are the so-called bubble functions, see Figure B.9.

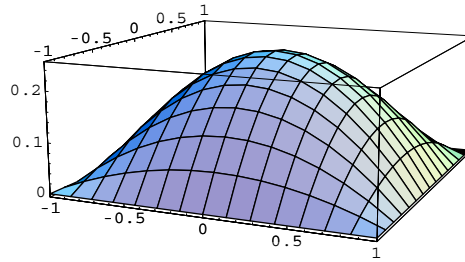


Figure B.9: Internal mode $\psi_{2,2}^I(\xi, \eta) = N_2(\xi)N_2(\eta)$

All in all with quadrilateral elements high order shape functions are as easy to obtain as in the one-dimensional case. This can be extended analogous (adding face basis functions) to three-dimensional cubes / hexahedral elements, see [11] for details.

Triangular Elements

For triangles the shape functions are not so easy to define. First of all a new coordinate system has to be introduced: *the barycentric coordinates* λ_1, λ_2 and λ_3 that are computed the

following way

$$\begin{pmatrix} x_1 & x_2 & x_3 \\ y_1 & y_2 & y_3 \\ 1 & 1 & 1 \end{pmatrix} \cdot \begin{pmatrix} \lambda_1 \\ \lambda_2 \\ \lambda_3 \end{pmatrix} = \begin{pmatrix} x \\ y \\ 1 \end{pmatrix}, \quad (\text{B.36})$$

with x, y the cartesian coordinates and $(x_i, y_i), i = 1, 2, 3$ the coordinates of the three vertices of the reference triangle. Here it is set as $(x_1, y_1) = (0, 0), (x_2, y_2) = (1, 0)$ and $(x_3, y_3) = (0, 1)$, the same reference triangle as before with the barycentric coordinates

$$\lambda_1(x, y) = x, \quad \lambda_2(x, y) = y, \quad \lambda_3(x, y) = 1 - x - y. \quad (\text{B.37})$$

These coordinates are the linear shape functions $\psi_i, i = 0, 1, 2$.

In order to define high order basis functions for triangular elements, the *scaled and scaled integrated Legendre polynomials* as

$$P_i^S(x, t) = P_i\left(\frac{x}{t}\right) t^i, \quad L_i^S(x, t) = L_i\left(\frac{x}{t}\right) t^i, \quad (\text{B.38})$$

have to be defined (with the Legendre polynomials P_i as in B.23 and the integrated Legendre polynomials as in B.24), see [26] for details. Again there are three groups of basis functions:

1. Nodal basis functions:

The Nodal basis functions

$$\psi^N(\lambda_\alpha) = \lambda_\alpha, \quad \alpha = 1, 2, 3, \quad (\text{B.39})$$

are exactly the barycentric coordinates and therefore the same as the linear shape functions (on this special reference element).

2. Edge basis functions:

The $p - 1$ edge-based functions are defined as

$$\psi_i^{E_{\alpha,\beta}}(\lambda_\alpha, \lambda_\beta) = L_i^S(\lambda_\alpha - \lambda_\beta, \lambda_\alpha + \lambda_\beta), \quad i = 2, \dots, p, \quad \alpha, \beta = 1, 2, 3. \quad (\text{B.40})$$

On each edge $E_{\alpha,\beta}$ there holds $\lambda_\alpha + \lambda_\beta = 1$, therefore the basis function equal L_i on this edge. On the other two edges the basis function vanish because

$$\frac{\lambda_\alpha - \lambda_\beta}{\lambda_\alpha + \lambda_\beta} = \pm 1, \quad \forall \alpha, \beta = 1, 2, 3, \quad (\text{B.41})$$

at the Edge $E_{\alpha,\beta}$ and $L_i(\pm 1) = 0$.

3. Internal basis functions:

The internal basis functions are defined as

$$\psi_{i,j}^I(\lambda_1, \lambda_2, \lambda_3) = L_i^S(\lambda_1 - \lambda_2, \lambda_1 + \lambda_2) P_j(2\lambda_3 - 1), \quad i \geq 2; j \geq 0; i + j \leq p - 1, \quad (\text{B.42})$$

with L_i^S the scaled integrated Legendre polynomial and P_j the Legendre polynomial as in B.23. The first term of $\psi_{i,j}^I$ vanishes at the edges with $\lambda_1 = 0$ and $\lambda_2 = 0$ whereas the second term vanishes for the edge $\lambda_3 = 0$. So $\psi_{i,j}^I$ is zero at all edges.

For the three dimensional case another barycentric coordinate λ_4 and basis functions for the faces have to be added, everything else works analogous, see [26] for more.

Bibliography

- [1] S. Abarbanel and D. Gottlieb. A Mathematical Analysis of the PML method. *Journal of Comp. Physics*, 134, pages 357–363, 1997.
- [2] Peter Arbenz and Michel E. Hochstenbach. A Jacobi-Davidson Method for Solving Complex Symmetric Eigenvalue Problems. *SIAM Journal of Sci. Comp.*, Vol. 25, pages 1655–1673, 2004.
- [3] E. Bécache and P. Joly. On the Analysis of Perfectly Matched Layers for Maxwell’s equation. *Mathematic Modelling and Numerical Analysis Num. Analysis*, 36, pages 87–119, 2002.
- [4] D. Braess. *Finite Elemente*. Springer, 2003.
- [5] Jean-Pierre Bérenger. A Perfectly Matched Layer for the Absorption of Electromagnetic Waves. *Journal of Computational Physics*, 114:185–200, 1994.
- [6] Jean-Pierre Bérenger. Improved PML for the FDTD Solution of Wave-Structure Interaction Problems. *IEEE Transactions on Antennas and Propagation*, 45, 1997.
- [7] Philippe G. Ciarlet. *Finite Element Method for Elliptic Problems*. Classics in Applied Mathematics, Vol. 40, SIAM, 2002.
- [8] Francis Collino and Peter B. Monk. Optimizing the perfectly matched layer. *Computer Methods in Applied Mechanics and Engineering*. 164, pages 157–171, 1998.
- [9] Francis Collino and Peter B. Monk. The perfectly Matched Layer in curvilinear Coordinates. *SIAM Journal of Sci. Comp.* 19, pages 2061–2090, 1998.
- [10] D. Colton and R. Kresse. *Inverse Acoustic and Electromagnetic Scattering Theory*. Springer-Verlag Berlin, 1992.
- [11] Alexander Düster. High Order FEM, Lecture Notes. www.inf.bv.tum.de/lehre/pfem/material/exercises.1.pdf, Summerterm 2005.
- [12] E. Bécache, A.-S. Bonnet-Ben Dhia and G. Legendre. Perfectly Matched Layers for the convected Helmholtz equation. *SIAM Journal of Num. Analysis*, 42, pages 409–433, 2001.
- [13] E. Bécache, P. Joly and Ch. Tsogka. Fictitious domain, Mixed Finite Elements and Perfectly Matched Layers for 2D Elastic Wave Propagation. *Journal of Comp. Acoustics*, 9, pages 1175–1203, 2001.

- [14] E. Bécache, S. Fauqueux and P. Joly. Stability of Perfectly Matched Layers, Group velocities and Anisotropic Waves method. *Journal of Comp. Physics*, 188, pages 399–433, 2003.
- [15] Heinz W. Engl. *Integralgleichungen*. SpringerWienNewYork, 1997.
- [16] David L. Harrar. A Shift-Invert Block Arnoldi Method with Deflation and Adaptive Parameter Selection. *Research Report MRR99-033*, 1999.
- [17] Frank Ihlenburg. *Finite Element Analysis of Acoustic Scattering*. Applied Mathematical Sciences 132, 1998.
- [18] W. Koch. Acoustic Resonances in Rectangular Open Cavities. *AIAA Journal*, Vol.43 , No. 11, 2005.
- [19] lapack@cs.utk.edu. LAPACK, Linear Algebra PACKage. www.netlib.org/lapack/.
- [20] M. Abramowitz and I. A. Stegun. *Handbook of Mathematical Functions*. New York, Dover Publications, 1965.
- [21] Intel MKL. Intel Math Kernel Library. www.intel.com/cd/software/products/asmo-na/eng/perflib/mkl/index.htm.
- [22] Olaf Schenk and Klaus Gärtner. PARDISO, PARallel sparse DIrect linear SOLver. www.computational.unibas.ch/cs/scicomp/software/pardiso/.
- [23] R. Klose, A. Schädle, F.Schmidt and L. Zschiedrich. A new Finite Element realisation of the Perfectly Matched Layer Method for Helmholtz scattering problems on polygonal domains in 2D. *Technical report 03-44, ZIB*, 2003.
- [24] S. Hein, W. Koch and J. Schöberl. Acoustic Resonances in a 2D Slat Cove and 3D Open Cavity. *11th AIAA/CEAS Aeroacoustics Conference, Monterey, CA*, 2005.
- [25] Joachim Schöberl. NETGEN. www.hpfem.jku.at/.
- [26] Joachim Schöberl and Sabine Zaglmayr. High Order Nédélec Elements with local complete sequence properties. *Journal for Computation and Mathematics in Electrical and Electronic Engineering (COMPEL)*, to appear.
- [27] B. A. Szabó and I. Babuška. *Finite Element Analysis*. John Wiley and Sons, 1991.
- [28] Thorsten Hohage, Frank Schmidt and Lin Zschiedrich. Solving timeharmonic scattering problems based on pole condition I: Theory. *SIAM J. Math. Anal.* 35, pages 183–210, 2003.
- [29] Thorsten Hohage, Frank Schmidt and Lin Zschiedrich. Solving timeharmonic scattering problems based on pole condition II: Convergence of the PML method. *SIAM J. Math. Anal.*, 35, pages 547–560, 2003.
- [30] Thorsten Hohage, Frank Schmidt and Lin Zschiedrich. A new Method for the solution of scattering Problems. In B. Michielsen and F. Decavele (eds) *Proceedings of the JEE'02 Symposium*, pages 251–256, Toulouse, ONERA, 2002.

- [31] C. H. Wilcox. *An expansion Theorem for electromagnetic fields*. Comm. Pure. Appl. Math., 115-134, 1956.
- [32] Z. Bai, J. Demmel, J. Dongarra, A. Ruhe and H. Van der Horst. *Templates for the Solution of Algebraic Eigenvalue Problems: A Practical Guide*. SIAM, 1987.

Eidesstattliche Erklärung

Ich, Maria Rechberger, erkläre an Eides statt, dass ich die vorliegende Diplomarbeit selbstständig und ohne fremde Hilfe verfasst, andere als die angegebenen Quellen und Hilfsmittel nicht benutzt bzw. die wörtlich oder sinngemäß entnommenen Stellen als solche kenntlich gemacht habe.

Linz, Nov 2005

Maria Rechberger

Curriculum Vitae

Name: Maria Rechberger

Nationality: Austria

Date and Place of Birth: 6 April, 1982 in Linz, Austria

Education:

2000-2005: Studies of Technical Mathematics,
Johannes Kepler University Linz, Austria

1996-2000: Adalbert-Stifter-Gymnasium (grammar school)
Linz, Austria

1992-1996: Hauptschule Ottensheim (secondary modern school)
Austria

1988-1992: Volksschule Walding (elementary school)
Austria

Special Activities:

August 2004: participant at 18th ECMI Modelling Week,
Lappeenranta, Finland

Sept.-Oct. 2004: practical training at National Economic University Kyiv,
Dep.of Mathematics, Kyiv, Ukraine